IMPROVEMENTS TO REAL TIME AEROSOL ANALYSIS USING AMBIENT
SAMPLING/IONIZATION MASS SPECTROMETRY

Kenneth Dakota Swanson

A dissertation submitted to the faculty at the University of North Carolina at Chapel Hill
in partial fulfillment of the requirements for the degree of Doctor of Philosophy in the
Department of Chemistry (Analytical) in the School of Arts and Sciences.

Chapel Hill
2018

Approved by:

James W. Jorgenson

Gary L. Glish

Brandie M. Ehrmann

Michel R. Gagné

Jason D. Surratt

ABSTRACT

Kenneth Dakota Swanson: Improvements to Real Time Aerosol Analysis using Ambient
Sampling/Ionization Mass Spectrometry
(Under the direction of Gary L. Glish)

Ambient ionization is a family of techniques that requires very few or no sample

preparation steps and has become an important area of research in analytical applications

using mass spectrometry. Extractive electrospray ionization (EESI) is an ambient

ionization technique that allows real-time sampling of organic aerosols. Similar to

electrospray ionization, the composition of the electrospray solvent used in extractive

electrospray ionization can easily be altered to change the chemistry of ionization. A novel

EESI source design is presented to improve the reproducibility of the interactions occurring

in EESI. This design uses three concentric capillaries to deliver solvent, sample and

nebulizing gas. Coaxial EESI was found to improve the inter-experiment variation by a

factor of four and intra-run relative standard deviation by a factor of 2.4. Unlike most

standard EESI designs, the device has the form factor of a standard electrospray (ESI)

emitter and can be used without any further instrument modifications. A simple design for

an open port sampling interface coupled to electrospray ionization (OPSI-ESI) is also

presented as a novel approach for the analysis of aerosols. The design uses minimal

modifications to a Bruker ESI emitter to create a continuous flow, self-aspirating open port

sampling interface. Upon comparison with EESI, this device has similar sensitivity with

increased reproducibility by nearly a factor of three.

Soli Deo gloria

ACKNOWLEDGEMENTS

I would like to begin by thanking my advisor, Professor Gary Glish, for taking in a student who loved building with LEGOs and training him to use that creativity for science. Gary, your infectious and limitless curiosity has provided me opportunities to explore chemistry in ways no other advisor could. I will be forever grateful and inspired by your dedication to cultivate well-rounded scientists by focusing on the quality of the science rather than the quantity of results.

To the current and former members of the Glish Group, thank you for being a constant source of support, critique, and humor. You have provided a safe space for the exploration of both good and bad ideas and those collective successes and failures have made me a better scientist. I would like to particularly recognize Matt for taking the time to write and continually modify programs to make data workup easier, and for pushing me, perhaps harder than anyone else, to strive for reproducibility over settling for interesting results. Some of the work in this dissertation was completed with the aid of some hard-working undergrads. Anne, Brandon, and Katherine, thank you for following my whims and striving to produce quality data. I am also very appreciative of the graduate students who aided me in editing this dissertation (Matt, James, Nick, Paul, Tavleen, Tiffany, and Nathan).

To my family and friends who have given me so much of their time and support on my seemingly endless journey through academia, thank you from the bottom of my heart. To my parents, thank you for the love and support you have given me throughout the years.

Mom, you have always told me I can do anything I set my mind to, and I foolishly believed you. Your faith in me has propelled me to where I am today. To my brother, Curt, you and Chenoa have provided me with an inexhaustible supply of love and support. Thank you for taking me into your family and always ensuring I had everything I needed to succeed. To Dan and the men of Glee Club, thank you for giving me the opportunity to sing with you. By deeming me a tenor, you challenged me to step outside of my comfort zone and I am a far better person for it. Jerome, thank you for befriending me on my first day, for challenging me with fun chemistry problems, and for showing me it is possible to balance a career in chemistry and a passion for music.

Finally, Brittni, whose daily encouragement was my sustaining force throughout my graduate career, words cannot express how much I love and appreciate you. Your warm smile makes each day, the good and the bad, worthwhile.

i carry your heart (i carry it in my heart)
e e cummings

TABLE OF CONTENTS

LIST OF TABLES

LIST OF FIGURES

LIST OF ABBREVIATIONS AND SYMBOLS

3D   three-dimensional

AIM   aerosol instrument manager

AMS   aerosol mass spectrometer

APCI   atmospheric pressure chemical ionization

°C   degrees Celsius

-C_{13} isotopically labeled with carbon-13

CID   collision induced dissociation

CO   carbon monoxide

COA   constant output atomizer

CPC   condensation particle counter

cm   centimeter

Da   unified atomic mass unit

DESI   desorption electrospray ionization

DFT   density functional theory

DIMS   differential ion mobility spectrometry

DMA   differential mobility analyzer

-d_n isotopically labeled with n deuterium atoms

EESI   extractive electrospray ionization

EI   electron ionization

EIC   extracted ion chronogram

ESI   electrospray ionization

FA   formic acid

FT-ICR   Fourier transform – ion cyclotron resonance

ft   foot

GC	gas chromatography
g	gram
H_2O	water
HESI	heated electrospray ionization
HOAc	acetic acid
HV	high voltage
hr	hour
ID	inner diameter
IEM	ion evaporation model
in	inch
kV	kilovolt
L	liter
LC	liquid chromatography
LPM	liters per minute
LTPI	low temperature plasma ionization
MeOH	methanol
MS	mass spectrometry
MS/MS	tandem mass spectrometry
MS^n	n stages of mass spectrometry
m	meter
m/z	mass-to-charge ratio
mA	milliampere
mL	milliliter
mM	millimolar
mg	milligram

mm	millimeter
ms	millisecond
min	minute
μA	microampere
μL	microliter
μM	micromolar
μg	microgram
μm	micrometer
μs	microsecond
n=4	number of replicates
N_2	nitrogen
NL	intensity of the most abundant peak
NNN	n-nitrosonornicotine
NPT	national pipe thread taper
nA	nanoampere
nm	nanometer
OD	outer diameter
OPSI	open port sampling interface
PILS	particle-into-liquid sampler
PLA	polylactic acid
ppm	part-per-million
psig	pounds per square inch gauge
QIT	quadrupole ion trap
RSD	relative standard deviation
S	seconds

SCFM	standard cubic feet per minute
SMPS	scanning mobility particle sizer
TIC	total ion chronogram
UR	unreactive rate
V	volts
Vpp	peak-to-peak voltage
v/v	volume/volume percent
ZDV	zero dead volume
$[M+H]^+$	positively charged protonated analyte
$[M+X]^+$	positively charged analyte with an adduct of X
$[M-H]^-$	negatively charged deprotonated analyte

CHAPTER 1: INTRODUCTION TO AEROSOL ANALYSIS BY AMBIENT IONIZATION
MASS SPECTROMETRY

1.1. Introduction to Aerosol Particle Analysis

Aerosol particle analysis presents a significant analytical challenge due to variations in size, composition, and phase[1]. An aerosol is a system of small particles suspended in a gas. A single aerosol particle is a conglomeration of molecules that can range in diameter from a few nanometers (nm), a collection of a two or more molecules, to ten microns (μm)[2]. The lifetimes of aerosol particles are inversely proportional to the particle size. The Environmental Protection Agency has set regulation standards for particles less than 10 μm in diameter because they can penetrate deep into the lungs[3]. Particular attention is given to aerosol particles 2.5 μm or less in diameter due to the environmental damage of particles that can travel long distances and settle onto the ground or into water sources. Depending on the chemical composition of these particles, this settling can cause reduction of visibility, acidification of lakes and streams, depletion of nutrients in soil, and damage to forestry and farm crops[4]. Further, the World Health Organization estimated that exposure to airborne pollution particles results in approximately 348,000 premature deaths every year[5]. Unless particles are specifically produced to be of a single diameter, or monodisperse, aerosol particles are typically polydisperse in size. This is important because aerosol activity in the lungs and in the environment is dependent on both size and composition. Assuming uniform composition, an aerosol can have varying activity simply due to the wide array of particle diameters. Uniform composition for aerosol particles is an invalid

assumption because the chemical composition of aerosol particles are often a function of particle size as shown in the literature[6,7].

Any single aerosol particle can be heterogeneous or homogeneous depending on the phase of the particle, where the phase can be a liquid, solid, or a mixture of both. Thus, analysis of the surface of a particle may not be representative of the whole particle, especially when constituents are insoluble in a liquid droplet, forming a heterogeneous particle. This becomes important in analyses where solubility is a factor in extracting compounds from the particle.

1.2. Analysis of the Chemical Composition of an Aerosol

The analysis of the chemical composition of an aerosol is critical to many different fields, including secondary organic aerosol formation[8,9], drug delivery[10,11], biological warfare agents[12], and biomass burning[13]. An analysis method can generally be grouped by two categories: amount of sample preparation and the ability to distinguish particles from one another. The amount of sample preparation required by an analysis determines whether an analysis is on-line (little or no sample preparation) or off-line (sample preparation is required). The ability to distinguish particles from one another determines whether the aerosol is sampled in bulk (particles analyzed without respect to size), size-separated prior to analysis, or analyzed on a single-particle level.

Typical compositional analysis includes off-line aerosol collection in bulk onto a filter, and then extraction followed by gas chromatography and mass spectrometric analysis (GC-MS)[14]. Filter analysis cannot distinguish between particle sizes. Such analyses suffer from chemical aging of compounds after collection onto the filter material, reactions with the filter material, evaporative losses from the filter material, and extraction bias depending on the solubility of the collected compounds in the extraction solvent[15,16]. Thus, the suite of compounds identified in an off-line analysis of a complex sample may not accurately

represent the compounds present in the aerosol particles immediately after generation. Further, no information regarding particle size or composition as a function of size is obtained.

Particles may be size-separated prior to either off-line or on-line analyses, but both present significant challenges[17]. Any off-line analysis will suffer from the aforementioned chemical aging, reactions with surfaces, and evaporative losses. On-line analyses of size-selected particles include the use of a scanning mobility particle sizer (SMPS) system[18]. An SMPS system, such as a differential mobility analyzer (DMA), separates particles by first charging particles uniformly and then separating the particles using an electric field[19]. The trajectory of smaller particles will be easily changed in a small electric field while larger particles require a larger electric field[20]. Size-separated particles are usually detected using a laser system such as a condensation particle counter[21]. While a laser system gives information on the distribution of sizes in an aerosol, it gives no information on the chemical composition of an aerosol.

Another method of aerosol size-separation is used prior to mass analysis in the commercial Aerodyne Aerosol Mass Spectrometer (AMS)[22–24]. This system utilizes a time-of-flight particle measurement where particles are accelerated with the same kinetic energy[22]. The velocity of each particle is determined by its mass, thus smaller particles arrive at the electron impact (EI) ionization source of the mass spectrometer earlier than larger particles yielding a separation of particles in time. For this analysis, a fast mass analyzer is required such as a quadrupole or a time-of-flight. The information obtained in this analysis includes size distribution of the aerosol particles, but the compositional analysis is limited to determination of compound classes rather than molecular assignment[25]. The EI source imparts enough internal energy to both ionize a compound and induce significant fragmentation[22]. In EI, a peak is rarely observed for the intact molecular ion. A structure

3

may be determined from the fragmentation pattern if only a single species if present, but compound identification is very difficult in a complex mixture due to overlapping fragmentation patterns. For this reason, the AMS system is ill-suited for compound identification in an aerosol. Custom-built mass spectrometers have been built for single-particle analyses, but these involve laser-induced ionization which suffers from the same drawbacks as EI where relative abundance of compound classes may be determined, but compound identification is very difficult[26–29].

1.3. Mass Spectrometry

Mass spectrometry is a fast, highly selective, and sensitive analysis technique that is uniquely suited for chemical analysis of complex mixtures. For successful mass analysis of the intact molecular ions from a sample, an analyte must be converted from its native state into gaseous ions. For an aerosol, particles must be dissociated into individual molecules and ionized. EI is often used in tandem with mass analysis due to the ability to control the energy of ionization. However, it typically imparts too much internal energy for the direct analysis of complex samples leading to excessive fragmentation and convoluted spectra. These ionization techniques are typically used in conjunction with chromatographic techniques such as liquid chromatography (LC) or gas chromatography (GC) to reduce sample complexity prior to mass analysis. Unfortunately, neither LC nor GC are very amenable to on-line aerosol analysis because both techniques usually begin with a sample in the liquid phase. To use chromatographic separations with an on-line aerosol analysis, an aerosol sample would have to be put into solution and injected onto a column on a fast timescale that reduces chemical aging.

Electrospray ionization (ESI) is an alternative ionization source to EI that imparts less internal energy and produces primarily intact analyte ions[30]. One of the most beneficial aspects of ESI is that it occurs at atmospheric pressure, unlike EI[31]. Some fragmentation

can occur, depending on the electric fields generated by the ion optics, but ESI is generally considered a soft-ionization technique. In ESI, an electric field is generated by applying a potential difference between the inlet to the mass spectrometer and a capillary containing the analyte of interest dissolved in solution[32]. Charge accumulates on the solution at the tip of the capillary and a Taylor cone of solution is formed from which small, highly charged droplets are ejected toward the mass spectrometer. By the ion evaporation model (IEM), a droplet desolvates until the surface charge reaches the Rayleigh limit[33] and the droplet explodes into smaller droplets due to columbic repulsion of the charges. Over time, solvated ions are ejected from the charged droplet. The solvent evaporates from the solvated ion until bare analyte ions are transmitted through the mass spectrometer for mass analysis[34]. Similar challenges exists for ESI as for LC or GC analysis. In ESI, the sample needs to be dissolved in solution before ionization. An aerosol would have to be put into solution and electrosprayed on a fast timescale that reduces chemical aging.

1.4. Ambient Ionization Mass Spectrometry

Ambient ionization refers to a family of ionization techniques in mass spectrometry in which ionization occurs at atmospheric pressure prior to introduction of the ions into the vacuum region of the mass spectrometer[35–39]. Benefits of ambient ionization include minimal or no sample preparation and the ability to analyze samples from their native state in real-time[39]. Ambient ionization can be broadly classified into laser-based techniques, atmospheric pressure chemical ionization (APCI)-related techniques, and electrospray-based techniques[40].

Several types of ambient ionization have been used in the analysis of aerosol particles. Desorption electrospray ionization (DESI) has been used by impacting an aerosol onto a plate prior to surface analysis[41]. Although surface analysis using DESI is an ambient ionization technique, the particles are no longer in a native state after impaction onto a

plate. This type of analysis allows for concentration of the aerosol for increased signal intensity; however, the technique suffers from problems similar to filter collection as discussed earlier. A particle-into-liquid sampler (PILS) has also been used to sample from aerosols resulting from biomass burning prior to electrospray ionization[42]. Both of these techniques require sample collection prior to analysis by mass spectrometry and are susceptible to chemical aging and evaporative losses.

Real-time ambient ionization has also been applied to aerosol particles. Low temperature plasma ionization (LTPI) has been used to characterize organic aerosols in which the plasma from a dielectric barrier discharge intersects a stream of organic aerosol particles[43,44]. The most reported technique for the on-line characterization of aerosol particles is extractive electrospray ionization (EESI)[45–47]. EESI involves a real-time extraction by colliding aerosol particles with the electrospray plume. This technique is one of the most versatile ionization techniques currently available for bulk aerosol analysis due to the ability to easily alter the extraction by manipulation of the electrospray solvent composition[48,49]. These techniques do not require significant instrument modifications as they can be used on any mass spectrometer with an atmospheric pressure interface.

1.5. Summary

Compositional analysis of complex aerosols is an analytical challenge that is prevalent in a variety of applications. Most current techniques involve off-line aerosol collection, which are susceptible to chemical reactivity and can provide misleading results. On-line ambient ionization mass spectrometry circumvents aerosol collection by sampling and ionizing compounds in aerosol particles directly. Further, electrospray-based ionization allows for tunability of the electrospray solvent to improve the extraction of compounds from an aerosol.

The experimental methods used in subsequent chapters are provided in **Chapter 2**. The instrumentation used is also covered, including information about the aerosol generation systems, the electrospray ionization source, the extractive electrospray ionization source, and the mass spectrometry systems used.

The work presented in **Chapter 3** involves the use of EESI to improve the sensitivity of multiple oxygen-containing compounds by using metal cations in the electrospray solvent. Fortuitously, this also led to improved dissociation patterns upon MS/MS of two of the compounds analyzed. Some studies are presented to show the similarity in the structures formed by EESI and ESI.

Chapter 4 discusses the drawbacks of the current EESI source and outlines a new design for a more stable source that can be used with the existing source housing. The fabrication of a coaxial EESI source is discussed and characterization of this source is presented in comparison to the existing EESI source. Solvent composition optimization for coaxial EESI is presented in the study of pyrolyzed cellulose.

A new electrospray-based aerosol sampling and ionization source is presented in **Chapter 5** that complements EESI. This open port sampling interface electrospray ionization (OPSI-ESI) source is contrasted to EESI and solvent optimization studies are discussed. Updates to the design are presented and characterized. Finally, **Chapter 6** provides a summary of the results of each chapter presented and considers potential future directions related to this work.

REFERENCES

1. Prather, K. A., Hatch, C. D. & Grassian, V. H. Analysis of Atmospheric Aerosols. *Annu. Rev. Anal. Chem.* **1,** 485–514 (2008).

2. Kaiser, J. Mounting Evidence Indicates Fine-Particle Pollution. *Science* **307,** 1858–1861 (2005).

3. Particulate Matter (PM) Basics. *US Environmental Protection Agency* (2016). Available at: https://www.epa.gov/pm-pollution/particulate-matter-pm-basics.

4. Health and Environmental Effects of Particulate Matter (PM). *US Environmental Protection Agency* (2003). Available at: https://www.epa.gov/pm-pollution/health-and-environmental-effects-particulate-matter-pm.

5. Joint WHO / Convention Task Force on the Health Aspects of Air Pollution. *Health risks of particulate matter from long-range transboundary air pollution.* (2006).

6. Lundgren, D. A. Atmospheric Aerosol Composition and Concentration as a Function of Particle Size and of Time. *J. Air Pollut. Control Assoc.* **20,** 603–608 (1970).

7. Noble, C. A. & Prather, K. A. Real-Time Measurement of Correlated Size and Composition Profiles of Individual Atmospheric Aerosol Particles. *Envionmental Sci. Technol.* **30,** 2667–2680 (1996).

8. Surratt, J. D. *et al.* Chemical Composition of Secondary Organic Aerosol Formed from the Photooxidation of Isoprene. *J. Phys. Chem. A* **110,** 9665–9690 (2006).

9. Krechmer, J. E. *et al.* Formation of Low Volatility Organic Compounds and Secondary Organic Aerosol from Isoprene Hydroxyhydroperoxide Low-NO Oxidation. *Environ. Sci. Technol.* **49,** 10330–10339 (2015).

10. Arunthari, V., Bruinsma, R. S., Lee, A. S. & Johnson, M. M. A Prospective, Comparative Trial of Standard and Breath-Actuated Nebulizer: Efficacy, Safety, and Satisfaction. *Respir. Care* **57,** 1242–1247 (2012).

11. Smith, J. H. *et al.* Nebulized live-attenuated influenza vaccine provides protection in ferrets at a reduced dose. *Vaccine* **30,** 3026–3033 (2012).

12. Pazienza, M. & Britti, M. S. Use of Particle Counter System for the Optimization of Sampling, Identification and Decontamination Procedures for Biological Aerosols Dispersion in Confined Environment. *J. Microb. Biochem. Technol.* **06,** 43–48 (2013).

13. Brito, J. *et al.* Ground-based aerosol characterization during the South American Biomass Burning Analysis (SAMBBA) field experiment. *Atmos. Chem. Phys.* **14,** 12069–12083 (2014).

14. Hoffmann, T., Huang, R. & Kalberer, M. Atmospheric Analytical Chemistry. *Anal. Chem.* **83,** 4664 (2011).

15. Bateman, A. P. *et al.* The effect of solvent on the analysis of secondary organic aerosol using electrospray ionization mass spectrometry. *Environ. Sci. Technol.* **42,** 7341–7346 (2008).

16. Turpin, B. J., Saxena, P. & Andrews, E. Measuring and simulating particulate organics in the atmosphere: Problems and prospects. *Atmos. Environ.* **34,** 2983–3013 (2000).

17. McMurry, P. A review of atmospheric aerosol measurements. *Atmos. Environ.* **34,** 1959–1999 (2000).

18. Keady, P. B., Quant, F. R. & Sem, G. J. Differential mobility particle sizer: a new instrument for high-resolution aerosol size distribution measurement below 1 μm. *TSI Q.* **9,** 3–11 (1983).

19. Liu, B. Y. H. & Pui, D. Y. H. Electrical neutralization of aerosols. *J. Aerosol Sci.* **5,** 465–472 (1974).

20. Hagen, D. E. & Alofs, D. J. Linear Inversion Method to Obtain Aerosol Size Distributions from Measurements with a Differential Mobility Analyzer. *Aerosol Sci. Technol.* **2,** 465–475 (1983).

21. Wiedensohlet, A. *et al.* Intercomparison study of the size-dependent counting efficiency of 26 condensation particle counters. *Aerosol Sci. Technol.* **27,** 224–242 (1997).

22. Canagaratna, M. R. *et al.* Chemical and microphysical characterization of ambient aerosols with the aerodyne aerosol mass spectrometer. *Mass Spectrom. Rev.* **26,** 185–222 (2007).

23. Shilling, J. E., King, S. M., Mochida, M., Worsnop, D. R. & Martin, S. T. Mass spectral evidence that small changes in composition caused by oxidative aging processes alter aerosol CCN properties. *J. Phys. Chem. A* **111,** 3358–3368 (2007).

24. Jimenez, J. L. *et al.* Evolution of Organic Aerosols in the Atmosphere: A New Framework Connecting Measurements to Models. *Science (80-.).* **326,** 1525–1529 (2009).

25. Zahardis, J., Geddes, S. & Petrucci, G. A. Improved Understanding of Atmospheric Organic Aerosols via Innovations in Soft Ionization Aerosol Mass Spectrometry. *Anal. Chem.* **83,** 2409–2415 (2011).

26. Denkenberger, K. A., Moffet, R. C., Holecek, J. C., Rebotier, T. P. & Prather, K. A. Real-time, single-particle measurements of oligomers in aged ambient aerosol particles. *Environ. Sci. Technol.* **41,** 5439–5446 (2007).

27. Moffet, R. C., Qin, X., Rebotier, T., Furutani, H. & Prather, K. A. Chemically segregated optical and microphysical properties of ambient aerosols measured in a single-particle mass spectrometer. *J. Geophys. Res. Atmos.* **113,** 1–11 (2008).

28. Hatch, L. E., Pratt, K. A., Huffman, J. A., Jimenez, J. L. & Prather, K. A. Impacts of Aerosol Aging on Laser Desorption/Ionization in Single-Particle Mass Spectrometers. *Aerosol Sci. Technol.* **48,** 1050–1058 (2014).

29. Axson, J. L., May, N. W., Colón-Bernal, I. D., Pratt, K. A. & Ault, A. P. Lake Spray Aerosol: A Chemical Signature from Individual Ambient Particles. *Environ. Sci. Technol.* **50,** 9835–9845 (2016).

30. Fenn, J. B. Electrospray Wings for Molecular Elephants (Nobel Lecture). *Angew. Chemie Int. Ed.* **42,** 3871–3894 (2003).

31. Covey, T. R., Thomson, B. A. & Schneider, B. B. Atmospheric pressure ion sources. *Mass Spectrom. Rev.* **28,** 870–897 (2009).

32. Wong, S. F., Meng, C. K. & Fenn, J. B. Multiple Charging in Electrospray Ionization of Poly(ethylene glycols). *J. Phys. Chem.* **92,** 546–550 (1988).

33. Rayleigh, Lord. XX. On the equilibrium of liquid conducting masses charged with electricity. *London, Edinburgh, Dublin Philos. Mag. J. Sci.* **14,** 184–186 (1882).

34. Iribarne, J. V. On the evaporation of small ions from charged droplets. *J. Chem. Phys.* **64,** 2287 (1976).

35. Ifa, D. R., Wu, C., Ouyang, Z. & Cooks, R. G. Desorption electrospray ionization and other ambient ionization methods: current progress and preview. *Analyst* **135,** 669–681 (2010).

36. Huang, M.-Z., Yuan, C.-H., Cheng, S.-C., Cho, Y.-T. & Shiea, J. Ambient Ionization Mass Spectrometry. *Annu. Rev. Anal. Chem.* **3,** 43–65 (2010).

37. Harris, G. A., Galhena, A. S. & Fernandez, F. M. Ambient sampling/ionization mass spectrometry: Applications and current trends. *Anal. Chem.* **83,** 4508–4538 (2011).

38. Yao, Z.-P. Characterization of proteins by ambient mass spectrometry. *Mass Spectrom. Rev.* **31,** 437–447 (2012).

39. Wu, C., Dill, A. L., Eberlin, L. S., Cooks, R. G. & Ifa, D. R. Mass spectrometry imaging under ambient conditions. *Mass Spectrom. Rev.* **32,** 218–243 (2013).

40. Weston, D. J. Ambient ionization mass spectrometry: current understanding of mechanistic theory; analytical performance and application areas. *Analyst* **135,** 661–668 (2010).

41. Laskin, J. *et al.* High-Resolution Desorption Electrospray Ionization Mass Spectrometry for Chemical Characterization of Organic Aerosols. *Anal. Chem.* **82,** 2048–2058 (2010).

42.   Bateman, A. P., Nizkorodov, S. A., Laskin, J. & Laskin, A. High-Resolution Electrospray Ionization Mass Spectrometry Analysis of Water-Soluble Organic Aerosols Collected with a Particle into Liquid Sampler. *Anal. Chem.* **82,** 8010–8016 (2010).

43.   Spencer, S. E., Tyler, C. A., Tolocka, M. P. & Glish, G. L. Low-Temperature Plasma Ionization-Mass Spectrometry for the Analysis of Compounds in Organic Aerosol Particles. *Anal. Chem.* **87,** 2249–2254 (2015).

44.   Spencer, S. E., Santiago, B. G. & Glish, G. L. Miniature Flow-Through Low-Temperature Plasma Ionization Source for Ambient Ionization of Gases and Aerosols. *Anal. Chem.* **87,** 11887–11892 (2015).

45.   Doezema, L. A. *et al.* Analysis of secondary organic aerosols in air using extractive electrospray ionization mass spectrometry (EESI-MS). *RSC Adv.* **2,** 2930 (2012).

46.   Gallimore, P. J. & Kalberer, M. Characterizing an extractive electrospray ionization (EESI) source for the online mass spectrometry analysis of organic aerosols. *Environ. Sci. Technol.* **47,** 7324–7331 (2013).

47.   Swanson, K. D., Spencer, S. E. & Glish, G. L. Metal Cationization Extractive Electrospray Ionization Mass Spectrometry of Compounds Containing Multiple Oxygens. *J. Am. Soc. Mass Spectrom.* **28,** 1030–1035 (2017).

48.   Swanson, K. D., Worth, A. L. & Glish, G. L. A coaxial extractive electrospray ionization source. *Anal. Methods* **9,** 4997–5002 (2017).

49.   Swanson, K. D., Worth, A. L. & Glish, G. L. Use of an Open Port Sampling Interface Coupled to Electrospray Ionization for the On-Line Analysis of Organic Aerosol Particles. *J. Am. Soc. Mass Spectrom.* **29,** (2018).

CHAPTER 2: EXPERIMENTAL METHODS AND MATERIALS

2.1.   Materials

All solvents used for electrospray ionization and related solvent-assisted ionization processes were purchased from either Thermo Fisher Scientific (Hampton, NH) or Sigma-Aldrich Corporation (St. Louis, MO) at a purity grade of Optima® unless otherwise noted. The solvents used include water (Fisher, W7-4), acetonitrile (Fisher, A996-4), methanol (Fisher, A454-4), chloroform (Fisher, Certified ACS, C298-500), toluene (Fisher, Certified ACS, T324-500), dichloromethane (Fisher, Certified ACS, D37-500). Acid additives to the electrospray solvent include acetic acid (Fisher, A113-50) and formic acid (Fisher, A117-50). Metal salt additives to the electrospray solvent include lithium acetate dihydrate (Sigma, Reagent-grade, L6883), sodium acetate (Fisher, Certified ACS, S-210), potassium acetate (Sigma, ACS reagent, 236497), and silver trifluoroacetate (Sigma, 98%, T62405). For metal cationization studies, the analytes targeted for analysis include levoglucosan (Carbosynth, 98%, ML06636 or Sigma, 99%, 316555), syringol (Sigma, 99%, D135550), maltol (Sigma, analytical standard, 18299), D-glucose (Sigma, >99.5%, G8270), and syringaldehyde (Sigma, 98%, S7602-5G). Other small molecules analytes used oleic acid (Fluka, >99%, 75090), nicotine (Sigma, >99%, N3876), N-Nitrosonornicotine (TRC, KIT0570), caffeine, (Sigma, ReagentPlus, C0750), methyl-α-D-glucopyranoside (Carbosynth, 98%, MM03961), and methyl- β-D-glucopyranoside (Carbosynth, 98%, MM03162). Isotopically labeled standards that were used include D-glucose-$^{13}C_6$ (Sigma, 99%, 389374), N-Nitrosonornicotine-d_4 (TRC, KIT0765), methanol-d_4 (Sigma, 99.96%, 444758), acetonitrile-d_3 (Sigma, 99.8%, 151807) and deuterium oxide (Sigma, >99.9%, 151882). For analysis of a

peptide in an aerosol, leucine enkephalin (Sigma, >95%, L9133) was used. For the analysis

of protein in an aerosol, lysozyme from chicken egg white (Sigma, >90%, L6876), ubiquitin

from bovine red blood cells (Sigma, BioUltra, U6253), and myoglobin from equine heart

(Sigma, >90%, M1882) were prepared in predominantly methanolic solutions with 10%

added water to enhance solubility. For the analysis of pyrolysis products of biomass,

microcrystalline cellulose (Alfa Aesar, A17730) was used. Sample extracts of lignin and

hemicellulose from tobacco were provided by R.J. Reynolds Tobacco Company (Winston-

Salem, NC). Raw tobacco that was genetically engineered to have low nicotine content was

also provided by R.J. Reynolds Tobacco Company.

2.2.   Aerosol Generation

2.2.1. Constant Output Atomizer (COA)

Two methods of aerosol generation were employed for the characterization of the

ambient sampling devices discussed in this dissertation. A constant output atomizer (Model

3076, TSI Inc., Shoreview, MN) was used to generate a polydisperse aerosol from a

standard solution or a mixture of standards[1]. Generally, the analyte was diluted to 100 ppm

in methanol unless otherwise stated. The aerosol solution was aspirated into the aluminum

block of the constant output atomizer as shown in Figure 2.1 using a flow of gas (nitrogen).

The nitrogen flow was restricted to a 350 µm aperture to increase the linear velocity of the

gas and nebulize the aspirated liquid such that small droplets are carried by the gas to the

dilution tube. Droplets that are too large to be carried by the gas are returned to the

solution reservoir by using the recirculation mode of operation. The pressure prior to the

aperture was maintained at 20 psig. The aperture acts as a conductance limiter and the

pressure inside the solution reservoir was less than 10 psig at all times as ensured by a 10

psig pressure relief valve on the cap of the solution reservoir that actuates whenever the

pressure in the reservoir exceeds 10 psig. Particles enter the dilution tube and are diluted
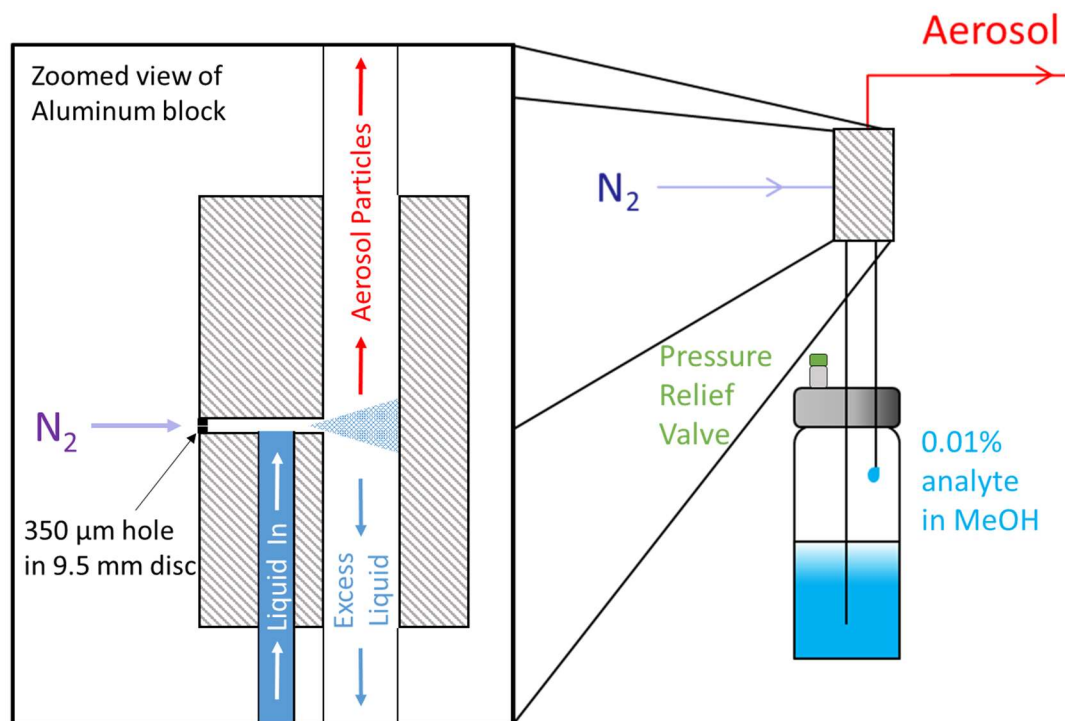
Figure 2.1. Schematic of the constant output atomizer system demonstrating atomization and flows.

by a second nitrogen flow to aid in desolvation. In some cases, the dilution tube was removed for analysis. Particles flow out of the output port of the dilution tube to the desired sampling apparatus with an aerosol gas flow that ranged from 0.5 to 12 L/min.

The solution reservoir intended to be used with the system is a 1L plastic-coated glass bottle designed with unique threads to fit the plastic cap provided with the system. The smallest amount of solution that one can use in the solvent reservoir is determined by the length of the metal tube that extends into solution. When there is insufficient solvent to reach the metal tube, aspiration no longer occurs. In time, the solution will evaporate with continued nitrogen flow. The minimum solution volume that can be used and generate an aerosol is about 200 mL. In an effort to reduce the volume of solution required for aerosol generation, a new plastic cap was designed in AutoCAD and 3D printed. Two designs were considered for 3D printing, a cap to fit a 20 mL scintillation vial and one to fit a 150 mL specimen container as shown in Figure 2.2. The threading was matched to the unique threads of each container so that the cap could be securely twisted onto the desired container. Three holes were printed or drilled into the caps for the pressure relief valve, the metal aspirating tube, and the solution return in recirculation mode. Each hole was printed or drilled to be slightly larger than 0.375" in diameter to accommodate NPT threads. A new metal aspirating tube was made using 0.125" stainless steel tubing, a stainless steel ultra-torr vacuum fitting (Swagelok, SS-8-UT-1-6), and appropriately sized o-rings. The tubing was cut to extend to the bottom of the container in each case and the tubing was secured to the vacuum fitting by sliding the o-rings onto one end of the tubing and inserting the assembly into the NPT end of the vacuum fitting. The vacuum fitting was then secured to the cap by threading onto the central-most hole in the cap to allow unobstructed access into the reservoir. The other two fittings, the solvent return, and

15
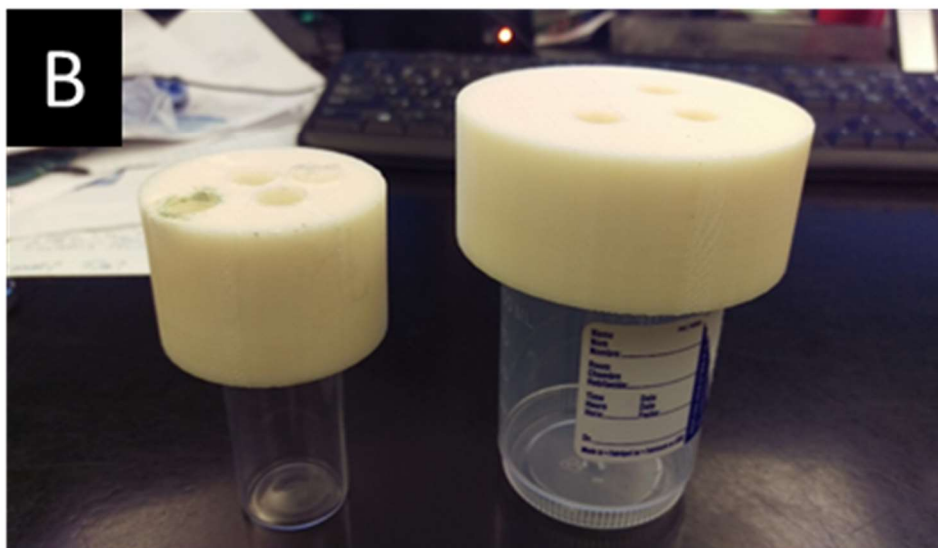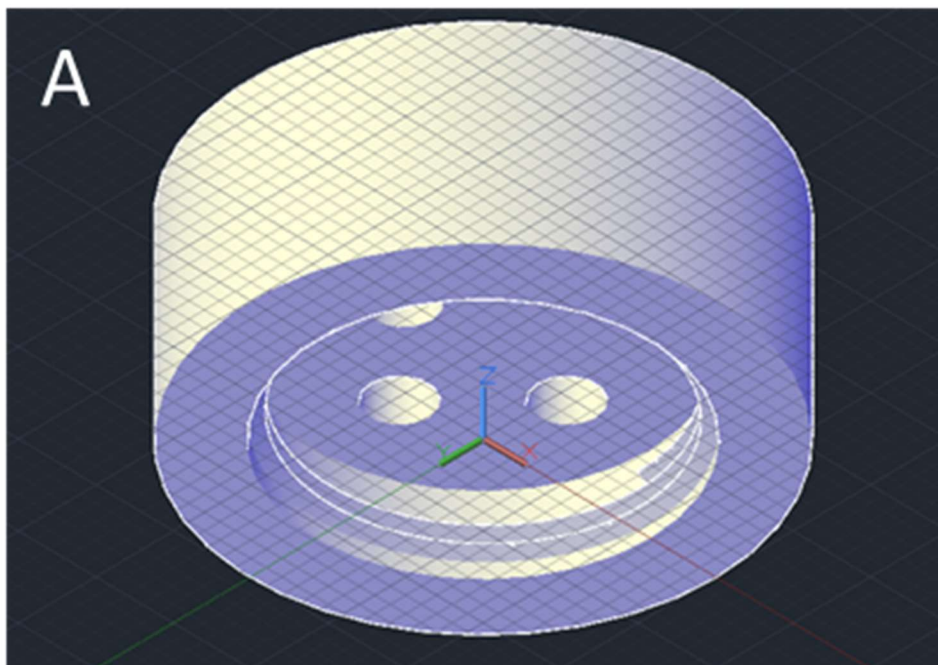
Figure 2.2. A) AutoCAD drawing of a cap to fit a 150 mL specimen vial. B) 3D printed caps attached to a 20 mL scintillation vial and 150 mL specimen vial.

pressure relief valve were transplanted from the original cap as shown in Figure 2.3. Care was taken in the design process to ensure enough room for the plastic tubing that accompanies the solvent return while keeping the holes far enough apart to avoid cracking the print material. When pressurized, the seal created by the scintillation vial threading onto the cap was not very good as methanol aerosol was observed leaking from the connection. One layer of electrical tape placed on the threads of the scintillation vial was enough to create a good seal.

For the 20 mL scintillation vial, a minimum of 5mL was necessary to form an aerosol. In this configuration, the aerosol solution disappeared at a much higher rate than expected. No single source of leakage was observed, instead the outer surface of the 3D printed cap became wet. It appears that even at high print resolution, the pores inherent to 3D printing are too large to create a sufficient seal for prolonged and reproducible aerosol generation.

It was determined that with the existing design, it was not ideal to place three 0.375" holes that fed into a 20 mL scintillation vial, so the design was altered to fit reusable glass media bottles (Fisher, FB-800). The mouth of different sized bottles are the same, which allows for one cap to fit multiple bottles (100 mL, 250 mL, 500 mL, and 1000 mL) with only the replacement of the metal aspiration tube. A cap was machined from Teflon™ and a metal aspiration tube was made using stainless steel tubing as described above for a 100 mL glass media bottle. A female NPT 90° elbow hydraulic hose adapter was used to connect the pressure relief valve to the cap to more easily connect each fitting. A minimum of about 20 mL solution is necessary to form an aerosol when using the 100 mL glass media bottle.

Figure 2.3. COA with 3D printed cap on 20 mL scintillation vial in operation.

The settings for the COA were studied and optimized using a scanning mobility particle sizer system (described in Section 2.3), and the results are displayed in Figure 2.4. The most crucial settings for the COA system are the pressure at the atomizer (COA pressure) and the flow rate of the dilution flow. The COA pressure and the solvent reservoir pressure that is regulated by the pressure relief valve are different due to a pressure drop across the system. A representative size distribution of oleic acid dissolved in methanol is shown in Figure 2.4a. The aerosol is polydisperse, but normally distributed around a mean diameter of 51 nm at 5 standard cubic feet per minute (SCFM) and 30 psig COA pressure. The green markers in Figure 2.4b-f represent 3 SCFM dilution flow and the blue markers represent 5 SCFM dilution flow. No significant difference was observed when the dilution flow was changed in this study. Shown in Figure 2.4b, the total aerosol concentration was observed to increase linearly as the COA pressure was increased. At COA pressures above 30 psig, the pressure relief valve on the solvent reservoir periodically released, which changed the pressure in the system. For this reason, no COA pressures above 30 psig were studied. Particle statistics of mean, geometric mean, median, and mode diameters at different COA pressures are shown in Figures 2.5c-f. Generally, the mean, geometric mean, and median diameters decreased as COA pressure increased, which suggests that smaller droplets are created by the larger linear velocity at the atomizer aperture. If smaller droplets are formed from the same volume, more droplets are formed.

2.2.2. Pyroprobe

As shown in Figure 2.5, A Pyroprobe 5250 (CDS, Oxford, PA) with an autosampler was used to generate an aerosol from the pyrolysis of biomass[2]. Pyrolysis is the thermal degradation of a material in an oxygen-free environment. Prior to sample introduction, a quartz filler rod (CDS, 10A1-3016L) is loaded into a quartz sample tube (CDS, 10A1-3015)
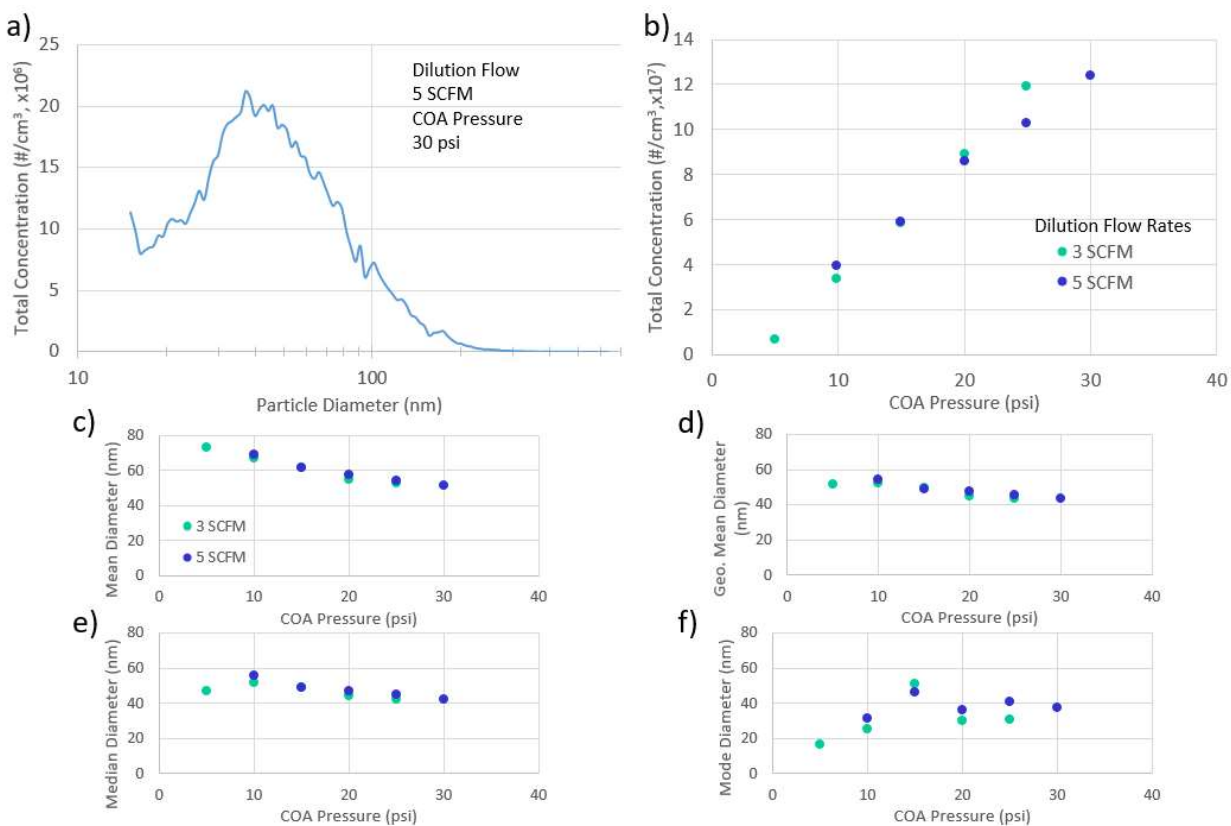
Figure 2.4. Results from the Optimization of COA parameters. a) Size distribution of the aerosol particles as it relates to aerosol concentration. b) Comparison of COA pressure and dilution flow rates in terms of aerosol concentration. Particle statistics shown include c) mean diameter, d) geometric mean diameter, e) median diameter, and f) mode diameter as a function of both COA pressure and dilution flow rate.
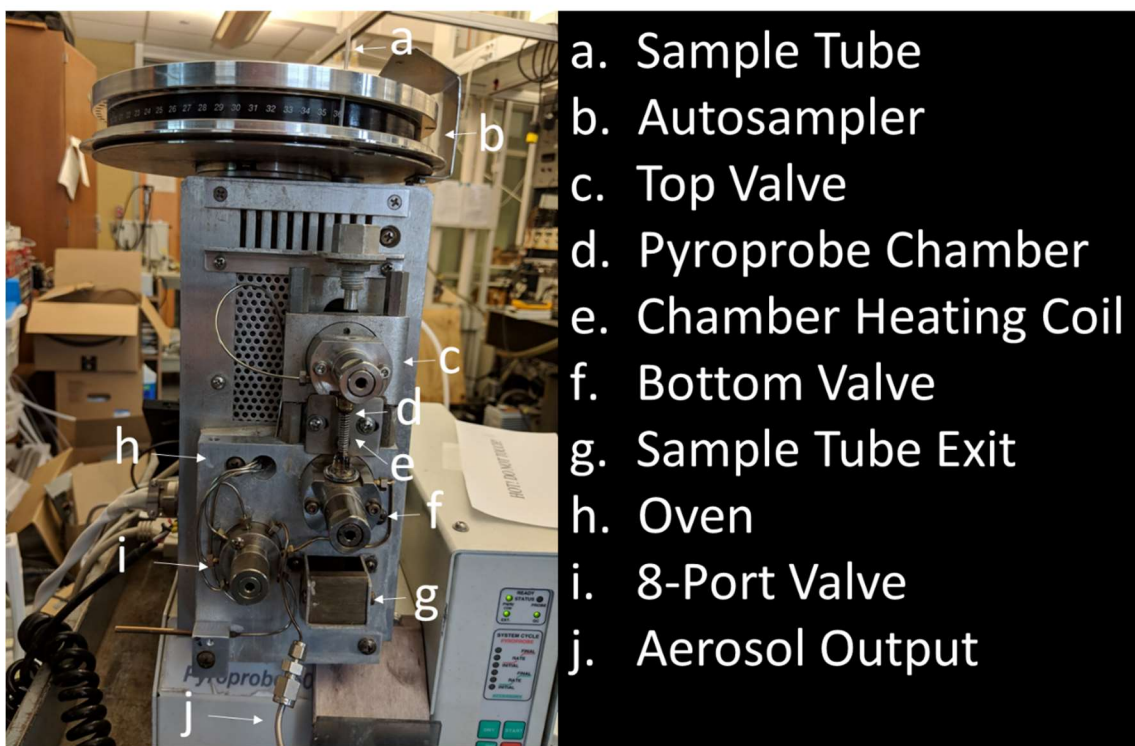
Figure 2.5. Picture of the Pyroprobe model 5250 with labeled components.

to provide a surface for a solid sample to rest inside the tube while allowing some flow through the sample. A sample is then loaded into the tube ranging from 5-20 mg of material. The filled sample tube is placed into the autosampler of the Pyroprobe 5250 shown in Figure 2.5. The valve oven is held at 300 °C at all times. This oven (Figure 2.5h), keeps the bottom valve, 8-port valve and tubing warm to avoid condensation of the aerosol particles onto surfaces. The autosampler (Figure 2.5b) actuates the sample tube (Figure 2.5a) to be in line with the pyrolysis chamber (Figure 2.5e), and the sample tube is dropped onto a closed top valve (Figure 2.5c). The top valve is then actuated into an open position, causing the sample tube to drop into the chamber (Figure 2.5d) onto a closed bottom valve (Figure 2.5f). The top valve then closes, sealing the sample tube into the pyrolysis chamber. The 8-port valve (Figure 2.5i) actuates to flow pure nitrogen through the pyrolysis chamber. A current is then applied to the chamber heating coil (Figure 2.5e) to heat the pyrolysis chamber. A typical heating program for most samples included in this work is as follows. The sample is equilibrated in the chamber for 10 seconds with the heating coil at 25 °C. The sample is then heated at a rate of 10 °C/s to a temperature of 650 °C and held at that temperature for 5 minutes. These values were typically used for analysis, but other settings were studied and the results are discussed below. At the end of the heating period, the bottom valve is actuated and the sample tube is ejected through the bottom chute (Figure 2.5g).

For most of the work presented in this dissertation, the system was plumbed as described in Figure 2.6. While heating the sample, the 8-port valve operates under position 1. Pure nitrogen flows into the 5th port of the 8-port valve and into the bottom valve. The gas flows upwards through the sample (opposite from the direction the sample tube is packed) and out the top valve, carrying any aerosol generated. The aerosol is then directed to the output. When the sample is being loaded, the 8-port valve operates under Position 2
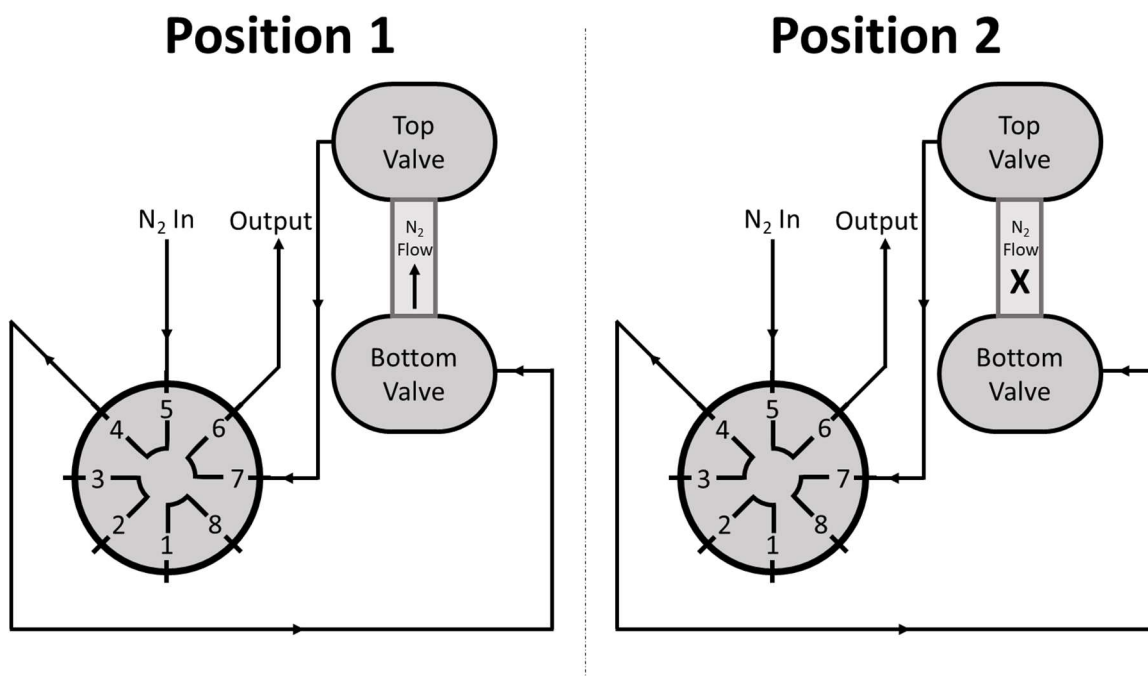
Figure 2.6. Schematic of the valve operation in the Pyroprobe model 5250 with arrows indicating the direction of aerosol/gas flow.

where there is no flow through the pyrolysis chamber. Pure nitrogen flows into the 5th port of the 8-port valve directly to the output. The plumbing in Figure 2.6 is not the manufacturer suggested mode of operation. The instrument was modified to this mode of operation for the purpose of improved signal intensity upon sampling of the generated aerosol[3]. The problems created by using this mode of operation include increased clogging, instability of the sample tube, and frequent breakage of sample tubes. The clogging observed has been attributed to two sources. The first source of clogging is due to the direction of gas flow in the pyrolysis chamber in position 1. Large sample particles and aerosol are easily blown out of the sample tube to the outlet of the top valve. The second source of clogging was condensation of particles inside the top valve and the following tubing due to a decrease in temperature. The top valve is not directly heated by the oven in the same way as the bottom valve, thus particles are more likely to settle and condense onto cooler surfaces. Clogging was frequently observed at the output of the top valve and in the tube connecting the top valve to the 8-port valve, which was only solved by flowing solvent in the opposite direction to the gas flow to dislodge the clog.

During heating, the gas flow actually caused the sample tube to levitate in the chamber. Interestingly, this often caused a spike in signal followed by a rapid decrease in signal. The increase in signal is most likely due to a burst of sample leaving the sample tube and depositing into the tubing on the outlet of the top valve. The rapid decrease in signal is likely due to the top of the sample tube resting on the top valve, preventing any pyrolyzed sample from leaving the tube after the first burst. The gas flow was often adjusted to have the sample tube levitate in between the top and bottom valves. The third problem that the incorrect mode of operation created was the coating of sample onto inside walls of the chamber and valves, making these surfaces sticky. Often, the sample tube would touch one of these walls either as the sample tube dropped into the chamber or as it

dropped out of the chamber. If the sample tube stopped falling inside either one of the valves, the valve would actuate based upon a timer and crush the sample tube. A crushed tube requires extensive cleaning of the valves and pyrolysis chamber to remove broken quartz pieces. Further, when the 8-port valve was in position 2, no sample was loaded into the probe, but no gas flowed through the chamber. Any sample material that had blown outside the tube would remain in the chamber, causing buildup of char inside the chamber which led to an ongoing need to clean the system.

These problems were not solved until the Pyroprobe was returned to manufacturer specifications as shown in Figure 2.7. In this mode, the flow of gas in the chamber is downward, in the direction of the sample packing, which leads to less sample dispersement outside the sample tube and the sample tube no longer levitates with the gas flow. Further, the manufacturer suggested mode of operation includes a purge gas flow (also pure nitrogen) that flows through the pyrolysis chamber when no sample tube is present. Thus, there was gas flow through the chamber at all times. This mode resulted in less clogging, less cleaning, and fewer sample tubes were broken upon entry into the pyrolysis chamber. A flow meter and pressure gauge were added in-line with the inlet nitrogen flow to maintain consistency in those parameters. No significant reduction in signal intensity was observed when sampling from the aerosol generated from pyrolysis of sample material using this improved mode of operation. As expected, this improved method of operation resulted in more consistent pyrolysis between samples and the lowered maintenance allowed the use of the autosampler for higher throughput analyses.

The settings for the Pyroprobe were studied and optimized using one of the sampling methods that will be described in Chapter 4. It is important to note that the temperature applied to the heating coil of the Pyroprobe does not accurately reflect the temperature of the sample inside the sample tube due to the constant flow of relatively cool nitrogen
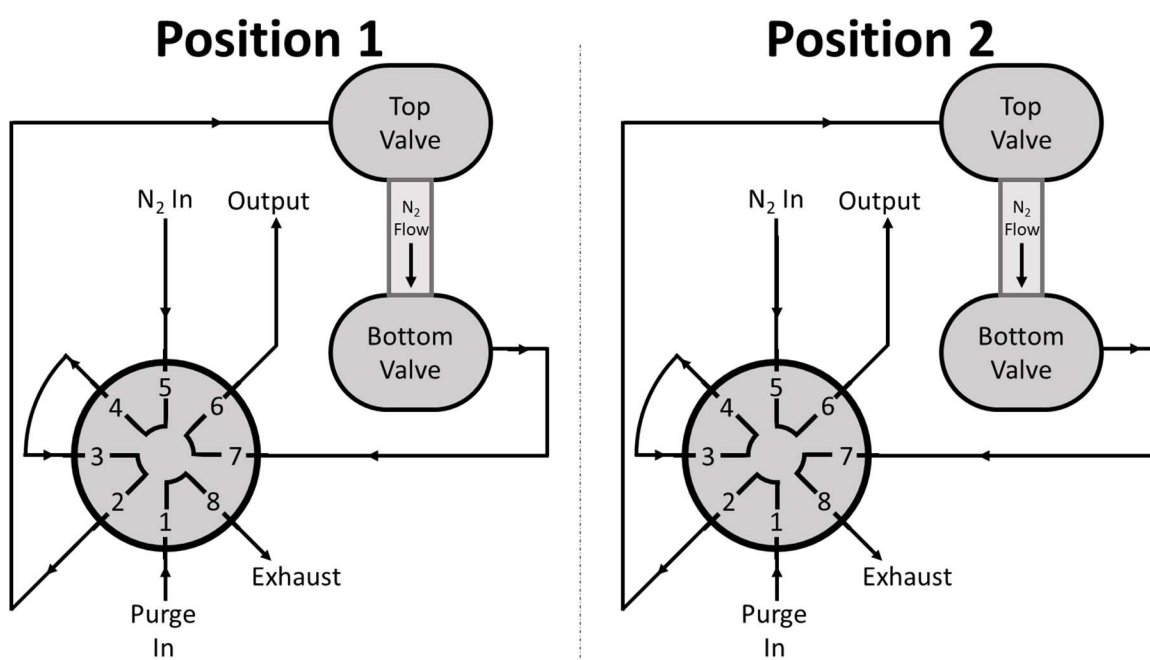
Figure 2.7. Schematic of the manufacturer suggested mode of operation of the Pyroprobe model 5250.

through the sample. Nonetheless, when a slow ramp rate (10 °C/s) is used to observe the pyrolysis of a sample of cellulose, the sample inside the tube changes color from white to brown at approximately 550 °C, indicated the onset of pyrolysis. Previous literature suggests 650 °C as the average temperature inside the pyrolysis region of a burning cigarette, so 650 °C was the setting used for most experiments. Multiple temperatures were used to examine the effect of temperature setting on the pyrolysis of cellulose as shown in Figure 2.8. The total ion chronogram (TIC) over pyrolysis runs at temperatures of 600, 700, 800, 900, and 1000 °C suggest there is no difference in the total signal observed as a function of temperature. Further, the mass spectrum obtained from each temperature setting is similar as displayed in Figure 2.9. The same peaks are observed in each spectrum and the absolute intensity of each peak does not change much as a function of temperature.

The setting for ramp rate in the heating program during pyrolysis was also studied by varying the ramp rate from 1 °C/s to 999 °C/s to a temperature of 650 °C. As shown in Figure 2.10 for 1 °C/s, pyrolysis occurs at 9 minutes and continues as the temperature reaches the maximum. For all others, pyrolysis occurs at approximately 0.5 minutes. This is evidence that the heating rate setting is the heating rate of the heater coil, not the sample. The heating rate of the sample is also a function of the gas flow rate through the system that acts to cool the sample as the heater coil warms the sample. The spectrum observed for each ramp rate was nearly identical. The area under the pyrolysis "peak" for the 1 °C/s ramp rate from 9 minutes to approximately 16 minutes is much larger than the area under any of the other peaks. This suggests that more aerosol is sampled from a single pyrolysis run at slow ramp rates. This is a way one could do an experiment that requires the collection of signal for a long amount of time. Theoretically, the ramp rate could be reduced to 0.01 °C/s, but this was not tested.
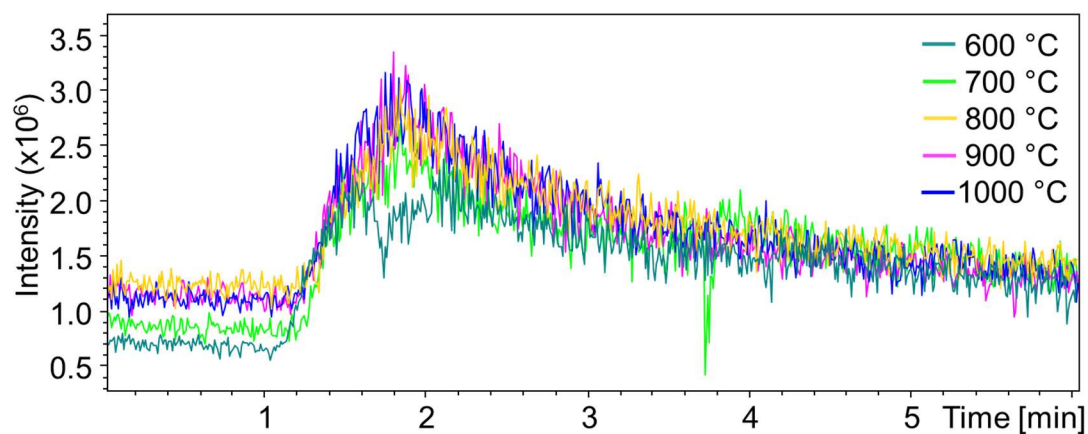
Figure 2.8. Time-resolved pyrolysis profiles of cellulose at varying temperatures.
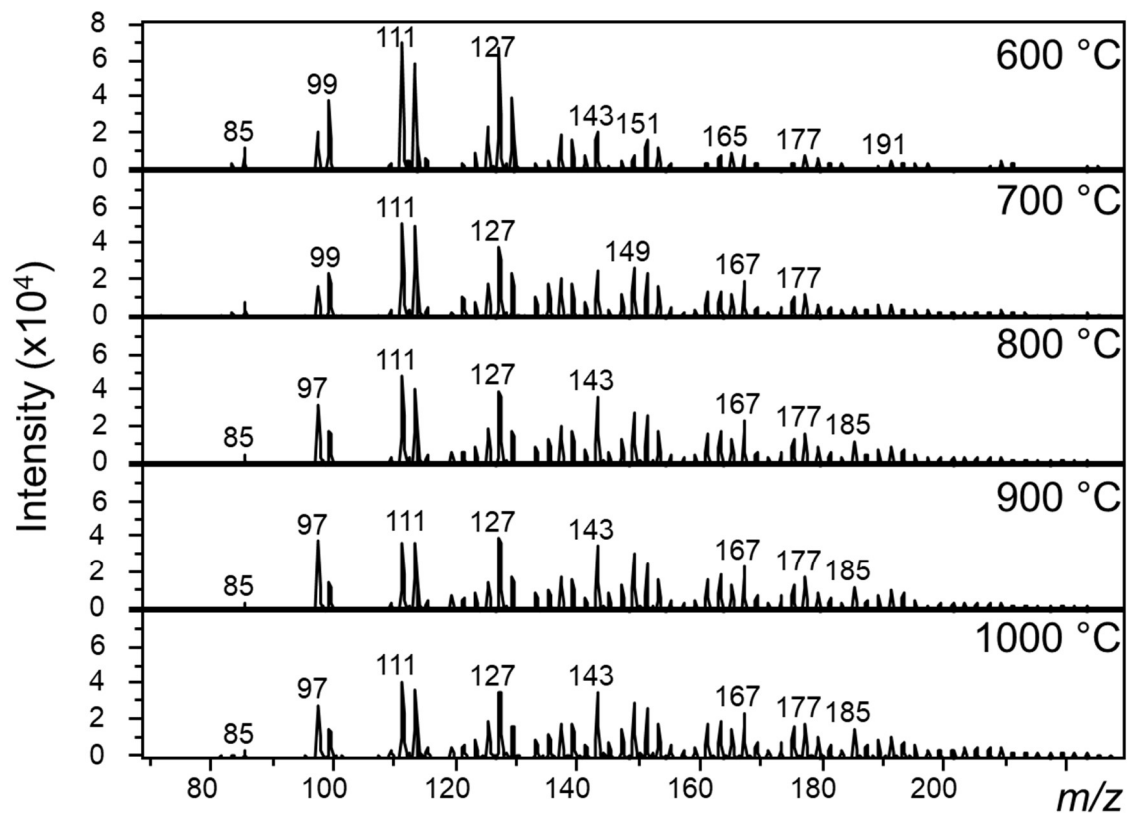
Figure 2.9. Mass spectra of cellulose pyrolysis at varying temperatures.
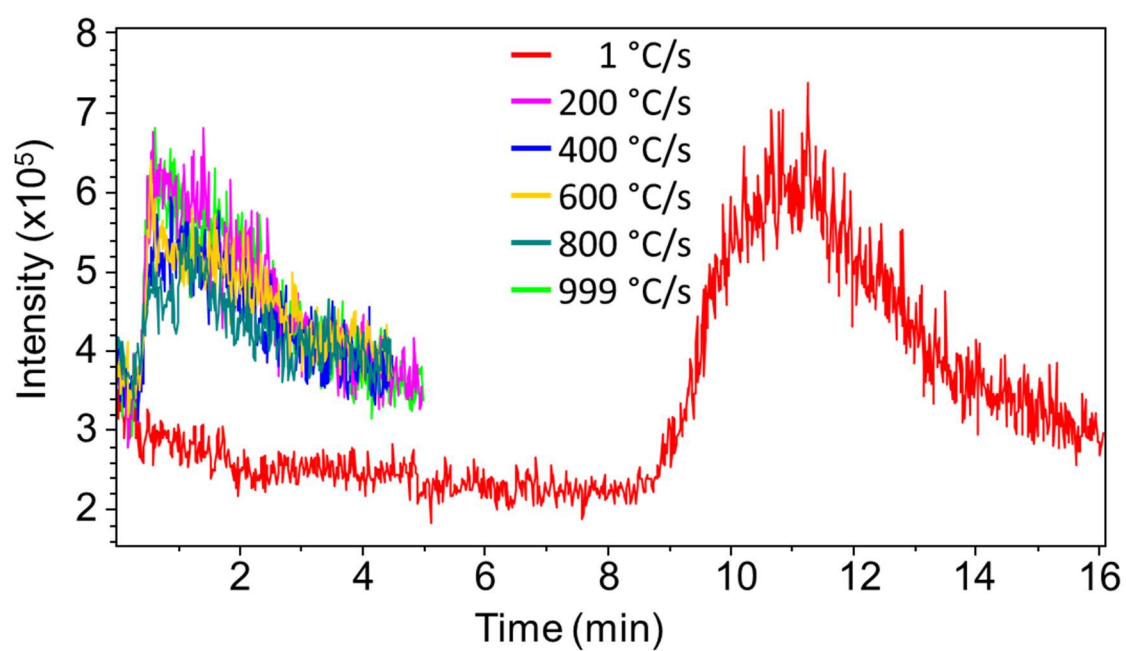
Figure 2.10. Time-resolved pyrolysis profiles of cellulose at varying temperature ramp rates.

2.3.   Aerosol Particle Size Measurement

The scanning mobility particle sizing (SMPS) system used includes a differential mobility analyzer (Model 3080, TSI Inc., Shoreview, MN) and a condensation particle counter (Model 3022A, TSI Inc. Shoreview, MN)[4,5]. A polydisperse aerosol was directed to the inlet of the differential mobility analyzer (DMA) with a flow rate not exceeding 1 L/min. If the flow of the gas carrying the aerosol particles was greater than 1 L/min, a Swagelok tee with a gate valve was used to divert a portion of the flow. The particles are uniformly charged then separated in size by an electric field. The sized particles are then sent to the condensation particle counter (CPC) for detection. In the CPC, particles are sent through a condensation chamber where a saturated t-butyl alcohol vapor condenses onto the particles to increase the particle diameter for measurement by light scattering. The number density of particles is correlated in time to the DMA voltage to generate a plot of particle number density versus particle diameter. Particle statistics can then be determined using the Aerosol Instrument Manager (AIM) software by TSI Inc[6]. The version of the software used was AIM 9.0.0.0.

2.4.   Mass Spectrometry

Although SMPS systems are useful for particle statistics, a mass spectrometer is the preferred detection method for aerosol analysis due to the chemical information obtained during mass analysis. The chemical information that mass spectrometry can yield includes mass, charge, structural information, and affinity for protons or metal cations. For mass analysis, compounds must be in the gas phase and charged. For liquid samples, this is most often accomplished using electrospray ionization (ESI) as described in Chapter 1. The ambient sampling and ionization techniques employed in this dissertation are all closely related to ESI and often ESI is used for comparison. Each instrument used was equipped with a standard commercial ESI source. The following instruments were employed for the

purposes of ESI or related techniques: Esquire 3000 Plus quadrupole ion trap mass spectrometer (Bruker, Billerica, MA) equipped with an Apollo I ESI source (Agilent, Santa Clara, CA), HCT-Ultra quadrupole ion trap mass spectrometer (Bruker, Billerica, MA) equipped with an Apollo I ESI source (Agilent, Santa Clara, CA), LTQ-FT linear ion trap and fourier transform – ion cyclotron resonance (FT-ICR) mass spectrometer (Thermo Scientific, Waltham, MA) equipped with an Ion Max ESI source (Thermo Scientific, IQLAAEGABBFACTMAJI).

2.5.   Ionization and Sampling

2.5.1   Electrospray Ionization

For the Esquire 3000 and HCT-Ultra mass spectrometers, the nebulizer used was either an Agilent (G1946-67098) or Bruker (A5940) nebulizer, both of which have nearly the same form factor for the Apollo I ESI source. For solvent delivery, a single-syringe infusion pump was used with various Hamilton gastight syringes. A schematic of an ESI nebulizer is shown in Figure 2.11. The solvent is delivered through a central capillary and the nebulizing gas (nitrogen) is delivered through an outer capillary to form a nebulized spray at the electrospray tip. More detail about the design of the nebulizer will be discussed in Chapter 4. The nebulizer is inserted into the Apollo I source housing and secured. A drying gas (nitrogen) is flowed around the inlet capillary of the mass spectrometer to heat the inlet capillary and aid in desolvation. The setting for the nebulizing gas pressure was 10 psig for most instances. This gas is heated prior to introduction into the ion source for interaction with charged droplets. In most cases, the dry gas flow is set to 5 L/min at 300 °C. After equilibration, the temperature of the inlet capillary, around which the drying gas flows,
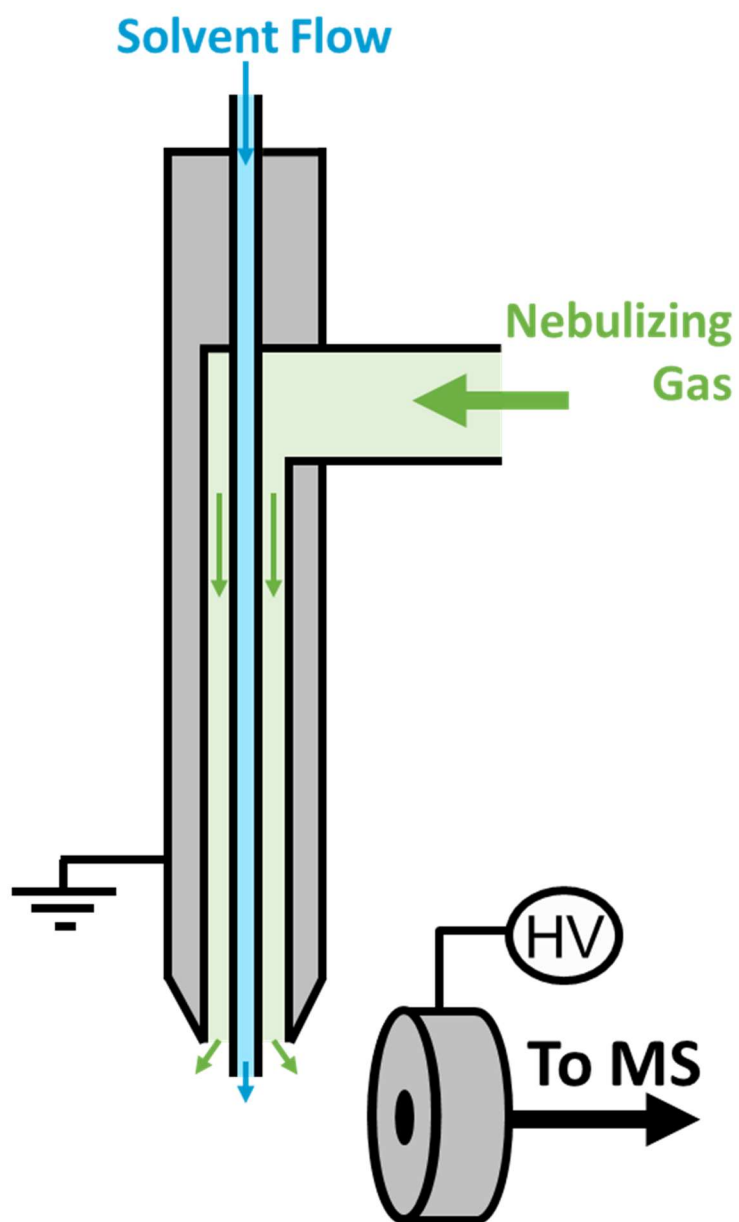
Figure 2.11. Schematic of an ESI nebulizer.

was measured to be 90 °C using a Klein Tool MM400 and a bead wire type K temperature probe. For the Bruker instruments, the high voltage (HV) is applied to the inlet of the mass spectrometer while the nebulizer is held at ground. In positive mode, the inlet is held at a negative potential to attract ions of a positive charge. In most cases, this inlet capillary voltage was set to -5 kV for positive mode. In negative mode, the inlet is held at a positive potential to attract ions of a negative charge. In most cases, this inlet capillary voltage was set to +4 kV for negative mode. For ESI, the analyte was dissolved in a 1:1 mixture of methanol and water with acid (acetic or formic) added at 1% by volume unless otherwise noted.

2.5.2   Extractive Electrospray Ionization (EESI)

The ambient ionization and ambient sampling techniques used in the research discussed in this dissertation are all variants on ESI. Extractive electrospray ionization occurs when a plume of charged droplets interact with airborne droplets or aerosol particles[7,8]. For analysis of an aerosol, this is accomplished by intersecting a stream of analyte-containing aerosol particles with an electrospray plume to generate analyte ions[9–11]. A schematic of this interaction is shown in Figure 2.12. The source housing on the instrument must be removed to have control over this interaction by choosing the angle of interaction and the distance of the outlet of the aerosol generator to the electrospray nebulizer and the inlet to the mass spectrometer. A picture of the instrument with the source housing in place is shown in Figure 2.13A. For custom arrangement of the ESI nebulizer and aerosol outlet tube, the source housing can be opened and lifted off the hinge as shown in Figure 2.13B. A ring stand can then be used with clamps to adjust the position and relative angles of the ESI nebulizer and the aerosol outlet tube. In most cases, with the
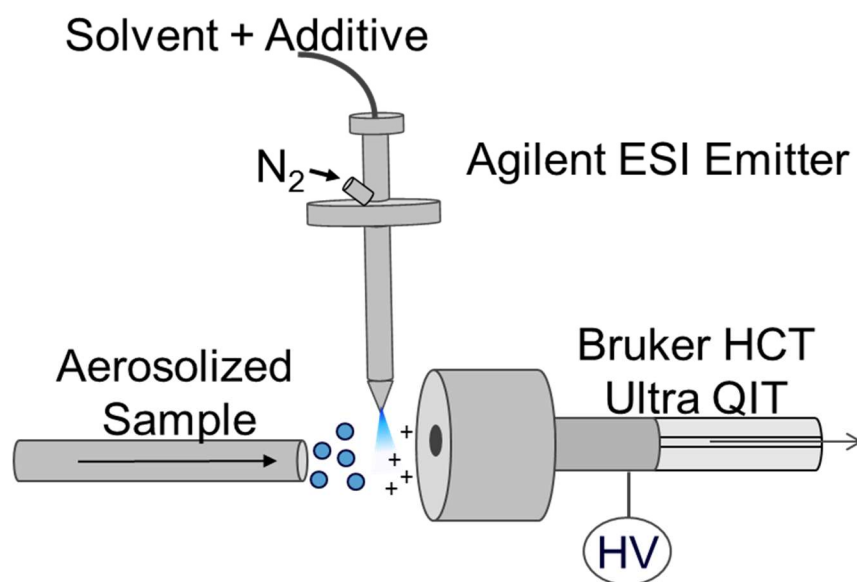
Figure 2.12. Schematic of EESI setup.
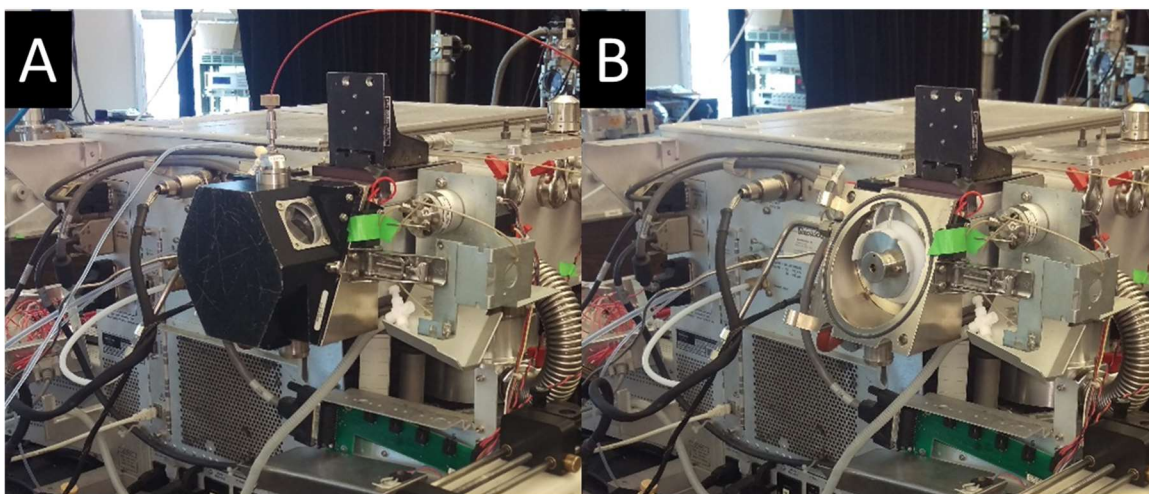
Figure 2.13. Picture of the Esquire 3000 Plus mass spectrometer A) with the source housing intact and B) with the source housing removed.
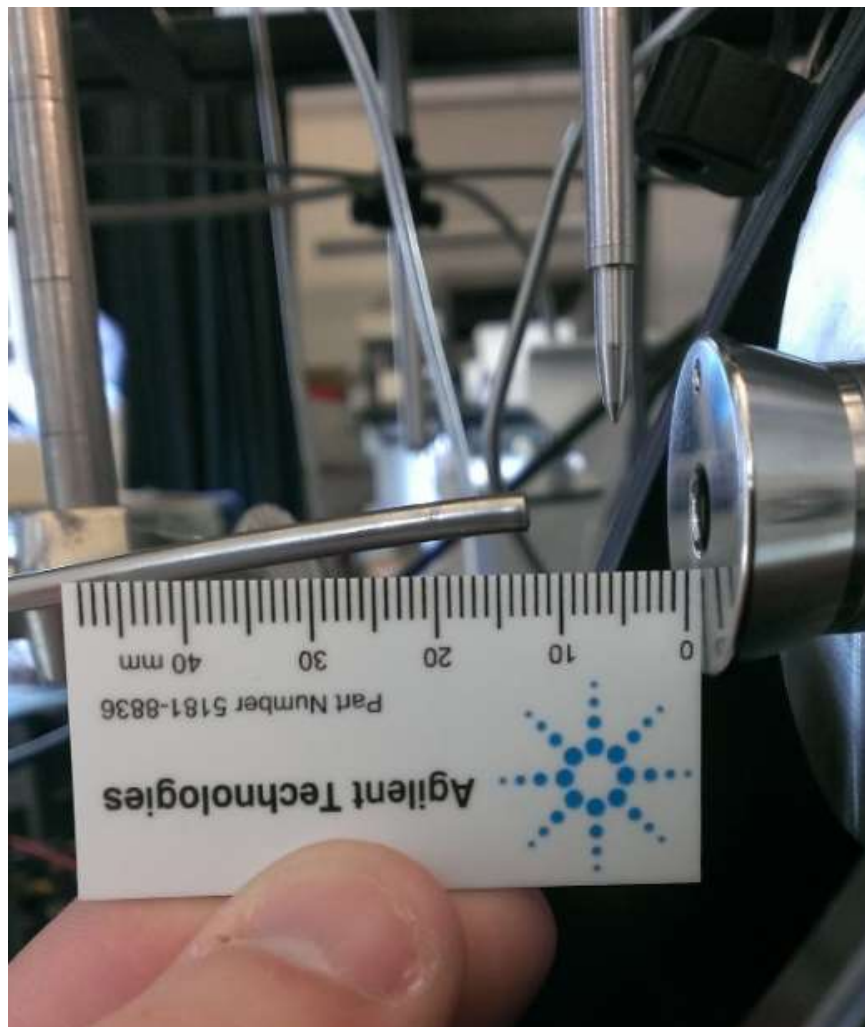
Figure 2.14. Picture demonstrating the arrangement of EESI in the standard configuration.

exception of the data shown in Chapter 3, the arrangement shown in Figure 2.14 was used. The emitter is placed 7 mm away from the inlet to the mass spectrometer, orthogonal to the inlet capillary, with the tip of the nebulizer situated just above the inner ring of the spray shield. The aerosol outlet tube is placed on-axis with the inlet capillary at a distance of 10-15 mm. Just as in conventional ESI described above, the potential is applied to the inlet capillary. Because the source housing was removed, the electrospray nebulizer is no longer held at ground in this configuration, thus it must be manually grounded using a grounding strap attached from the body of the nebulizer to a grounded point on the mass spectrometer. The electrospray solvent used in most cases was a 1:1 mixture of methanol and water with acid (acetic or formic) added at 1% by volume. This was altered in some studies to change the selectivity of the extraction by using different ratios, different solvents or different additives.

2.5.3   Coaxial Extractive Electrospray Ionization (Coaxial EESI)

To address the challenges associated with EESI, a new device was developed to simplify the setup and improve upon the operation of EESI in the standard configuration[12]. This device is used with the source housing intact and operation is similar to ESI. The absolute magnitude of the electrospray voltage in both positive and negative modes was increased by 1000 V due to the increased distance from the tip of the coaxial EESI nebulizer to the inlet capillary. Further details, including the construction and optimization of coaxial EESI parameters may be found in Chapter 4.

2.5.4   Open Port Sampling (OPSI)

An ambient aerosol sampling technique was also developed to complement the analysis of aerosols using EESI[13]. This design uses an open solvent interface to sample from a given aerosol and deliver the dissolved compounds to an ionization source by aspiration. Although either ESI or atmospheric pressure chemical ionization may be used with OPSI, most of the

results presented in this dissertation used ESI. Only initial testing for the use OPSI with

APCI for the analysis of aerosols was done, but the use of OPSI-APCI for the analysis of

other sample types is described elsewhere[14–16]. The OPSI-ESI device is used with the source

housing intact. The construction and operation of the device is described in detail in

Chapter 5.

REFERENCES

1. TSI. Model 3076 Constant Output Atomizer Instruction Manual. (2005).

2. CDS Analytical. Pyroprobe 5000 Manual. (2012).

3. Spencer, S. E. Development of an Aerosol Mass Spectrometry System for the Analysis of the Composition of Aerosol Particles in Real Time. *Ph. D. Dissertation* (University of North Carolina, 2015).

4. TSI. Series 3080 Electrostatic Classifiers Manual. (2008).

5. TSI. Model 3022A Condensation Particle Counter Manual. (2002).

6. TSI. Aerosol Instrument Manager Software Manual. (2005).

7. Chen, H., Venter, A. & Cooks, R. G. Extractive electrospray ionization for direct analysis of undiluted urine, milk and other complex mixtures without sample preparation. *Chem. Commun.* **19,** 2042–2044 (2006).

8. Law, W. S. *et al.* On the Mechanism of Extractive Electrospray Ionization. *Anal. Chem.* **82,** 4494–4500 (2010).

9. Doezema, L. A. *et al.* Analysis of secondary organic aerosols in air using extractive electrospray ionization mass spectrometry (EESI-MS). *RSC Adv.* **2,** 2930 (2012).

10. Gallimore, P. J. & Kalberer, M. Characterizing an extractive electrospray ionization (EESI) source for the online mass spectrometry analysis of organic aerosols. *Environ. Sci. Technol.* **47,** 7324–7331 (2013).

11. Swanson, K. D., Spencer, S. E. & Glish, G. L. Metal Cationization Extractive Electrospray Ionization Mass Spectrometry of Compounds Containing Multiple Oxygens. *J. Am. Soc. Mass Spectrom.* **28,** 1030–1035 (2017).

12. Swanson, K. D., Worth, A. L. & Glish, G. L. A coaxial extractive electrospray ionization source. *Anal. Methods* **9,** 4997–5002 (2017).

13. Swanson, K. D., Worth, A. L. & Glish, G. L. Use of an Open Port Sampling Interface Coupled to Electrospray Ionization for the On-Line Analysis of Organic Aerosol Particles. *J. Am. Soc. Mass Spectrom.* **29,** (2018).

14. Van Berkel, G. J. & Kertesz, V. An open port sampling interface for liquid introduction atmospheric pressure ionization mass spectrometry. *Rapid Commun. Mass Spectrom.* **29,** 1749–1756 (2015).

15. Van Berkel, G. J. & Kertesz, V. Rapid sample classification using an open port sampling interface coupled with liquid introduction atmospheric pressure ionization mass spectrometry. *Rapid Commun. Mass Spectrom.* **31,** 281–291 (2017).

16.   Van Berkel, G. J. *et al.* Combined Falling Drop/Open Port Sampling Interface System for Automated Flow Injection Mass Spectrometry. *Anal. Chem.* **89,** 12578–12586 (2017).

CHAPTER 3: EXTRACTIVE ELECTROSPRAY IONIZATION

3.1.   Introduction

Ambient ionization is a family of techniques that requires very few or no sample preparation steps and has become an important area of research in analytical applications using mass spectrometry[1–5]. Extractive electrospray ionization (EESI) is an ambient ionization technique in which a solvent is electrosprayed through a nebulized sample[6–13]. EESI is simple in design and can be implemented with most commercial electrospray ionization (ESI) sources[8]. It has also been shown that EESI can be used to sample from aerosols in real time as an alternative to aerosol collection, extraction, and derivatization followed by lengthy analysis by gas chromatography-mass spectrometry (GC-MS) or liquid chromatography-mass spectrometry (LC-MS)[14,15]. One area of interest in our lab is characterization of aerosols formed in the pyrolysis of biomass[16,17].

EESI is similar to ESI because the electrospray solvent composition is a primary factor in determining ionization efficiency[18]. Compounds in the nebulized sample are ionized and typically detected as [M+H]$^+$. Although a number of studies of ESI have focused on the influence of solvent composition[19–22], only a few studies have focused on the influence of

solvent composition in EESI[18,23]. In previous studies using EESI, the electrospray solvent

typically contains a proton source (often formic or acetic acid)[2].

3.2. Metal Cationization Extractive Electrospray Ionization Mass Spectrometry

3.2.1. Introduction to Metal Cationization EESI

Trace sodium is adventitious in electrosprayed samples and can increase the

number of peaks in mass spectra and decrease sensitivity due to formation of $[M+Na]^+$ in

addition to the normal $[M+H]^+$. The source of sodium in the sample is typically attributed to

salts leached from glassware or impurities in analytical grade solvents[24]. To reduce cation

formation, on-line desalting methods have been used[25]. However, the addition of metal salts

to the electrospray solvent in ESI has been shown to enhance sensitivity in some cases,

including the ionization of peptides[26], ethoxylate surfactants[27], polyether ionophores[28], and

carbohydrates[29]. In ESI, large carbohydrates are most efficiently ionized by large metals

such as cesium; however, smaller carbohydrates such as sugars are more efficiently ionized

by smaller metals, such as lithium[30]. One example of this effect is the analysis of

levoglucosan, a glucose derivative. Levoglucosan is a pyrolysis product of carbohydrate

polymers such as cellulose and is a tracer of biomass burning in atmospheric particles[31]. In

a solvent mixture of water, methanol, and acetic acid, levoglucosan is observed only as

$[M+Na]^+$ in ESI-MS. However, EESI-MS of levoglucosan using the same solvent generates

$[M+H]^+$ and no sodium cationized molecules. This result motivated studying the addition of

metal salts to the electrospray solvent to induce metal cationization in EESI. Because

carbonyl and oxy compounds are most commonly observed to be adventitiously metal

cationized in ESI, lithium, sodium, potassium and silver salts were added to the EESI

electrospray solvent separately to evaluate the ability to metal cationize some compounds of

that type.

After ionizing by EESI, tandem mass spectrometry (MS/MS) of each metal cationized compound was investigated as a method to obtain more information on the structure of compounds than can be obtained from MS/MS of the protonated species. Metal cationization has been used to obtain structural information from collision induced dissociation (CID) in the study of ginsenosides[32], polyglycols[33], monosaccharides[34], disaccharides[35], and polysaccharides[36].

3.2.2. Unique Experimental Details

A constant output atomizer was used to generate aerosol from a solution of 100 ppm of analyte in methanol using nitrogen gas. The analytes used for the evaluation of metal cationization in EESI-MS were levoglucosan, syringol, maltol, glucose and syringaldehyde. The gas flow rate carrying the aerosol to the EESI source was approximately 12 L/min. Mass spectrometric measurements were carried out using an Esquire 3000 ion trap mass spectrometer. The source housing on the Apollo I ESI source was removed and the ESI nebulizer was affixed orthogonally to the inlet axis of the mass spectrometer, 7 mm from the spray shield as shown in Figure 3.1. The output of the constant output atomizer was positioned 8 mm from the inlet of the mass spectrometer at approximately 135° with respect to both the inlet of the mass spectrometer and the ESI nebulizer. This was empirically found to give the most intense signal, but a systematic characterization of angles and distances was not performed at this time. The nebulization gas pressure for the electrospray solvent was 1260 Torr, dry gas temperature was set to 300 °C, and dry gas flow rate was 3 L/min. The syringe and ESI nebulizer were rinsed thoroughly with methanol before changing the EESI solvent. Solvent flow rate through the ESI nebulizer was 2 µL/min.
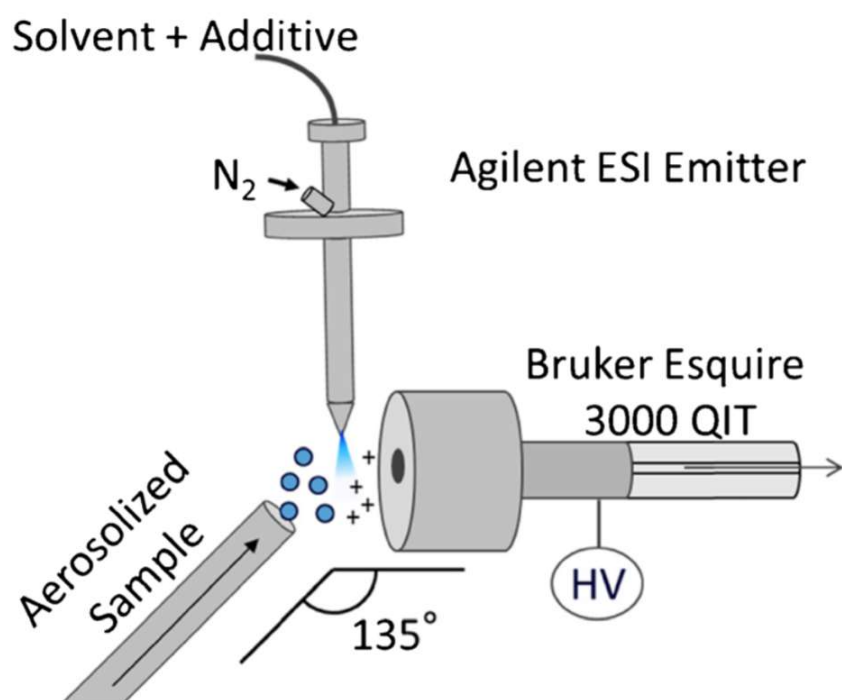
Figure 3.1. Schematic of experimental setup

The electrospray solvent was a 1:1 mixture of water and methanol (v/v) prior to inclusion of an additive. For EESI with an acid, the additive used was acetic acid (Fisher, Hampton, NH) at a concentration of 175 mM. To study interactions with metals, sodium acetate, lithium acetate, potassium acetate, and silver trifluoroacetate were added to the electrospray solvent at concentrations ranging from 0.5 mM to 25 mM.

3.2.3. Metal Cationization EESI of Levoglucosan

Metal salts were individually added to the electrospray solvent for EESI-MS to ionize aerosolized levoglucosan and compare signal intensities. Protonated levoglucosan is observed in the mass spectrum when acetic acid is used as an additive with no trace of sodiated levoglucosan. When a metal salt was used as the additive for EESI, the corresponding metal cationized levoglucosan was observed, with no protonated molecule, in the mass spectrum. The intensity of each metal cationized molecule observed was compared to the ion intensity of the protonated molecule measured when acetic acid was used as an additive (n=4). The same concentration of levoglucosan was used in the constant output atomizer for all experiments, thus any increase in signal intensity is related to an increase in sensitivity. When lithium was used as an additive, the signal for [levoglucosan+Li]$^+$ (m/z 169) was 4.3 ± 0.9 times greater than the signal for [levoglucosan+H]$^+$ (m/z 163) when acetic acid was used as an additive. Similarly, the signal for [levoglucosan+Na]$^+$ (m/z 185) was 3.0 ± 0.7 times greater when sodium was used as an additive, and the summed signal for [levoglucosan+Ag]$^+$ (m/z's 269 and 271) was 1.5 ± 0.6 times greater when silver was used as an additive. Conversely, when potassium was used as an additive, the signal for [levoglucosan+K]$^+$ (m/z 201) was reduced to only 0.3 ± 0.2 times the protonated molecule when acid was used as an additive. Thus, an increase in the sensitivity of levoglucosan was observed from cationization with each metal additive except potassium. Silver has two isotopes of similar intensity, so the normalized intensity of [M+Ag]$^+$ is presented as the sum

of $[M+^{107}Ag]^+$ and $[M+^{109}Ag]^+$. While the sensitivity of a single isotopic peak is slightly less than the protonated species, the isotope pair provides a characteristic signature in the mass spectrum. Compounds that have undergone silver cationization can easily be distinguished from other species by the isotopic peak doublet.

Lithium and sodium were found to increase sensitivity of levoglucosan detection much more than silver, thus experiments were carried out to separately determine the optimal concentration of lithium and sodium in the electrospray solvent to form metal cationized levoglucosan. The concentration of each metal additive was individually varied from 0.5 mM to 25 mM added to the electrospray solvents. In Figure 3.2, intensity of $[M+X]^+$, where X represents the metal additive, is plotted as a function of metal concentration. At all metal concentrations, $[M+Li]^+$ is formed in greater abundance than $[M+Na]^+$, and at salt concentrations higher than 10 mM, $[M+Li]^+$ and $[M+Na]^+$ intensity plateaued. A decrease in the intensity of $[M+X]^+$ was observed above 10 mM lithium and 20 mM sodium concentrations as metal acetate clusters became the dominant peaks in the mass spectrum. To maximize sensitivity while minimizing metal acetate clusters, 5 mM metal concentration was used for the remainder of the study. Although this was determined to be the optimal metal concentration for EESI, this concentration is much higher than metal concentrations reported for ESI in the literature[29–32].
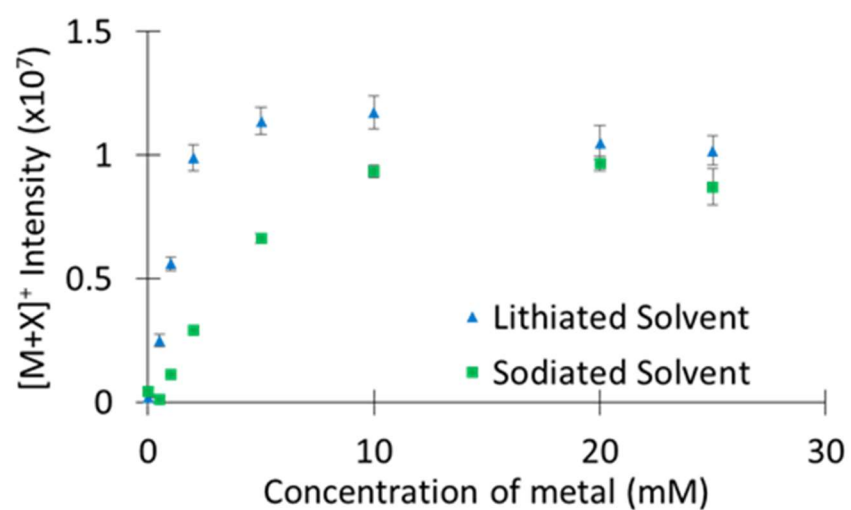
Figure 3.2. Comparison of concentration profiles of both $[M+Li]^+$ and $[M+Na]^+$ for levoglucosan by EESI. Both metals reached an optimal intensity between 5 and 10 mM.

To investigate the competitive formation of $[M+Li]^+$ and $[M+Na]^+$ for levoglucosan, mixtures of lithium and sodium acetate were used as additives to the electrospray solvent. The total metal concentration was held constant at 5 mM, but the ratio of lithium to sodium was varied as displayed in Figure 3.3. The intensities of both $[M+Li]^+$ and $[M+Na]^+$ for each mixture were normalized to the intensity of $[M+Li]^+$ when the additive was 100% lithium. The absolute value of the slope of the line corresponding to $[M+Li]^+$ is more than double the slope of the line corresponding to $[M+Na]^+$. This result suggests that levoglucosan has a higher cation affinity for lithium than sodium, which is consistent with results displayed in Figure 3.2.

3.2.4. Metal Cationization of Other Compounds Containing Multiple Oxygens

To determine the applicability of metal cationization for other compounds, analytes with other functional groups containing oxygen were studied using both EESI with an acid additive and EESI with different metal additives. Two mixtures were aerosolized, one containing levoglucosan, syringol, and maltol, and the other consisting of glucose and syringaldehyde. Both mixtures were aerosolized using a volume concentration of 100 ppm in methanol for each analyte. In general, peaks corresponding to syringol and maltol appeared at much lower intensity than those corresponding to levoglucosan. The difference in sensitivity is likely due to differences in ionization efficiency. As a result of using metal additives, $[\text{syringol} + X]^+$ (where X is the added metal) increased in intensity relative to the protonated molecule, while maltol decreased in sensitivity. In Figure 3.4, the ratio of $[M+X]^+$ to $[M+H]^+$ (the later when just using acetic acid as the additive) is plotted for each compound and metal studied. The signal response of $[M+Li]^+$ and $[M+Na]^+$ for levoglucosan,
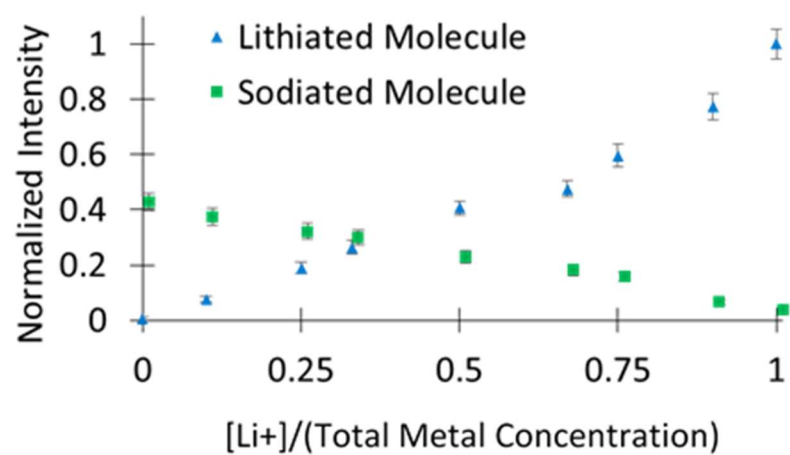
Figure 3.3. Comparison of $[M+Li]^+$ and $[M+Na]^+$ for levoglucosan from EESI in a mixture of the two metals. Total metal concentration was 5 mM.
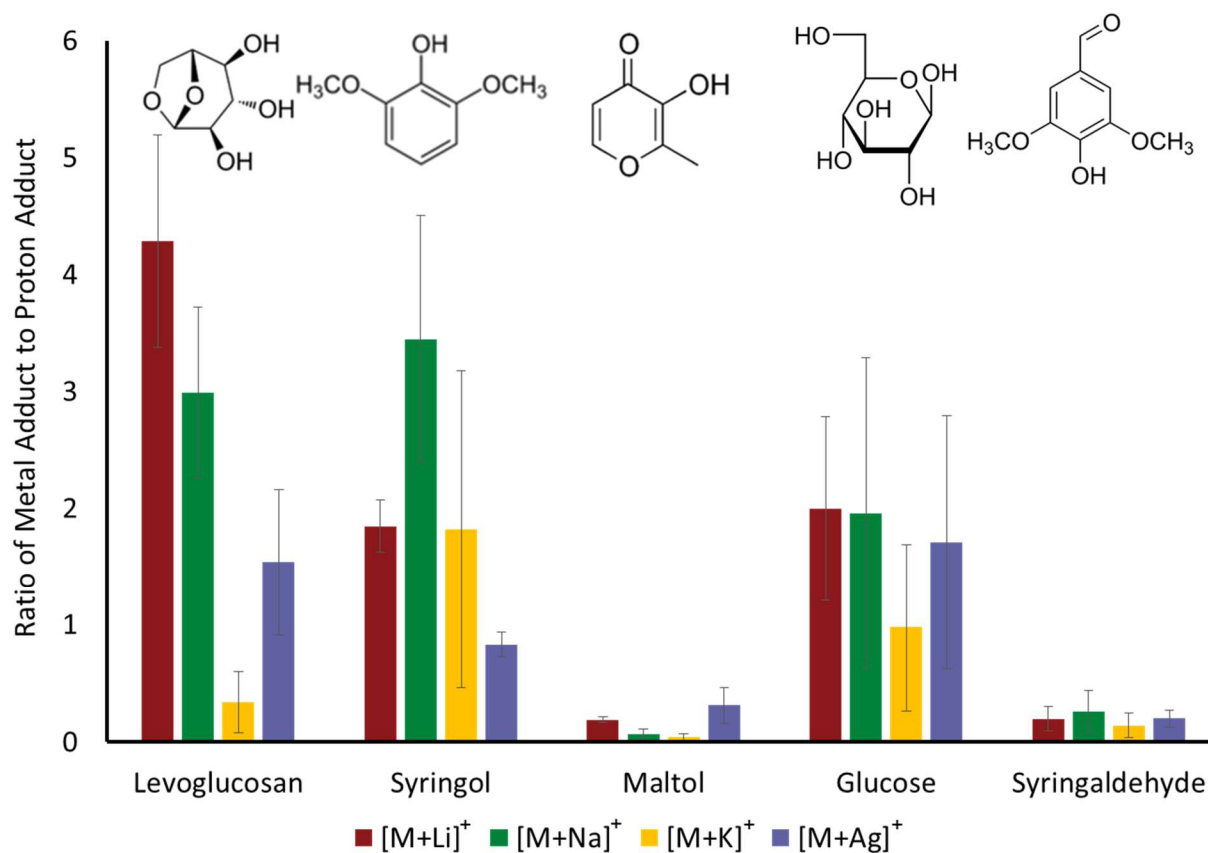
Figure 3.4. Comparison of intensities resulting from cationization of different analytes. All values were normalized to the observed ion intensity of the protonated species in the absence of added metal salt. The ratio for [M+Ag]+ is representative of the sum of the ion intensities of both isotopes.

syringol and glucose is greater with the addition of the metal salts to the electrospray

solvent as compared to the protonated molecule. The combined intensity of [glucose+^{107}Ag]$^+$

and [glucose+^{109}Ag]$^+$ showed a slight increase in intensity. The uncertainty for the ratio of

[M+X]$^+$ to the protonated molecule for glucose is large due to low sensitivity of [M+H]$^+$. This

low sensitivity is due in part to fragmentation as an ion corresponding to a water loss from

protonated glucose was consistently observed as the base peak in the mass spectrum, with

very little of the protonated molecule observed[37]. An analogous fragment ion was not

observed in the mass spectrum for metal cationized glucose.

Both levoglucosan and glucose were studied using electrospray ionization by

dissolving standards in the same electrospray solvents described above. Neither

levoglucosan nor glucose are observed as a protonated molecule, instead both are present as

sodiated molecules, even without added sodium. If lithium, potassium, or silver is added to

the ESI solvent, the sodiated form of each molecule is still present and often dominant. This

is in contrast with the finding above that levoglucosan has a higher affinity for Li$^+$ than

Na$^+$. ESI is much more sensitive to salt concentration as any concentration greater than

100 μM of metal acetate salts yield metal acetate cluster ions that dominate the mass

spectrum.

3.2.5. Tandem Mass Spectrometry of Metal Cationized Compounds

One benefit to coupling EESI to an ion trap is the ability to do MS^n for structural

elucidation. However, in general, very little information is gained from CID MS/MS of

protonated monosaccharides and related anhydrides. Figure 3.5a shows a CID MS/MS

spectra of [levoglucosan+H]$^+$ in which only two product ions are present. One of the product

ions corresponds to a water loss, which is very common among carbohydrates and other

oxygen containing compounds. The second product ion is a water adduct, which is an

unexpected
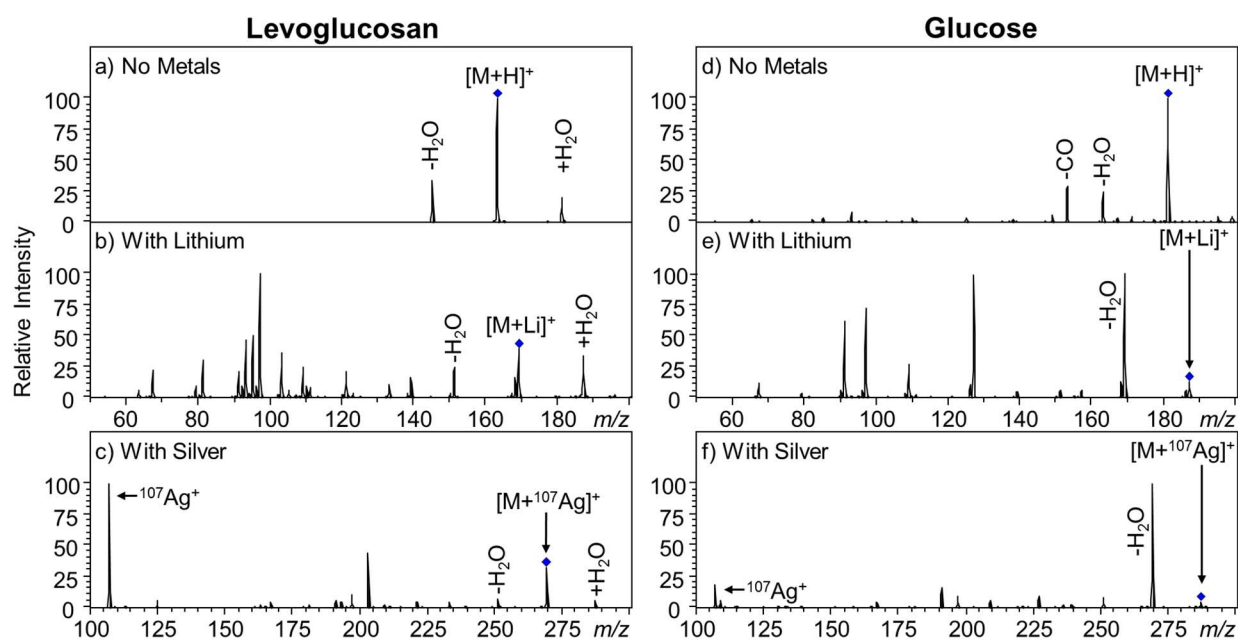
Figure 3.5. CID MS/MS spectra of (a) [levoglucosan+H]$^+$, (b) [levoglucosan+Li]$^+$, (c) [levoglusocan+^{107}Ag]$^+$, (d) [glucose+H]$^+$, (e) [glucose+Li]$^+$, and (f) [glucose+^{107}Ag]$^+$.

product ion. This product ion spectrum is suspected to be due to a contaminant at *m/z* 163 that is highly reactive with water. This will be discussed further in Section 3.4. In Figure 3.5b, a spectrum obtained from MS/MS of lithium cationized levoglucosan is shown. Both ions corresponding to the water adduct and the water loss are present; however, product ions corresponding to carbon-carbon bond cleavages as well as multiple losses of water are detected. Similar product ions are observed in the MS/MS spectrum of silver cationized levoglucosan as displayed in Figure 3.5c. Two product ions for protonated glucose (Figure 3.5d) are water loss and CO loss, which are not very structurally informative. Lithium and silver cationized glucose both resulted in informative MS/MS spectra upon CID with product ions corresponding to more structurally informative dissociation pathways as shown in Figure 3.5e-f. A detailed list of product ion masses and neutral losses for Figure 3.5 can be found in Table 1. For both levoglucosan and glucose, lithium and silver cationization produced similar spectra but with different relative intensities of the structurally significant product ions. Although MS/MS experiments for both $[M+Na]^+$ and $[M+K]^+$ for levoglucosan and glucose were performed, no product ions were observed. This is because the only product ion that is formed is the metal cation. These product ions, Na^+, and, K^+, are not observed in the MS/MS experiment because of the low mass cutoff during the ion trap CID experiment. No product ions are observed in the MS/MS spectra of the sodium or potassium cationized molecules generated by ESI.

Table 3.1. Product ion mass and neutral loss data for MS/MS of protonated, lithiated and silver-cationized levoglucosan and glucose as shown in Figure 3.5. Only one isotope (Ag[107]) of silver-cationized analyte is tabulated.

	Levoglucosan		Glucose	
	Product Ion Mass (Da)	Neutral Loss (Da)	Product Ion Mass (Da)	Neutral Loss (Da)
[M+H]⁺	181	+18	181	0
	163	0	163	-18
	145	-18	153	-28
[M+Li]⁺	187	+18	187	0
	169	0	163	-24
	151	-18	127	-60
	139	-30	109	-78
	133	-36	97	-90
	121	-48	91	-96
	109	-60	67	-120
	103	-66		
	97	-72		
	95	-74		
	93	-76		
	91	-78		
	81	-88		
	67	-102		
[M+Ag¹⁰⁷]⁺	287	+18	287	0
	269	0	269	-18
	251	-18	251	-36
	233	-36	227	-60
	221	-48	209	-78
	203	-66	197	-90
	197	-72	191	-96
	193	-76	167	-120
	191	-78	107	-180
	181	-88		
	167	-102		
	107	-163		

3.2.6. Conclusions

Metal cationization is effective for ionizing compounds from aerosolized mixtures using EESI. Lithium and sodium are both capable of more efficient ionization than protonation of the compounds studied except maltol. This effect is likely due to a combination of two factors, one increasing the likelihood of metal cationization and the other increasing the likelihood of protonation. Efficient metal cationization will be dependent on the ability for the metal to bind to the compound, oxygen containing or other heteroatoms, in a multi-dentate fashion. We are currently using theoretical modeling to understand this in more detail. Lithium cationization is also effective in aiding in improved dissociation upon CID. Both of these points will be beneficial using EESI in the study of complex aerosols produced by biomass burning.

3.3. Metal Cationization during Pyrolysis of Cellulose

Although metal cationization may be used for improved sensitivity and dissociation of some compounds, generally it is regarded as a nuisance. If a sample or the electrospray solvent is prepared in glass, the corresponding spectrum will contain sodium cationized molecules if the compounds in the sample have a high sodium affinity. This is the case for compounds generated from the pyrolysis of cellulose or ethyl cellulose. When the method of metal cationization in EESI was applied to the pyrolysis of ethyl cellulose, the results in Figure 3.6 were observed. The spectrum when acetic acid was added to a 1:1 mixture of methanol and water closely resembles the spectrum when sodium acetate was added. Further, when lithium is added, a shift in mass of -16 is observed corresponding to the difference between the mass of a sodium atom and a lithium atom. This suggests that the electrospray solvent with added acetic acid contained a significant amount of sodium. When silver was used as an additive, a shift toward higher masses was observed consistent with
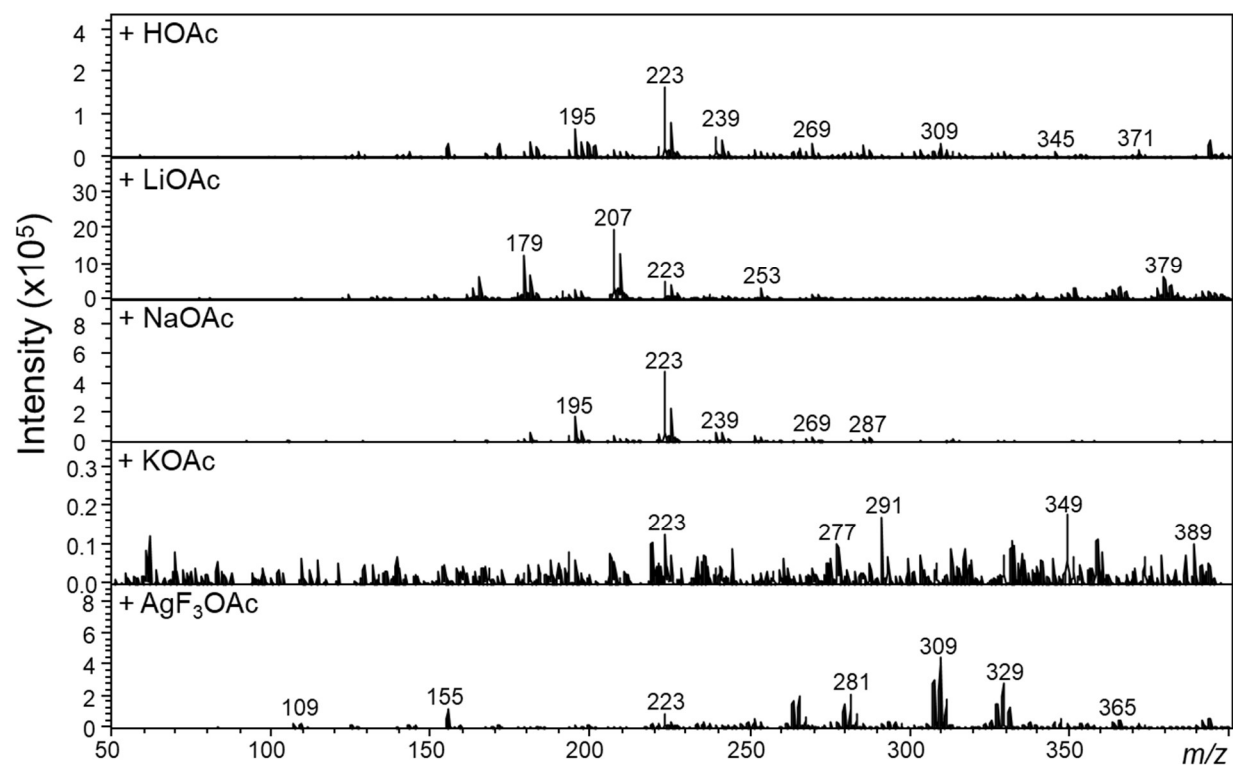
Figure 3.6. Full scan mass spectra of EESI of pyrolyzed ethyl cellulose with metal salt additives.

the difference between a silver isotope distribution and the mass of a sodium atom. Potassium was also used as an additive, but no potassium cationized molecules were observed. The spectrum observed when acetic acid was the additive was previously considered a standard mass spectrum for protonated compounds from the pyrolysis of ethyl cellulose prior to the presentation of these results. From this point forward, electrospray solvents were prepared in plastic containers rather than glass containers to limit sodium contamination. The focus was also moved away from pyrolysis of ethyl cellulose to the more prevalent natural polymer, cellulose.

3.4.   Influence of Acid Additive on EESI

As mentioned in Section 3.2.5 and shown in Figure 3.5a, the MS/MS spectrum obtained from m/z 163, the protonated molecule, from EESI of aerosolized levoglucosan with acetic acid used as an additive shows a peak corresponding to a water loss (m/z 145) and a peak corresponding to a water adduct (m/z 181). The observation of protonated levoglucosan is not shown elsewhere in the literature, as it is always observed in negative mode[38] or as a sodium[39] or ammonium cationized molecule[40]. Nothing about this product ion spectrum was considered abnormal until formic acid was used as an additive for the analysis of levoglucosan by EESI.

In blank runs using acetic acid as an additive (1% by volume) to a 1:1 mixture of water and methanol, a small peak for m/z 163 was always observed. Although blanks were recorded frequently, this was often disregarded as carry over from a prior experiment because it was present at low intensities compared to the intensity observed during EESI of a levoglucosan aerosol. A comparison of the MS spectra observed from the blank using acetic and formic acid as additives is shown in Figure 3.7. A peak for m/z 163 is present in
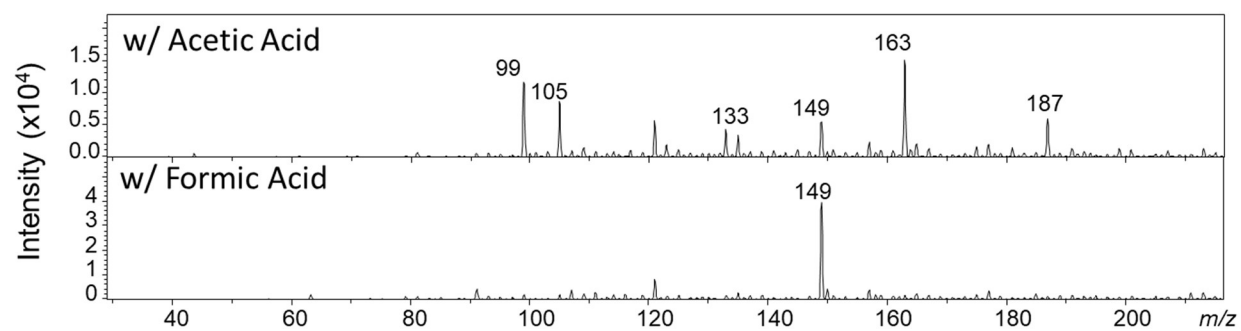
Figure 3.7. Mass spectra of the solvent blanks using acetic acid and formic acid as additives.

the mass spectrum when acetic acid was used, but not when formic acid was used. When each of these solvents are used for EESI of an aerosol of levoglucosan, a large peak at m/z 163 corresponding to protonated levoglucosan is observed. MS/MS of protonated levoglucosan in each solvent produces very different product ion spectra. In Figure 3.8, the product ion spectra for each solvent is shown at different fragmentation voltage settings. As fragmentation voltage is increased, the selected mass, m/z 163, is accelerated more quickly to force more frequent collisions with the helium collision gas and impart more internal energy to the ions at m/z 163. The only peaks present in the product ion spectra for the solvent with acetic acid (Figure 3.8A) are a loss of water (m/z 145) and an adduct of water (m/z 181). This is identical to the spectra in Figure 3.5a. When the solvent with formic acid is used, a different MS/MS spectra is observed. In Figure 3.8B, peaks are observed that correspond to the same neutral losses observed in Table 1 for lithiated levoglucosan. This suggests that the product ion spectra obtained from MS/MS of levoglucosan using formic acid as an additive (Figure 3.8B) is representative of levoglucosan, but the product ion spectra obtained from MS/MS of levoglucosan using acetic acid as an additive is representative of a different structure. This structure could be the ion from the blank in Figure 3.7. One method that can be used to distinguish isomers or isobars using an ion trap is the ion-molecule reaction of water adduction[41].

We have found that the structure(s) of lithiated compounds can be probed by allowing the lithiated compound to react with adventitious water in an ion trap and measuring the fraction of the structures that do not react with water even after long trapping times[41–43]. The likelihood that a structure reacts with water is dependent on the availability of sites where lithium can cationize. If the lithium can have a tridentate or tetradentate interaction with a structure, the complex is much less likely to react with
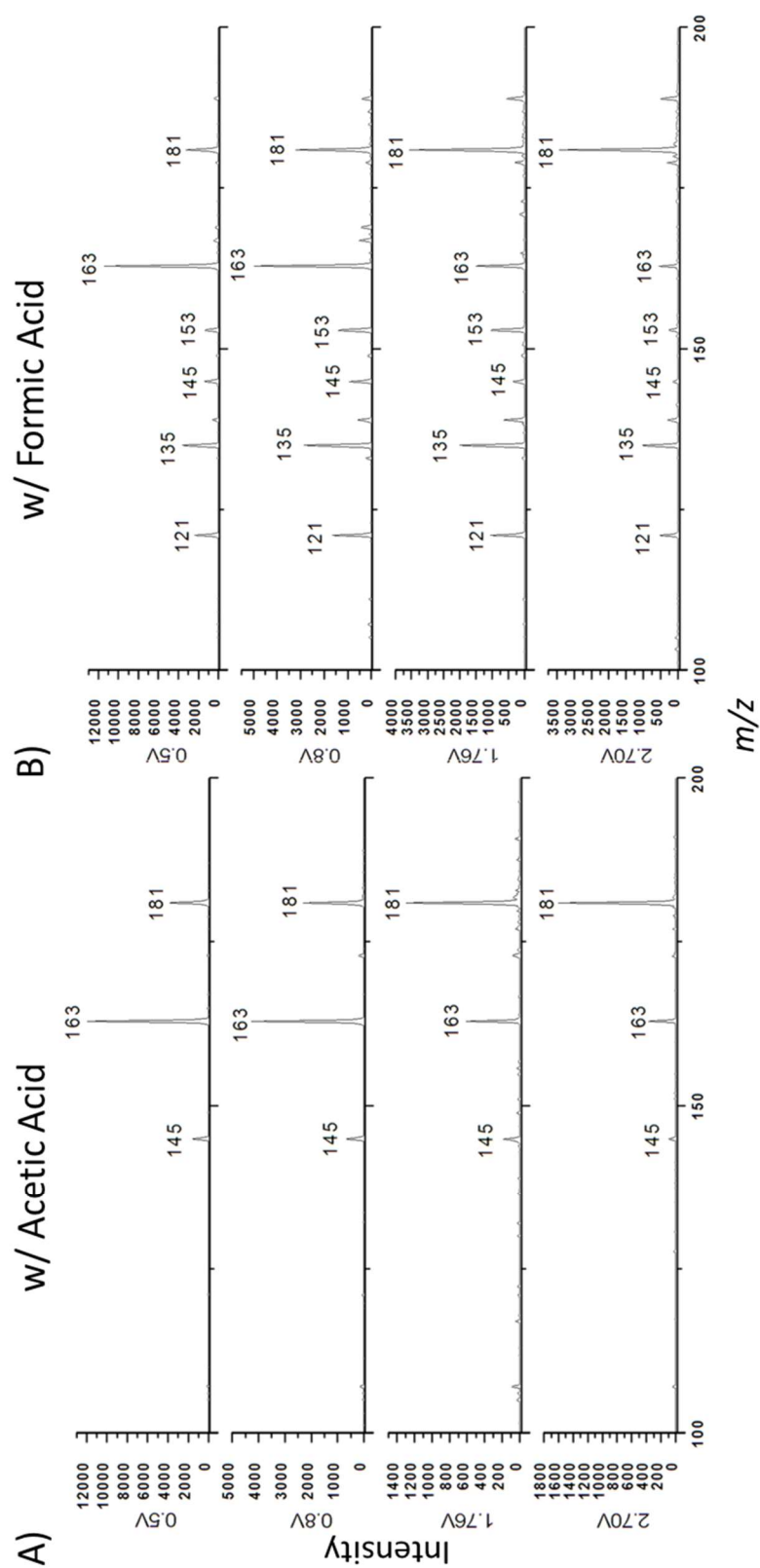
Figure 3.8. CID MS/MS spectra at varying fragmentation voltage settings of the solvent blanks using A) acetic acid and B) formic acid.

59

water in an ion trap. If the lithium forms a bidentate interaction with the structure, then the structure is more likely to bind with water in the ion trap. After long trapping/reaction times, there is typically a group of reactive ions that adduct to water observed at a shift in mass of +18 relative to the parent mass and there is another group of unreactive ions, observed at the parent mass, that do not adduct to water. The unreactive fraction of the lithiated complex is defined as the ion population that is unreactive divided by the total population of ions. This value for an analyte in solution has been demonstrated to be extremely reproducible[41].

Levoglucosan in particular has a very steady unreactive fraction due to a stable, bicyclic structure. Lithiated levoglucosan, analyzed by both ESI and EESI, has a slow reaction rate and a high unreactive fraction compared to many other sugars that we have analyzed using the water adduction technique. The majority of work in the water adduction method has focused on lithium cationized molecules. Nonetheless, water adduction can still be observed experimentally for a protonated molecule as seen in Figure 3.5B and an unreactive fraction can be measured using the same trapping parameters adjusted for the mass of the protonated molecule rather than the lithiated molecule.

EESI of aerosolized levoglucosan using an acid additive generates a protonated levoglucosan that is mostly unreactive with water, yielding an unreactive fraction of 0.85. This means that for protonated levoglucosan, 85% of the unreacted structure remains while only 15% has reacted with adventitious water in the ion trap after 10 seconds of trapping time. Figure 3.9 compares the unreactive fraction of protonated levoglucosan to the unreactive fraction of *m/z* 163 in each of the blanks using acetic acid and formic acid as an additive. The majority of the m/z 163 of aerosolized levoglucosan ionized with acetic acid is the protonated molecule, but there is some reactive contributor in the blank. The error
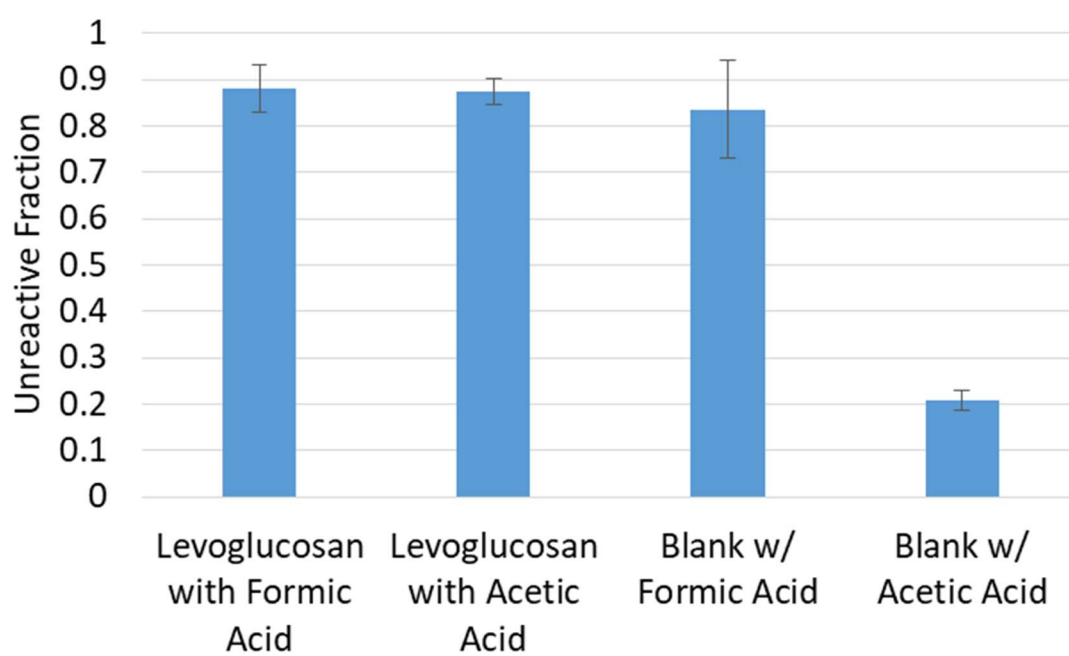
Figure 3.9. Bar graph of the unreactive fraction from *m/z* 163 observed in the analysis of aerosolized levoglucosan using acetic acid and formic acid as additives.

associated with the blank using formic acid can be attributed to very low signal intensity. The signal measured for the blank using formic acid is still likely levoglucosan at barely detectable amounts in the background. The unreactive fraction for *m/z* 163 in the blank with acetic acid added is different from the rest with a value of 0.21. For the blank with an acetic acid additive, only 21% of the unreacted structure remains while 79% has reacted with water in the ion trap after 10 seconds of trapping time. This data supports the hypothesis that a contaminant is present in the solvent mixture of water and methanol with acetic acid used as an additive.

Although the contaminant is from acetic acid, the identity of the contaminant is still unknown. An array of acid sources described in Table 2 were used as additives to a mixture of 1:1 methanol and water to test for the presence of a contaminant at *m/z* 163 with high water reactivity. The unreactive fraction for each of the acid sources is shown in Figure 3.10A. As expected, the unreactive fraction when formic acid is used as an additive to the blank is approximately 0.85. Interestingly, the unreactive fraction when using various acetic acid sources as an additive to the blank varied from 0.08 to 0.45, which suggests the possibility of multiple contaminants. The unreactive fraction of HOAc 1 was expected to match the results displayed in Figure 3.9 because the same acid source was used in both solvents; however, the results were different, likely due to variation in solution preparation. The two acetic acid sources with the largest intensity at *m/z* 163 were HOAc 1 and 8 in Figure 3.10B. These sources are the most often used acetic acid sources in the Glish lab. Notice both of these sources have unreactive fractions below 0.1. If the scan delay is increased to 10 seconds without isolation of any mass, all ions that adduct to adventitious water in the trap may be monitored. For the solvent made with HOAc 1, analysis of the

Table 3.2. Description of the acid sources used to investigate the acetic acid contaminant.

Acid Source	Description
HOAc 1	Optima – used most often
HOAc 2	Optima
HOAc 3	Abandoned scintillation vial labeled "acetic acid"
HOAc 4	ACS grade
HOAc 5	ACS Plus grade
HOAc 6	Sequencing grade
HOAc 7	ACS Plus grade (separate from HOAc 5)
HOAc 8	Optima – used by another project
FA	Optima – used most often
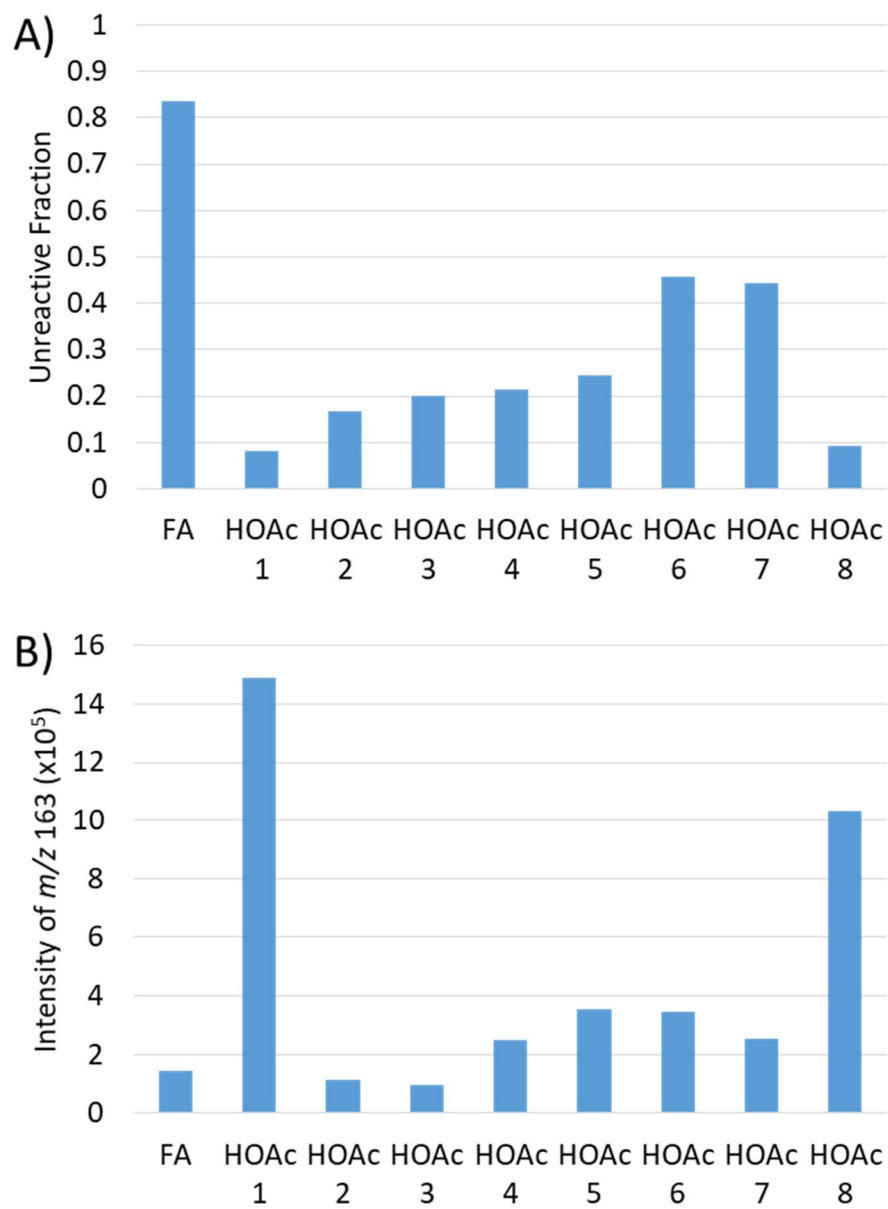
Figure 3.10. Analysis of different acid sources to observe the A) unreactive fraction and B) intensity of m/z 163. A description of the acid labels are given in Table 3.2.

mass spectrum before and after a scan delay suggests there are many structures in the mass spectrum that are highly reactive with water.

In an effort to obtain more information about the contaminant at *m/z* 163, two blank solvents, one with HOAc 1 as an additive and the other with formic acid as an additive were analyzed using a Thermo Scientific Q Exactive HF-X hybrid quadrupole-orbitrap. The data zoomed in at *m/z* 163 is presented in Figure 3.11. There is a peak present at *m/z* 163.02714 (highlighted by a red circle) in the solvent with acetic acid that is not as prevalent in the solvent with formic acid. The other peaks at *m/z* 163 stay approximately the same. The accurate mass does not correspond to a valid molecular formula using only carbon, oxygen, nitrogen, and hydrogen atoms. More information is necessary for successful identification of the contaminant.

3.5.   Summary and Conclusions

Presented in this chapter are results demonstrating the utility of metal cationization in EESI for the on-line sampling and ionization of compounds in an aerosol. EESI is described in detail and practical aspects of EESI operation are discussed. Protonation of sugars, which is currently not efficient enough to detect using ESI, were demonstrated using EESI with an acid additive. One of the primary benefits to an electrospray-based ionization method is the ability to choose the electrospray solvent for the best extraction of an analyte of interest or to improve ionization using an additive such as a metal cation. The efficacy of using metal cationization to improve analyses of levoglucosan and glucose was evaluated and resulted in improved signal intensity and improved MS/MS dissociation for glucose. The results from dissociation of levoglucosan are obscured by a contaminant present when using acetic acid as a solvent additive for EESI.
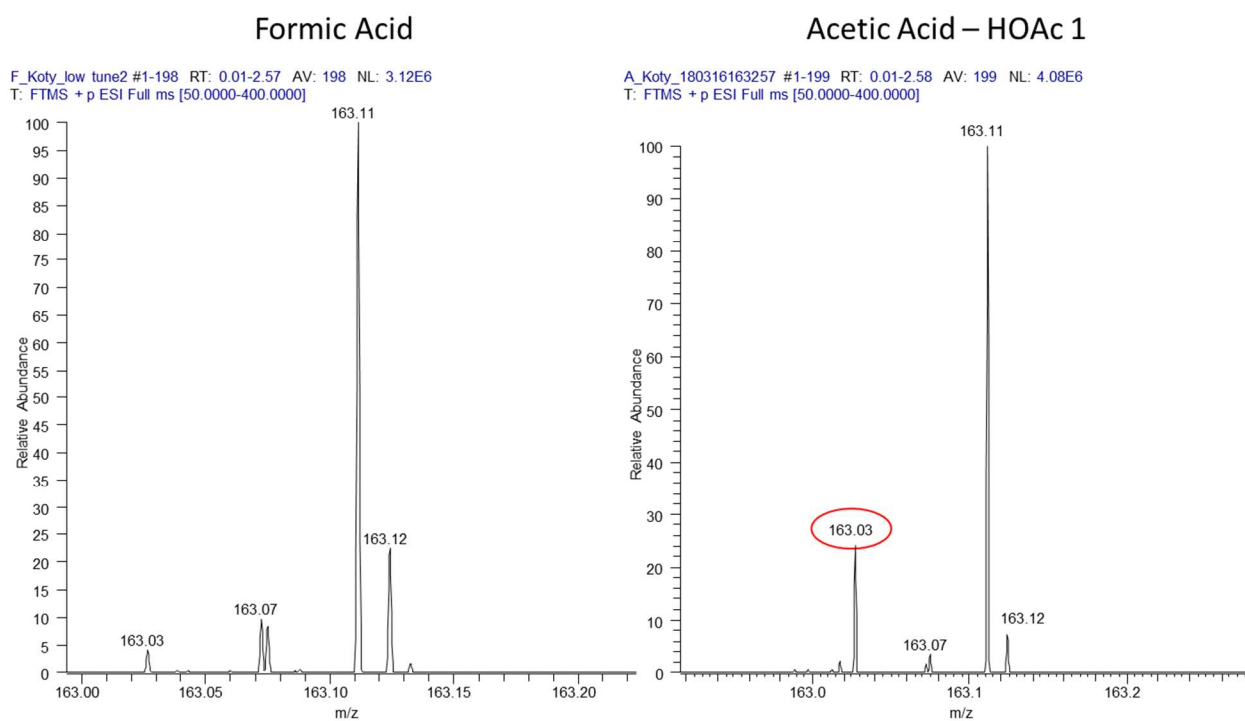
Figure 3.11. High resolution mass spectra of the solvent blanks containing both formic acid and acetic acid as an additive.

Metal cationization in EESI was also demonstrated for the analysis of the pyrolysis products of ethyl cellulose. Results suggest that extra care must be taken to prepare solutions in non-glass containers to avoid sodium contamination. Previous results for EESI of the pyrolysis products of ethyl cellulose were likely contaminated with sodium and the peaks observed were sodiated rather than protonated as assumed.

In the search for the identity of the contaminant at *m/z* 163 that obscured the dissociation data presented in Section 3.2, it was shown that the contaminant was present in solvents with acetic acid as an additive and not present in solvents with formic acid as an additive based upon MS/MS studies. The water reactivity of the structures present at *m/z* 163 were assessed using an ion-molecule reaction in a quadrupole ion trap. Ions of interest were isolated in the trap and allowed to adduct to water for 10 seconds before mass analysis. These results showed that the contaminant present in acetic acid was very reactive with water while protonated levoglucosan is barely reactive with water.

REFERENCES

1. Ifa, D. R., Wu, C., Ouyang, Z. & Cooks, R. G. Desorption electrospray ionization and other ambient ionization methods: current progress and preview. *Analyst* **135,** 669–681 (2010).

2. Huang, M.-Z., Yuan, C.-H., Cheng, S.-C., Cho, Y.-T. & Shiea, J. Ambient Ionization Mass Spectrometry. *Annu. Rev. Anal. Chem.* **3,** 43–65 (2010).

3. Harris, G. A., Galhena, A. S. & Fernandez, F. M. Ambient sampling/ionization mass spectrometry: Applications and current trends. *Anal. Chem.* **83,** 4508–4538 (2011).

4. Yao, Z.-P. Characterization of proteins by ambient mass spectrometry. *Mass Spectrom. Rev.* **31,** 437–447 (2012).

5. Wu, C., Dill, A. L., Eberlin, L. S., Cooks, R. G. & Ifa, D. R. Mass spectrometry imaging under ambient conditions. *Mass Spectrom. Rev.* **32,** 218–243 (2013).

6. Chen, H., Venter, A. & Cooks, R. G. Extractive electrospray ionization for direct analysis of undiluted urine, milk and other complex mixtures without sample preparation. *Chem. Commun.* **19,** 2042–2044 (2006).

7. Chen, H., Yang, S., Wortmann, A. & Zenobi, R. Neutral Desorption Sampling of Living Objects for Rapid Analysis by Extractive Electrospray Ionization Mass Spectrometry. *Angew. Chem.* **46,** 7591–7594 (2007).

8. Chen, H. & Zenobi, R. Neutral desorption sampling of biological surfaces for rapid chemical characterization by extractive electrospray ionization mass spectrometry. *Nat. Protoc.* **3,** 1467–1475 (2008).

9. Chingin, K., Gamez, G., Chen, H., Zhu, L. & Zenobi, R. Rapid classification of perfumes by extractive electrospray ionization mass spectrometry (EESI-MS). *Rapid Commun. Mass Spectrom.* **22,** 2009–2014 (2008).

10. Venter, A., Nefliu, M. & Cooks, R. G. Ambient desorption ionization mass spectrometry. *TrAC Trends Anal. Chem.* **27,** 284–290 (2008).

11. Gu, H., Xu, N. & Chen, H. Direct analysis of biological samples using extractive electrospray ionization mass spectrometry (EESI-MS). *Anal. Bioanal. Chem.* **403,** 2145–2153 (2012).

12. Li, L.-P. *et al.* Applications of ambient mass spectrometry in high-throughput screening. *Analyst* **138,** 3097–3103 (2013).

13. Wang, Y., Liu, S., Hu, Y., Li, P. & Wan, J.-B. Current state of the art of mass spectrometry-based metabolomics studies – a review focusing on wide coverage, high throughput and easy identification. *RSC Adv.* **5,** 78728–78737 (2015).

14. Doezema, L. A. *et al.* Analysis of secondary organic aerosols in air using extractive electrospray ionization mass spectrometry (EESI-MS). *RSC Adv.* **2,** 2930 (2012).

15. Gallimore, P. J. & Kalberer, M. Characterizing an extractive electrospray ionization (EESI) source for the online mass spectrometry analysis of organic aerosols. *Environ. Sci. Technol.* **47,** 7324–7331 (2013).

16. Spencer, S. E., Tyler, C. A., Tolocka, M. P. & Glish, G. L. Low-Temperature Plasma Ionization-Mass Spectrometry for the Analysis of Compounds in Organic Aerosol Particles. *Anal. Chem.* **87,** 2249–2254 (2015).

17. Spencer, S. E., Santiago, B. G. & Glish, G. L. Miniature Flow-Through Low-Temperature Plasma Ionization Source for Ambient Ionization of Gases and Aerosols. *Anal. Chem.* **87,** 11887–11892 (2015).

18. Law, W. S. *et al.* On the Mechanism of Extractive Electrospray Ionization. *Anal. Chem.* **82,** 4494–4500 (2010).

19. Chowdhury, S. K., Katta, V. & Chait, B. T. Probing conformational changes in proteins by mass spectrometry. *J. Am. Chem. Soc.* **112,** 9012–9013 (1990).

20. Zhou, S. & Hamburger, M. Effects of solvent composition on molecular ion response in electrospray mass spectrometry: Investigation of the ionization processes. *Rapid Commun. Mass Spectrom.* **9,** 1516–1521 (1995).

21. Kostiainen, R. & Kauppila, T. J. Effect of eluent on the ionization process in liquid chromatography-mass spectrometry. *J. Chromatogr. A* **1216,** 685–699 (2009).

22. Crotti, S., Seraglia, R. & Traldi, P. Some thoughts on electrospray ionization mechanisms. *Eur. J. Mass Spectrom. (Chichester, Eng).* **17,** 85–100 (2011).

23. Wang, R. *et al.* On the mechanism of extractive electrospray ionization (EESI) in the dual-spray configuration. *Anal. Bioanal. Chem.* **402,** 2633–2643 (2012).

24. Cech, N. B. & Enke, C. G. Practical implications of some recent studies in electrospray ionization fundamentals. *Mass Spectrom. Rev.* **20,** 362–387 (2002).

25. Emmett, M. R. & Caprioli, R. M. Ultra-High-Sensitivity Analysis of Peptides and Proteins. *J. Am. Soc. Mass Spectrom.* **5,** 605–613 (1994).

26. Leitner, A., Emmert, J., Boerner, K. & Lindner, W. Influence of Solvent Additive Composition on Chromatographic Separation and Sodium Adduct Formation of Peptides in HPLC–ESI MS. *Chromatographia* **65,** 649–653 (2007).

27. Jonkers, N., Govers, H. & Pim, D. V. Adduct formation in LC-ESI-MS of nonylphenol ethoxylates: Mass spectrometrical, theoretical and quantitative analytical aspects. *Anal. Chim. Acta* **531,** 217–228 (2005).

28. Schneider, R. P., Lynch, M. J., Ericson, J. F. & Fouda, H. G. Electrospray ionization mass spectrometry of semduramicin and other polyether ionophores. *Anal. Chem.* **63,** 1789–1794 (1991).

29. Harvey, D. J. Structural determination of N-linked glycans by matrix-assisted laser desorption/ionization and electrospray ionization mass spectrometry. *Proteomics* **5,** 1774–1786 (2005).

30. Bruggink, C., Maurer, R., Herrmann, H., Cavalli, S. & Hoefler, F. Analysis of carbohydrates by anion exchange chromatography and mass spectrometry. *J. Chromatogr. A* **1085,** 104–109 (2005).

31. Simoneit, B. R. T. *et al.* Levoglucosan, a tracer for cellulose in biomass burning and atmospheric particles. *Atmos. Environ.* **33,** 173–182 (1999).

32. Ackloo, S. Z., Smith, R. W., Terlouw, J. K. & McCarry, B. E. Characterization of ginseng saponins using electrospray mass spectrometry and collision-induced dissociation experiments of metal-attachment ions. *Analyst* **125,** 591–597 (2000).

33. Chen, R. & Li, L. Lithium and transition metal ions enable low energy collision-induced dissociation of polyglycols in electrospray ionization mass spectrometry. *J. Am. Soc. Mass Spectrom.* **12,** 832–839 (2001).

34. Heaton, A. L., Moision, R. M. & Armentrout, P. B. Experimental and Theoretical Studies of Sodium Cation Interactions with the Acidic Amino Acids and Their Amide Derivatives. *J. Phys. Chem. A* **112,** 3319–3327 (2008).

35. Hofmeister, G. E., Zhou, Z. & J.A., L. Linkage position determination in lithium-cationized disaccharides: Tandem mass spectrometry and semiempirical calculations. *J. Am. Chem. Soc.* **113,** 5964–5970 (1991).

36. Asam, M. R. & Glish, G. L. Tandem mass spectrometry of alkali cationized polysaccharides in a quadrupole ion trap. *J. Am. Soc. Mass Spectrom.* **8,** 987–995 (1997).

37. Schaller-Duke, R. M., Bogala, M. R. & Cassady, C. J. Electron Transfer Dissociation and Collision-Induced Dissociation of Underivatized Metallated Oligosaccharides. *J. Am. Soc. Mass Spectrom.* **29,** 1021–1035 (2018).

38. Dye, C. & Yttri, K. E. Determination of Monosaccharide Anhydrides in Atmospheric Aerosols by Use of High-Performance Liquid Chromatography Combined with High-Resolution Mass Spectrometry. *Anal. Chem.* **77,** 1853–1858 (2005).

39. Swanson, K. D., Spencer, S. E. & Glish, G. L. Metal Cationization Extractive Electrospray Ionization Mass Spectrometry of Compounds Containing Multiple Oxygens. *J. Am. Soc. Mass Spectrom.* **28,** 1030–1035 (2017).

40. Hurt, M. R. *et al.* On-line mass spectrometric methods for the determination of the primary products of fast pyrolysis of carbohydrates and for their gas-phase manipulation. *Anal. Chem.* **85,** 10927–10934 (2013).

41. Campbell, M. T., Chen, D. & Glish, G. L. Identifying the D-Pentoses Using Water Adduction to Lithium Cationized Molecule. *J. Am. Soc. Mass Spectrom.* **28,** 1420–1424 (2017).

42. Campbell, M. T., Chen, D., Wallbillich, N. J. & Glish, G. L. Distinguishing Biologically Relevant Hexoses by Water Adduction to the Lithium-Cationized Molecule. *Anal. Chem.* **89,** 10504–10510 (2017).

43. Campbell, M. T., Chen, D. & Glish, G. L. Distinguishing Linkage Position and Anomeric Configuration of Glucose–Glucose Disaccharides by Water Adduction to Lithiated Molecules. *Anal. Chem.* **90,** 2048–2054 (2018).

CHAPTER 4: COAXIAL EXTRACTIVE ELECTROSPRAY IONIZATION

Portions of this chapter are adapted from the following reference with permission from The Royal Society of Chemistry.

4.1.   Introduction

Several types of ambient ionization have been used in the analysis of aerosol particles. Desorption electrospray ionization (DESI) has been used by impacting an aerosol onto a plate prior to surface analysis[1]. A particle-into-liquid sampler (PILS) has also been used to sample aerosols generated from biomass burning prior to electrospray ionization[2]. Both of these techniques require sample collection prior to analysis by mass spectrometry and are susceptible to chemical aging and evaporative losses[3]. Real-time ambient ionization has also been applied to aerosol particles. Low temperature plasma ionization (LTPI) has been used to characterize organic aerosols in which the plasma from a dielectric barrier discharge intersects a stream of organic aerosol particles[4,5]. An ambient electrospray ionization (AESI) source has also been used where aerosol was flowed through the nebulization gas inlet of a conventional electrospray source[6]. The most reported technique for the on-line characterization of aerosol particles is extractive electrospray ionization (EESI)[7–9]. As discussed in the previous chapter, EESI is a technique in which a nebulized sample is passed through an electrospray plume near the atmospheric pressure inlet of a mass spectrometer[10–17]. EESI is likely to be the most broadly applicable ambient ionization technique for the ionization of organic aerosols because of the ability to use different

solvents and additives to enhance ionization of different classes of molecules[18,19]. Compounds in the nebulized sample are typically ionized as $[M+H]^+$ or $[M-H]^-$, although it has been shown that adding a metal salt to the electrospray solvent can improve sensitivity for some compounds by metal cationization as demonstrated in Chapter 3.2[9].

One major challenge associated with EESI of aerosol particles is the difficulty in aligning the aerosol stream and electrospray plume in the source region[19]. The nebulized solvent spray must intersect an aerosol-gas stream, which is invisible to the eye at typical aerosol concentrations. Small differences in the position of either the ESI emitter or aerosol stream can lead to large differences in sampling efficiency and electric field, resulting in a loss in sensitivity. There is also variation in the signal trace as a function of time that results in large coefficients of variations in the analysis, unrelated to fluctuations in the aerosol. This chapter presents a novel EESI source design to address limitations with existing designs.

4.2.   Using the Aerosol-Gas flow as the Nebulization Gas

EESI faces similar challenges as LTPI in that the plasma gas must intersect the stream of aerosol particles[4]. This challenge was overcome by using the aerosol-gas flow as the plasma gas in a mode called flow-through LTPI[5]. A similar solution was attempted for EESI, where the aerosol-gas flow was used as the nebulization gas. In pneumatically-assisted ESI, the nebulization gas flows around a solvent capillary and nebulizes the solvent into small charged droplets. In this configuration, the aerosol-gas serves as the nebulization gas while also delivering aerosol particles for interaction with the charged solvent droplets. The outlet of the COA was piped into the nebulization gas port on the ESI nebulizer EESI analysis. For analysis of an oleic acid aerosol in negative mode, the results are presented in Figure 4.1. When oleic acid is analyzed by standard ESI, as shown in
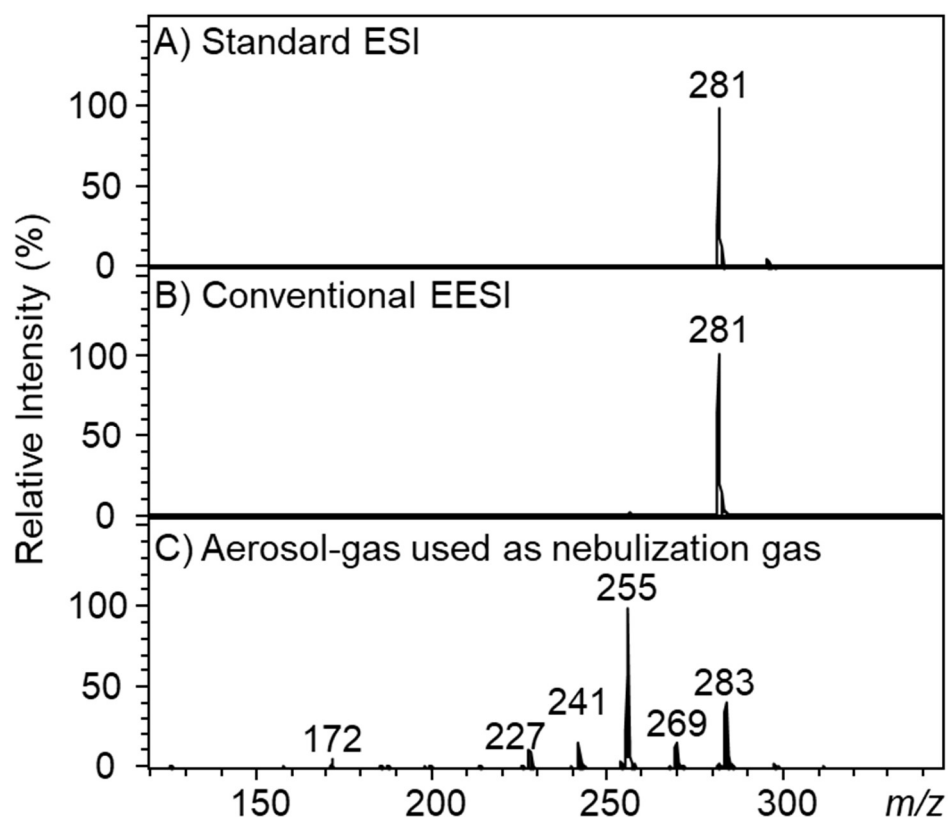
Figure 4.1. Mass spectra of deprotonated oleic acid ([M-H]⁻) using different ionization sources.

Figure 4.1A, a peak is observed for [M-H]⁻ at *m/z* 281. This *m/z* 281 is also the only peak observed in Figure 4.1B when an oleic acid aerosol is analyzed by conventional EESI as described in Chapter 3. However, when analyzed by EESI using the aerosol-gas as the nebulization gas, as shown in Figure 4.1B, an array of peaks are observed, none of which correspond to [M-H]⁻. Instead, an unusual peak corresponding to [M+H]⁻ is observed at *m/z* 283 with in-source fragmentation products corresponding to a neutral mass loss of $-CH_2$, a typical loss observed for alkyl chains. For this mode of ionization, the current readout from the end plate of the mass spectrometer reads 9 μA when it typically reads in the nA range for conventional EESI. This increase in end plate current is indicative of a corona discharge which can be observed as a purple glow at the tip of the inline EESI emitter. The corona discharge can be avoided by reducing the capillary voltage, but the signal intensity suffers at lower capillary potentials. The corona discharge can be suppressed by increasing the flow of the nebulizing gas[20,21]. This method would likely work well in a high aerosol-gas flow environment, but not at low flow rates. A design that allows for independent nebulization of the electrospray solvent is needed to avoid corona discharge while maintaining the capillary potential necessary to generate ions.

4.3.   Coaxial EESI

A novel device was designed and fabricated to overcome many of the challenges associated with EESI. The specific device was designed for use on any Bruker instrument with an Apollo I ESI source. The standard configuration of EESI, detailed in Chapters 2 and 3, was used to compare and evaluate the performance of the new device. The standard configuration of EESI, as shown in Figure 4.2, will henceforth be referred to as standard EESI. A list of experimental parameters used on the Bruker HCT Ultra and Bruker Esquire3000 Plus are presented in Tables 4.1 and 4.2.
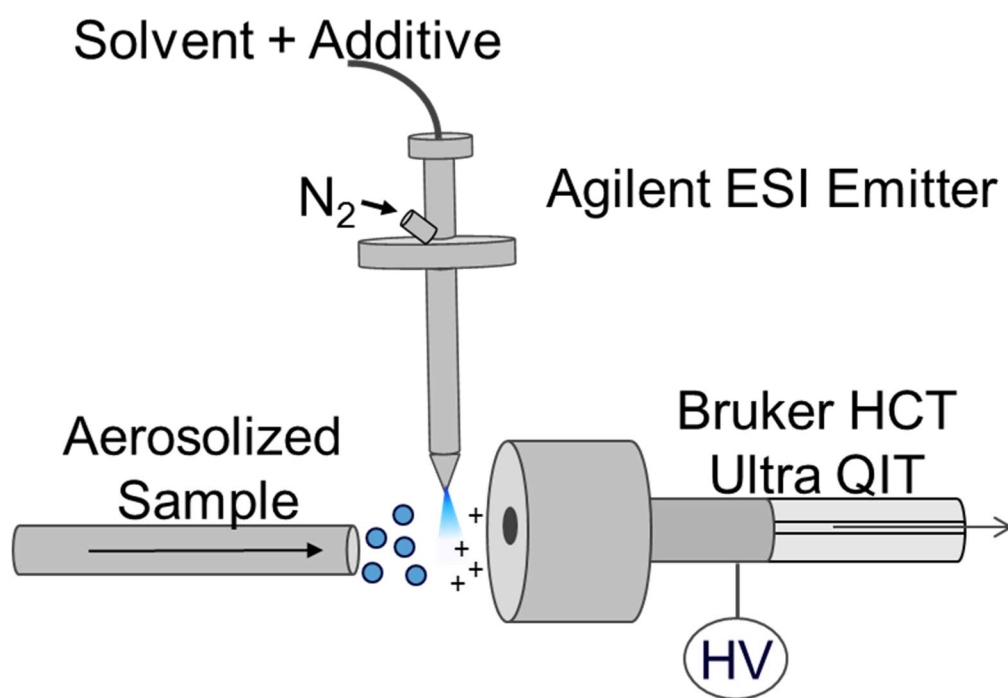
Figure 4.2. Diagram of standard EESI.

Table 4.1. Tuning parameters for the comparing standard and coaxial EESI in the analysis of oleic acid aerosol using a Bruker HCTultra ion trap mass spectrometer. Differences between the two configurations are bolded.

	Standard EESI	Coaxial EESI
Trap Drive (V)	41.0	41.0
Octopole RF Amplitude (Vpp)	149.0	149.0
Lens 2 (V)	52.0	52.0
Capillary Exit (V)	-133.3	-133.3
Skimmer (V)	-40.5	-40.5
Lens 1 (V)	6.5	6.5
Octopole 1 (V)	-12.0	-12.0
Octopole 2 (V)	-1.7	-1.7
Dry Gas Temperature (°C)	300	300
Nebulizer Gas Pressure (psi)	10.0	10.0
Dry Gas Flow Rate (L/min)	8.0	8.0
HV Capillary (V)	**5000**	**6000**
HV End Plate Offset (V)	-500	-500
Solvent Flow Rate (µL/min)	**2.0**	**3.0**

Table 4.2. Tuning parameters for the comparing standard and coaxial EESI in the analysis of aerosolized pyrolysis products of cellulose using a Bruker Esquire 3000 ion trap mass spectrometer. Differences between the two configurations are bolded.

	Standard EESI	Coaxial EESI
Trap Drive (V)	41.7	41.7
Octopole RF Amplitude (Vpp)	150.0	150.0
Lens 2 (V)	-60.0	-60.0
Capillary Exit (V)	87.4	87.4
Skimmer 1 (V)	19.4	19.4
Skimmer 2 (V)	6.0	6.0
Lens 1 (V)	-5.0	-5.0
Octopole (V)	2.4	2.4
Dry Gas Temperature (°C)	300	300
Nebulizer Gas Pressure (psi)	10.0	10.0
Dry Gas Flow Rate (L/min)	5.0	5.0
HV Capillary (V)	**5000**	**6000**
HV End Plate Offset (V)	-500	-500
Solvent Flow Rate (µL/min)	**2.0**	**3.0**

4.3.1. Design and Fabrication of a Coaxial EESI source

For coaxial EESI, two identical ESI emitters (Agilent, G1946- 67098) were modified to form three concentric capillaries where the solvent, aerosol stream, and nebulization gas interact at the tip of the source in an electric field as shown in Figure 4.3. In this design, the flow rates of the solvent, aerosol stream, and nebulization gas are uncoupled. The nebulization gas ensures that nebulization of the solvent is independent of the aerosol flow rate. The solvent is flowed through the central capillary because typical aerosol and nebulization gas flow rates cannot be achieved using the 0.1 mm inner diameter (ID) capillary without excessive gas pressure in each system.

A schematic of the device is shown in Figure 4.4a with solvent, nebulization gas and aerosol inputs labeled. An exploded view of the device is shown in Figure 4.4b. To fabricate the device, one ESI emitter (F in Figure 4.4b) was modified by removing the inner capillary and cutting the long stock of the nebulizer body that includes the electrospray tip. In place of the stock, a 20-gauge needle (G in Figure 4.4b, Fisher, 14-825-15AA) was cut to 75 mm and silver-soldered onto the device. A needle holder (I in Figure 4.4b, Agilent, G1946-20174) was cut in half and the needle was inserted into the holder and silver-soldered in place. A second ESI emitter (K in Figure 4.4b) was modified at the tip opening (L in Figure 4.4b) to be 1.3 mm in diameter, large enough to accommodate the 20-gauge needle (G in Figure 4.4b) with ample area for nebulization gas flow. F was then threaded onto K at I to form two concentric capillaries, with the 20-gauge needle extending 0.2 mm past the outside of L. Finally, a stainless steel inner capillary with 0.1 mm ID (D in Figure 4.4b, Vitaneedle, 32RW gauge) was cut to 122 mm and affixed using a needle holder (C in Figure 4.4b, Agilent, G1946-20174) and then threaded onto F to protrude 0.2 mm past the end of G. The solvent may be introduced into the central capillary using a zero dead volume (ZDV) fitting (A in Figure 4.4b) attached to the needle holder (C in Figure 4.4b). Nebulizing gas can be
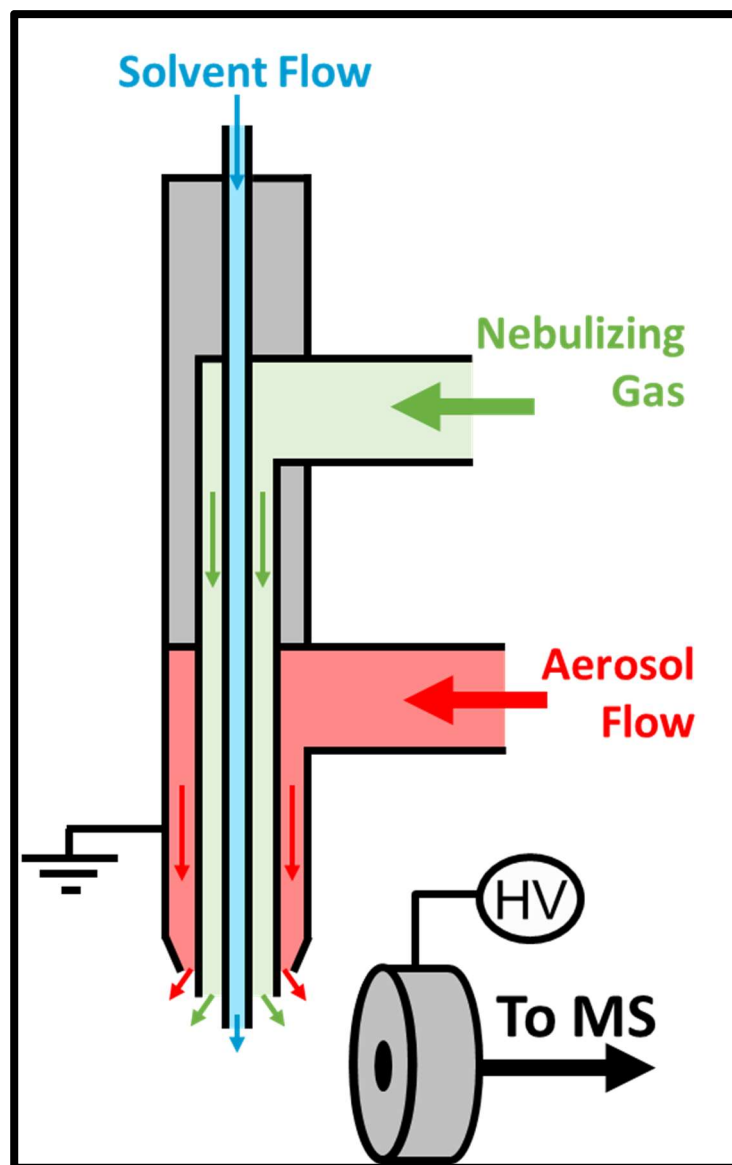
Figure 4.3. Diagram of coaxial EESI. Solvent (blue) flows down a center capillary surrounded by a sheath of nebulizing gas (green). Aerosol (red) flows through the outer capillary and interacts with the solvent and nebulizing gas at the tip of the emitter within the source region.
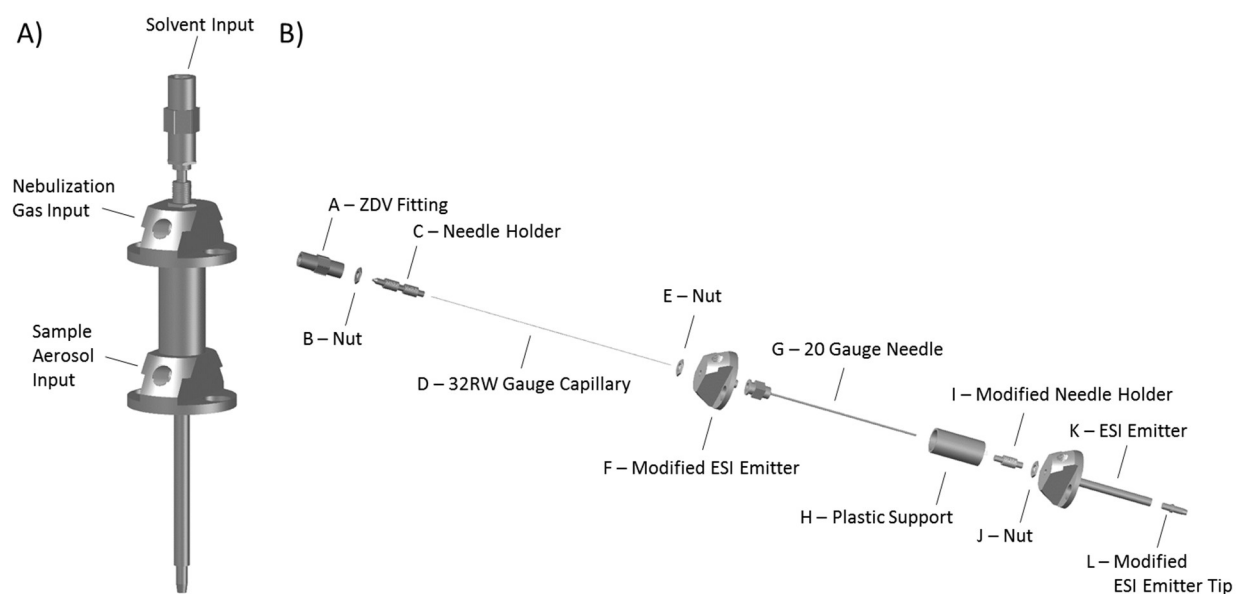
Figure 4.4. (A) Assembled coaxial EESI device measuring 136 mm in length with a maximum radius of 28 mm. (B) Explosion view of the device with all pieces labeled. All pieces are assembled along the axis shown.

flowed through the inner shell using the port on F, and the aerosol can be introduced into the outer shell using the port on K. Although the device may be configured such that the aerosol flow is through the inner shell and nebulizing gas flow is through the outer shell, experiments, described in Section 4.6, show that the two configurations perform similarly. Due to the fragility of the device at the soldered joints between F, G, and I, the configuration of the aerosol and nebulization gas shown in Figure 4.3 was chosen to reduce mechanical stress on the device arising from the attachment of gas and aerosol tubes to ports F and K. A 3D printed piece (H in Figure 4.4b) was designed to reinforce the fragile joints between F, G, and I. The assembled device is shown in Figure 4.4a. Overall, the device measures 136 mm in length. The images of the device as well as the zoomed views of the tip are given in Figure 4.5.

The form factor of the coaxial EESI emitter allows the device to be placed into the source housing of the Apollo 1 ion source in place of a standard ESI emitter. Because the length of the emitter tip L was trimmed 3 mm to have an inner diameter greater than the outer diameter of the 20 gauge needle (G in Figure 4.4b), the emitter tip is farther from the central axis of the inlet capillary and thus farther from the inlet to the mass spectrometer than a standard electrospray emitter tip. To compensate, the absolute magnitude of the electrospray voltage used for all of the coaxial experiments was increased as compared to standard EESI. For the experiments described here, the standard Bruker arrangement was used in that the electrospray voltage is applied to the capillary inlet of the mass spectrometer. However, coaxial EESI has also been successfully performed with the electrospray voltage applied to the coaxial EESI device. An insulating piece was 3D printed in a wood/PLA composite to isolate the coaxial EESI device from the grounded source housing.
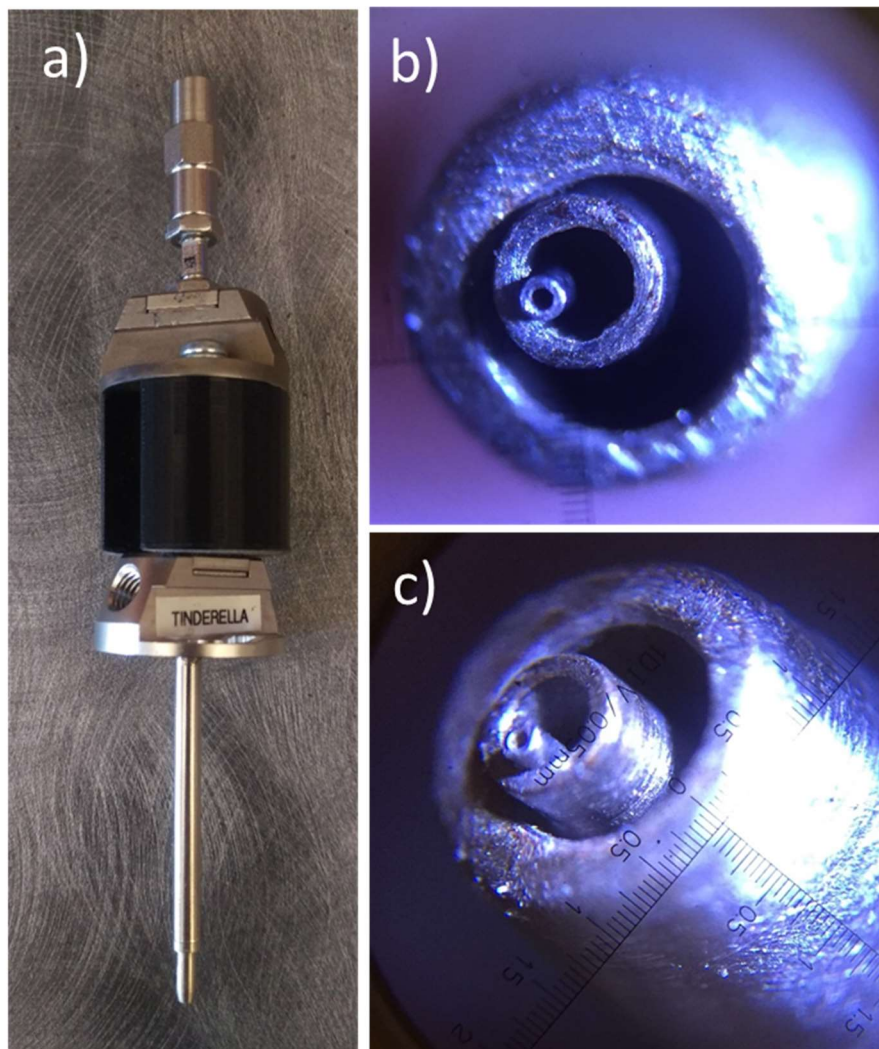
Figure 4.5. (a) Fabricated coaxial EESI device measuring 136 mm in length. (b) Zoomed image of the tip of the device showing the three concentric capillaries. (c) Zoomed image of the tip of the device to illustrate the distance each capillary extends from the device.

4.3.2. Comparison of Coaxial EESI to Standard EESI

To compare coaxial and standard EESI, an experiment was performed where each configuration was used for a period of six minutes using an aerosol of oleic acid. A standard EESI source was assembled and analysis was performed. The setup was then disassembled and a coaxial EESI emitter was inserted into the source housing into the slot for the ESI emitter. The results when each configuration was set up nine times, over several days, are shown in Figure 4.6. The average intensity of each configuration across six minutes of continuous signal is shown in the left panel. The signal for deprotonated oleic acid, $[M-H]^-$ (*m/z* 281), using coaxial EESI decreased by a factor of three as compared to standard EESI. Although the signal decreased, the variation across nine measurements shows that the interexperiment variation associated with standard EESI is four times greater than the interexperiment variation associated with coaxial EESI. The large interexperiment variation in standard EESI most likely arises from the removal of the ion source from the source region and repositioning the source for another experiment. One representative run of each standard and coaxial EESI is shown in the central panel of Figure 4.6. The signal intensity for standard EESI, shown in red, varies significantly across the experiment. The signal observed for $[M-H]^-$ using coaxial EESI is plotted in blue and has a smaller variation across the same time period. The intra-run relative standard deviation (RSD) was calculated for the signal intensity across each run spanning six minutes. The mean of these calculated RSDs was taken and is reported in the right panel in Figure 4.6. Standard EESI resulted in a mean RSD of 19% and coaxial EESI had a mean RSD of 8%. This represents an improvement of the intra-run RSD of a factor of 2.4. The mean RSD for coaxial EESI is more similar to the 5% RSD observed from a standard ESI experiment with oleic acid.

The spectral fingerprint from the aerosolized pyrolysis products of cellulose may be used to assess the ability of coaxial EESI to ionize the same compounds from a complex mixture
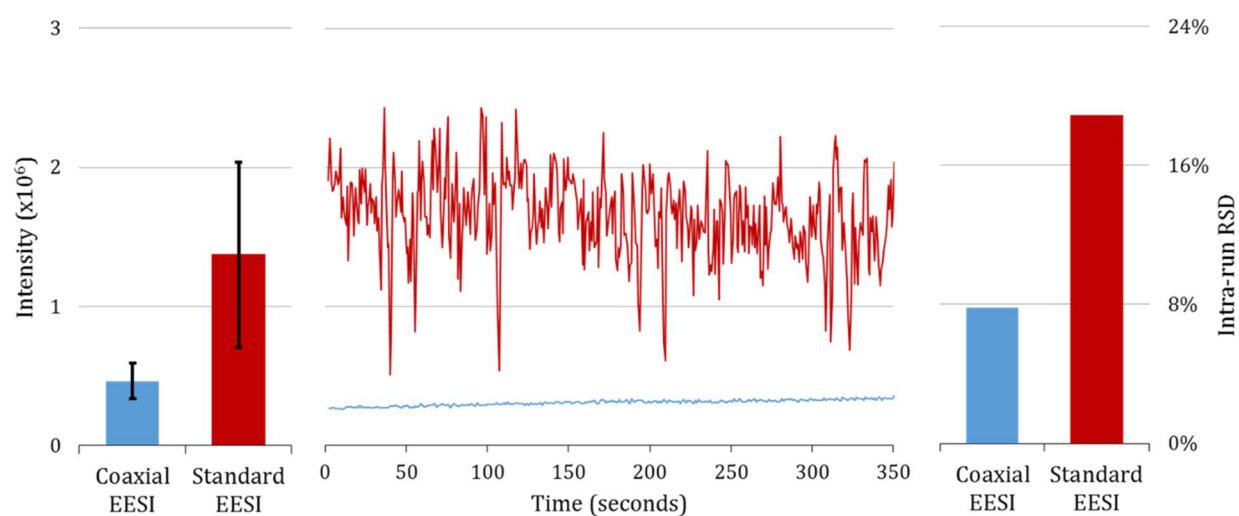
Figure 4.6. Comparison between standard (red) and coaxial (blue) EESI for the study of deprotonated oleic acid aerosol ([M-H]-) from oleic acid aerosol. The left pane is the absolute intensity of each configuration (n=9) after disassembly and reassembly of the configuration. The center pane is a representative trace of the absolute intensity as a function of time for each configuration. The right pane is the average (n=9) of the intra-run relative standard deviations for each trace as a function of time.

compared to standard EESI. A comparison of the spectra obtained from each configuration can be seen in Figure 4.7. The spectral fingerprints obtained using the two configurations are nearly identical with relative intensities varying only slightly. The absolute intensities are very similar for each peak as well, which means there is no loss in sensitivity for this type of analysis using coaxial EESI.

The trace of the total ion signal from each configuration as a function of time can be seen in Figure 4.8. The green trace represents the temperature program with temperatures corresponding to the green y-axis on the right side of the graph. For standard EESI, the change in signal as a function of time is convoluted by the variation in the signal. At the top of the temperature ramp, the aerosol reaches its maximum concentration. This point is not very distinct in the standard EESI trace due to the variation in the signal. The blue trace corresponds to the total ion signal for coaxial EESI in a separate pyrolysis experiment. The average intensity across the length of the experiment using coaxial EESI is similar to the average intensity for standard EESI; however, there is less variation in signal for coaxial EESI than standard EESI. For coaxial EESI, the maximum aerosol concentration at the top of the temperature ramp can be observed more clearly than in standard EESI. The primary difference between standard EESI and coaxial EESI is the geometry between aerosol particles and charged solvent droplets. In standard EESI, the solvent is first nebulized using a nebulization gas. The gas stream carrying charged droplets that orthogonally intersects the gas stream carrying aerosol particles is also affected by the heated dry gas stream which aids in the desolvation of the charged droplets. The intersection of these three gas streams leads to a turbulent interaction at the inlet of the mass spectrometer, which is likely the cause of large variability from scan to scan. Coaxial EESI reduces this turbulent interaction by flowing the aerosol coaxially to the solvent and nebulization gas. It may be possible to improve the overlap of the aerosol particles and the charged solvent droplets. As
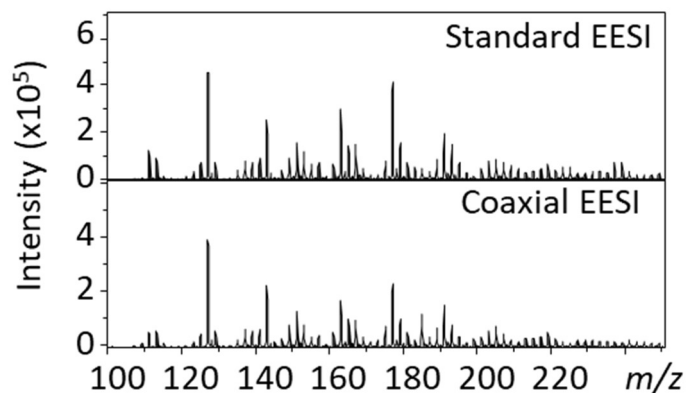
Figure 4.7. Comparison between standard (top) and coaxial (bottom) EESI of the spectra obtained from EESI of the aerosol generated from the pyrolysis of cellulose.
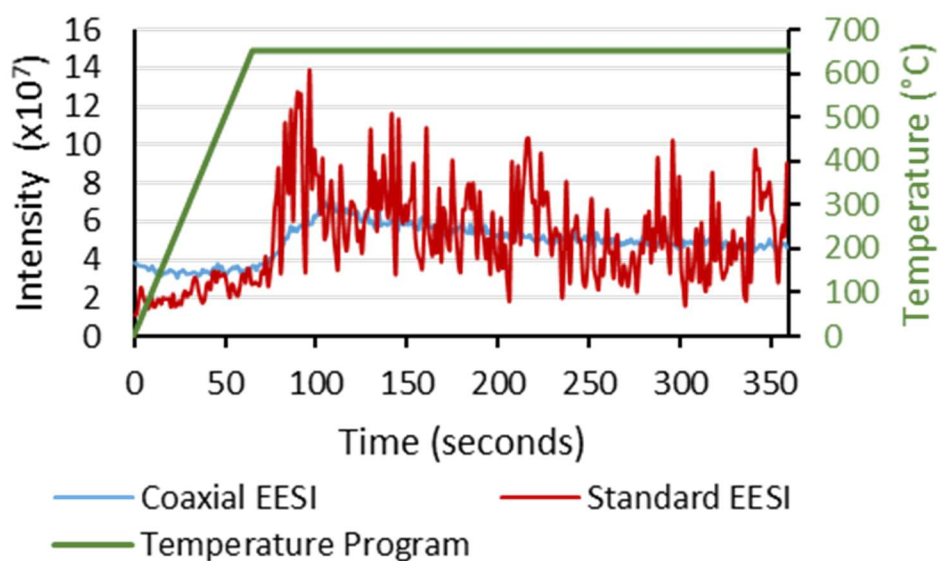
Figure 4.8. Comparison of the total ion chronogram between standard (red) and coaxial (blue) EESI in the study of the aerosol generated from the pyrolysis of cellulose over the course of a pyrolysis experiment. The temperature program (green) is also shown corresponding to the green axis.

aerosol particles tend to follow gas streamlines, particles will tend to move radially away from the charged solvent droplets during electrospray due to gas expansion from the tip of the emitter. This may lead to less efficient mixing, resulting in a decrease in intensity. This challenge can be addressed by improved mixing between the aerosol particles and the solvent droplets. One way to improve mixing would be to alter the configuration shown in Figure 4.3 such that the aerosol-gas flow would expand into the solvent. This would require that the aerosol flows through the central capillary. The primary challenge to be addressed in this method is the conductance limit created by the 0.1 mm central capillary and the pressure that will be distributed throughout the aerosol generation process. Although the central capillary may be enlarged to decrease this effect and increase the aerosol flow, the current design cannot accommodate this. The second method to increase mixing is to alter the tip such that the gas streamlines intersect with the solvent droplets. This could be done by altering the tip (L in Figure 4.4b) to have a twist to cause a vortex motion. Both methods of mixing have the potential to increase sensitivity.

4.4.   Thermo-coaxial EESI

A few issues arise when using the coaxial EESI emitter with non-Bruker instruments. One problem is that the emitter has the incorrect form factor for use with the existing source housing. For use, the source housing must be removed and safety interlocks must be overridden for the high voltage to be applied. A second problem is that the device was originally designed and tested on an instrument that applies the voltage to the MS inlet capillary, while the emitter rests at ground potential. This is abnormal for instrument manufacturers as the emitter is typically held at high voltage and the MS inlet capillary rests near ground potential. To use the device described in Section 4.3 on a non-bruker instrument, the coaxial device must be electrically isolated from a clamp and stand so that the position of the device may be altered while in operation and to avoid a short circuit.

Multiple holders were designed and 3D printed, but the one that worked best was a simple

cylindrical collar to slide over the ZDV fitting (Figure 4.4A) at the top of the device for a

clamp to hold. A Polylactic acid (PLA)/wood composite was used to print the collar as it was

found to have good insulating properties for high voltages. The coaxial EESI device with the

insulating collar is shown in Figure 4.9. The aerosol generator must also be isolated from

the device. For use with the Pyroprobe, the output of the aerosol was connected to a PEEK

union which electrically isolated the Pyroprobe from the tube that was threaded into the

coaxial EESI device. This configuration was successfully used with a Thermo Scientific

LTQ-FT (linear trap quadrupole - fourier transform ion cyclotron resonance) mass

spectrometer to sample from an aerosol of pyrolyzed cellulose or pyrolyzed tobacco, but

reproducibility of sprayer placement was difficult. Additionally, an external nebulization

gas source was required because the LTQ-FT supplies gases through the source housing,

which was removed for this analysis.

A coaxial EESI device that used the existing source housing was desired to improve

reproducibility and simply setup for analysis using the LTQ-FT. One way this could be

accomplished is by using an existing Ion Max Heated-ESI (HESI) probe (Thermo Scientific,

97055-60140). For the Ion Max ESI probes, two gas inlets are used to deliver gas separately

to the electrospray tip of the probe. Sheath and auxiliary gases function to nebulize and

focus the electrospray plume, respectively. These two channels are analogous to the

concentric capillaries in the coaxial EESI emitter, thus aerosol could be introduced to one of

the channels during direct infusion of a clean solvent to form ions from an aerosol.

The use of the HESI probe with the Ion Max ESI source housing in place to do coaxial

EESI was termed thermo-coaxial EESI because of the instrument manufacturer as well as
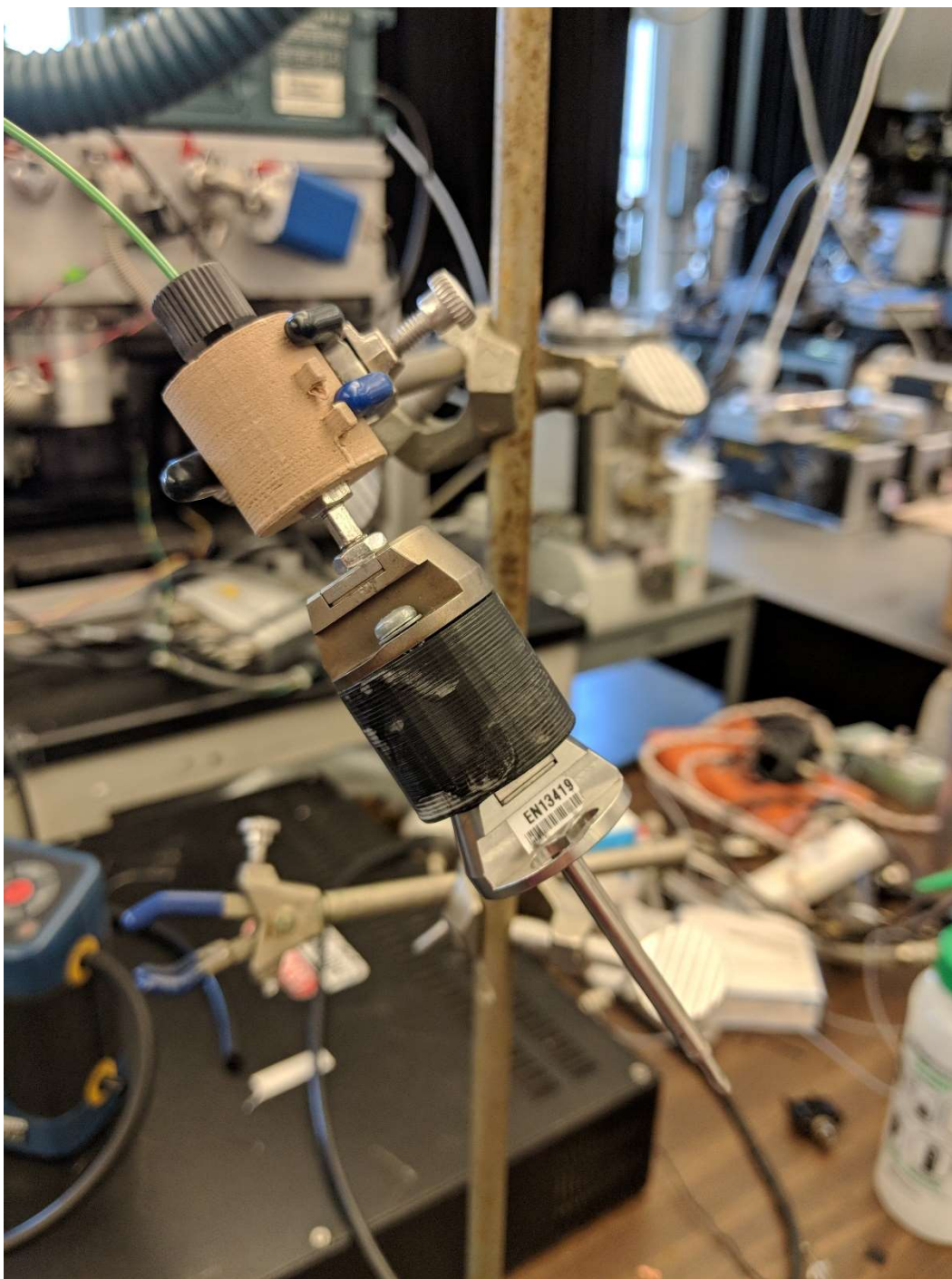
Figure 4.9. Picture showing coaxial EESI insulated from the clamp by a 3D printed collar (brown).

the ability to heat the probe during aerosol analysis. In a similar configuration as discussed in Section 4.2, the solvent was delivered through a central capillary, nitrogen was flowed through the sheath gas inlet, and aerosol was piped into the auxiliary gas inlet. Isolation from the high voltage is provided by the original probe design, so no precautions were taken to manually isolate the aerosol generator. Analysis of an oleic acid aerosol using the COA was successfully performed as shown in Figure 4.10. In this experiment, the COA was turned on and off for the time range highlighted in green on the inset chronogram in Figure 4.10, and the rise and decay of signal for [M-H]$^-$ for oleic acid was observed in black. The heating capabilities of thermo-coaxial EESI were evaluated, but no signal corresponding to the aerosolized analyte was observed at temperature settings greater than 150 °C. A temperature setting of 50 °C improved signal intensity, likely due to improved desolvation, but the experiments presented here were performed with the heater set to off.

The purpose of using coaxial EESI on the LTQ-FTICR instrument was to obtain accurate mass information on the pyrolysis of cellulose and related natural polymers. Such an approach would yield a mass spectrum with resolved isobars and allow molecular formula assignment to each peak. The LTQ-FT allows easy switching between the mass analyzers without modification to the ion source. One primary difference observed between the two modes of operation is that the FT-ICR heavily biases against the transmission of ions of m/z less than 200, which yields a slightly different distribution of ions. This difference could be problematic in a quantitative analysis, but with sufficient signal intensity, an accurate mass may be assigned to each peak.

Thermo-coaxial EESI was compared to standard EESI for the analysis of the aerosol generated form pyrolyzed cellulose. Two photographs are shown in Figure 4.11 where
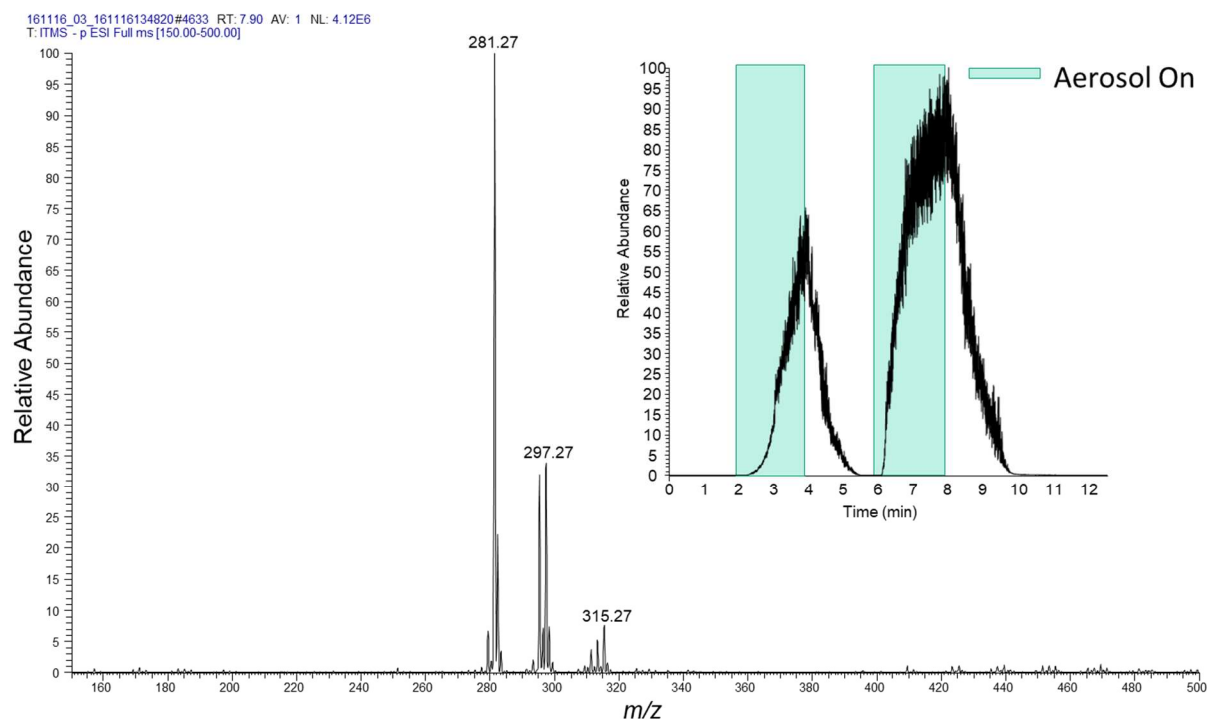
Figure 4.10. Mass spectrum of deprotonated oleic acid ([M-H]⁻) analyzed by thermo-coaxial EESI. The inset chronogram shows the signal response as aerosol is introduced to the source.
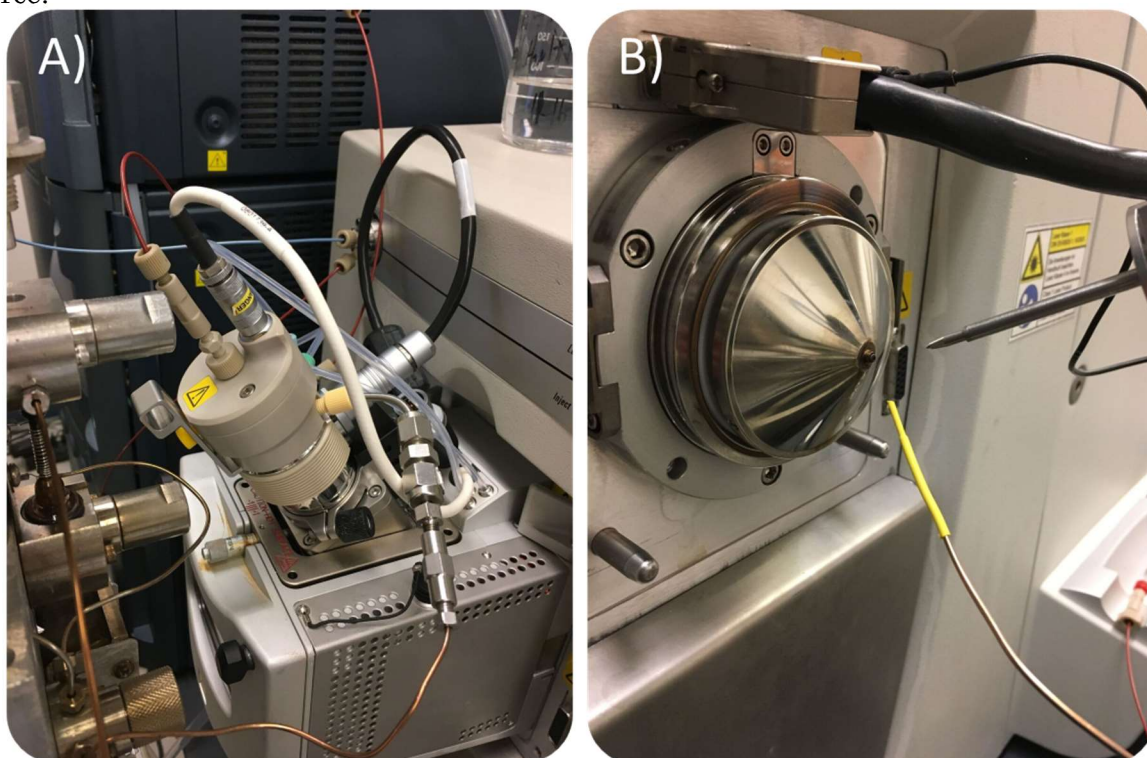
Figure 4.11. Pictures showing A) thermo-coaxial EESI in operation and B) standard EESI in operation on the Thermo Scientific LTQ-FTICR mass spectrometer.

thermo-coaxial EESI is used with the source housing intact (Figure 4.11A) and standard

EESI is used with the source housing removed (Figure 4.11B). For thermo-coaxial EESI,

the aerosol was input into the auxiliary gas port and the instrument's sheath gas was piped

into the sheath gas port. In standard EESI, the 3D printed collar was used with an Agilent

ESI emitter so that the high voltage can be applied to the emitter isolated from the stand. A

custom electronics connector was used to connect from the high voltage connection on the

instrument to an alligator clip that clipped onto the emitter. The Pyroprobe was

electronically isolated using the PEEK connector described above and by placing a small

sleeve of shrink wrap onto the end of the metal tube to avoid charging of the metal. The

solvent used was a mixture of 1:1 methanol and water with 1% formic acid added by

volume. The results using the ion trap are shown in Figure 4.12. The two spectra are

similar both in ion distribution as well as overall intensity. An inset in each spectrum is

given that shows the total ion chronogram over the course of the pyrolysis experiment. The

signal is much more stable in thermo-coaxial EESI over standard EESI which was expected

from the results of coaxial EESI discussed above.

Ion generation is the same regardless of the mass analyzer, so the results when using

the FT-ICR for mass analysis, shown in Figure 4.13 corroborate the results when using the

ion trap, shown in Figure 4.12. The ion distribution is shifted toward larger masses, but

there is enough ion signal to obtain useful information from the lower mass ions. The

spectra are similar, but the inset total ion chronogram shows that the signal is more stable

for thermo-coaxial EESI than standard EESI. Only one decimal place is shown for each

mass for simplicity, but the data is accurate to 5 ppm, per instrument specifications. The

signal stability is further demonstrated by three replicate selected ion chromatograms at
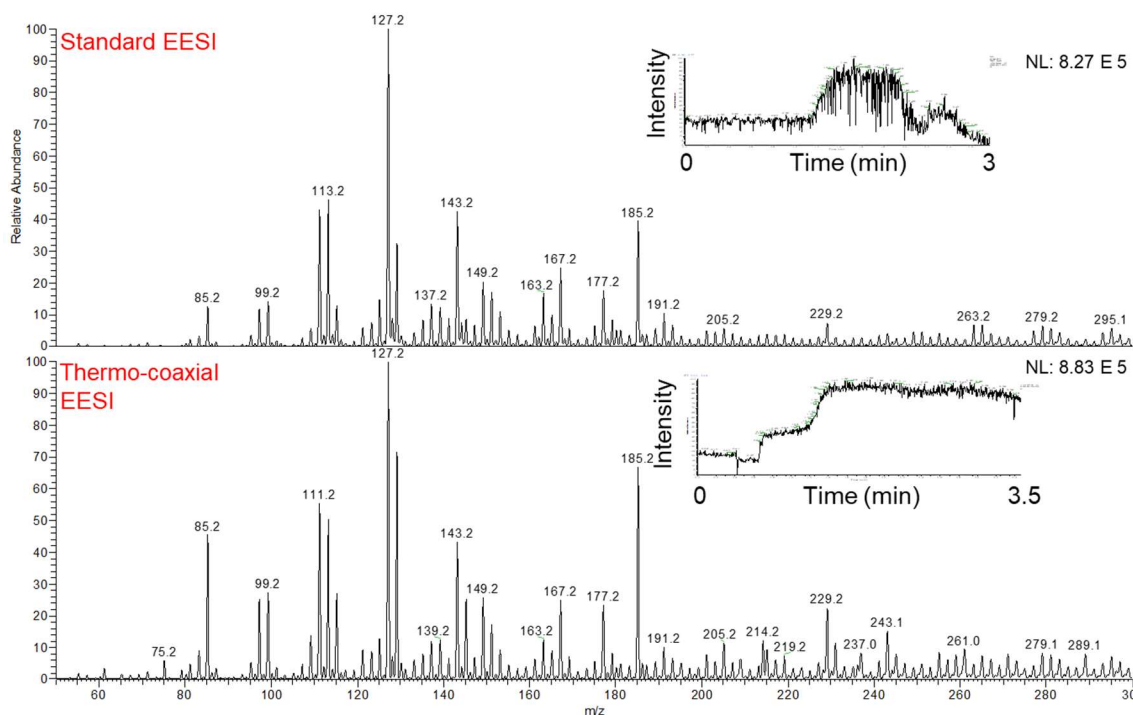
Figure 4.12. Mass spectra comparing standard and thermo-coaxial EESI using the LTQ mass analyzer.
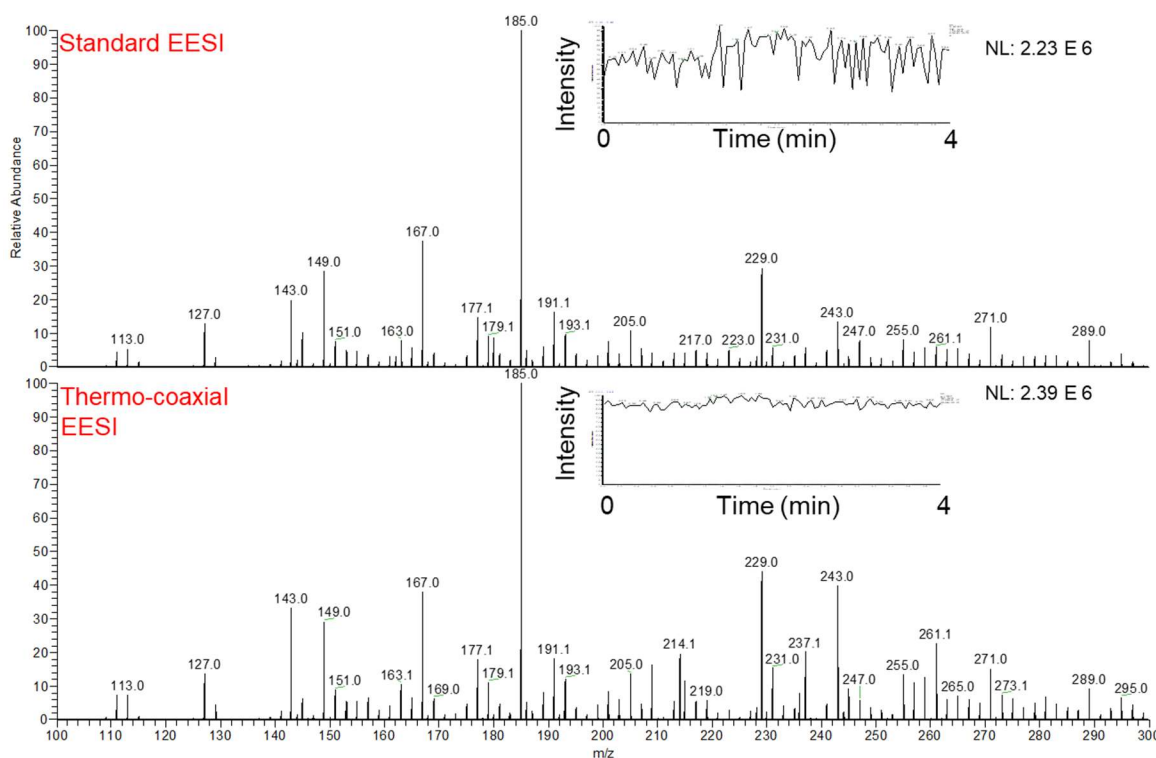
Figure 4.13. Mass spectra comparing standard and thermo-coaxial EESI using the FT-ICR mass analyzer.

m/z 185, sodiated levoglucosan, over the course of a pyrolysis experiment using standard EESI (Figure 4.14A) and thermo-coaxial EESI (Figure 4.14B).

We can also use FT-ICR to observe isobaric species in the aerosol generated from pyrolyzed cellulose. Three ion populations are present at m/z 163 as shown in Figure 4.15A. In a spectrum collected using an ion trap mass spectrometer, these three isobaric peaks would not be resolved. Molecular formulas were assigned based upon the closest molecular formula match allowing only carbon, hydrogen, and oxygen as possible atomic composition because cellulose pyrolysis should only form compounds that contain those atoms. In Figure 4.15B, the red and blue traces follow a typical pyrolysis pattern where the intensity reaches a maximum at the top of the temperature ramp then decays. The green trace follows an opposite pattern, where the intensity decreases as the red and blue ions increase in intensity which suggests the ions represented by the green trace is a contaminant in the solvent.

Thermo-coaxial EESI has been demonstrated as a method to analyze an aerosol by EESI on an instrument with an Ion Max ESI source. This method improves upon standard EESI on the same instrument by improving reproducibility and simplicity of setup. Thermo-coaxial EESI can be operated with the source housing intact, leaving no high voltages exposed. Further, a similar signal intensity was observed when using both standard EESI and thermo-coaxial EESI. No carry-over effects were noticed and a few milliliters of solvent was used to rinse through the auxiliary gas port after use. No modifications to the existing HESI probe were required, and setup was as simple as exchanging the probe. There is no particular reason the HESI probe is necessary for thermo-coaxial EESI unless further heating studies were of interest. The standard ESI probe should suffice.
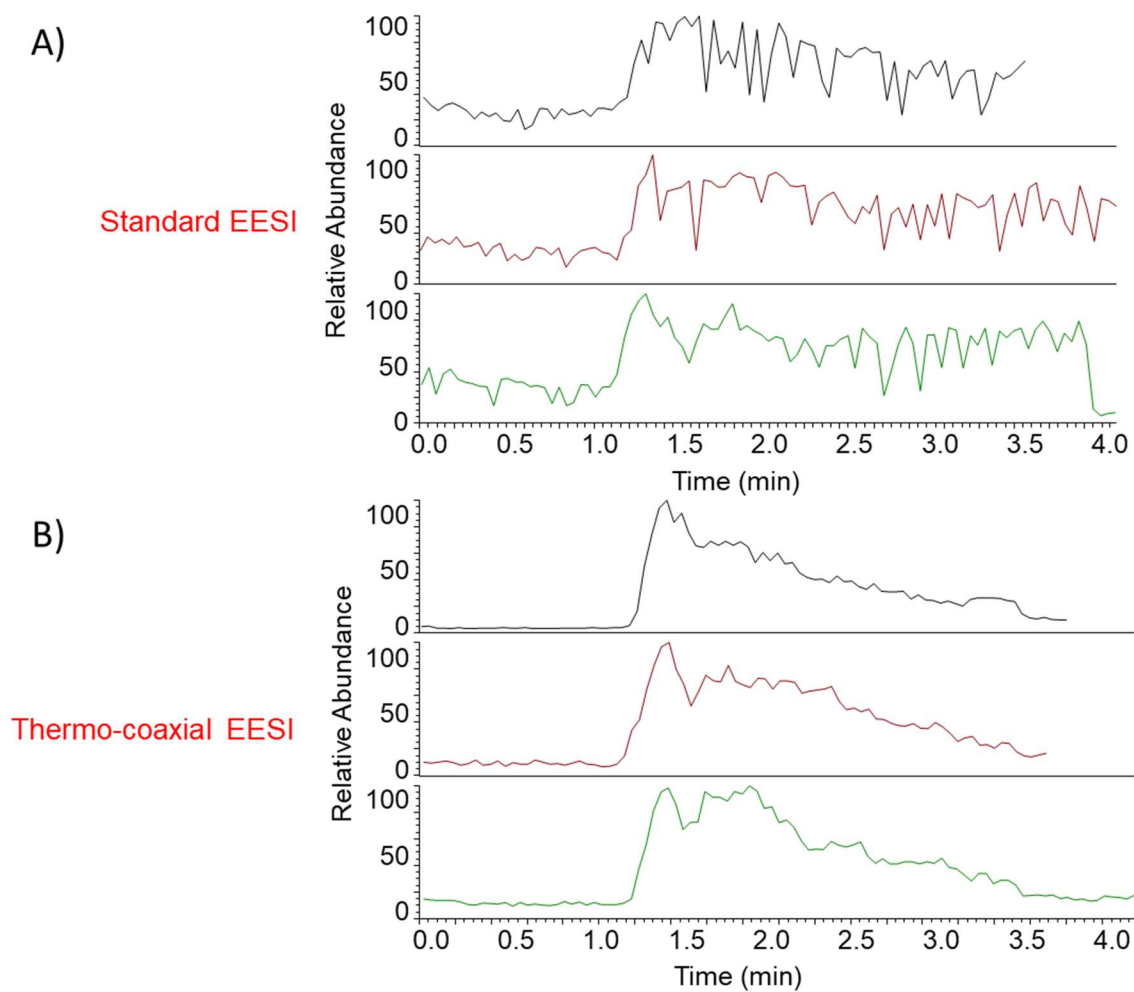
Figure 4.14. Chronograms of three replicate runs tracing *m/z* 185 during the analysis of the aerosol generated from the pyrolysis of cellulose using A) standard EESI and B) thermo-coaxial EESI.
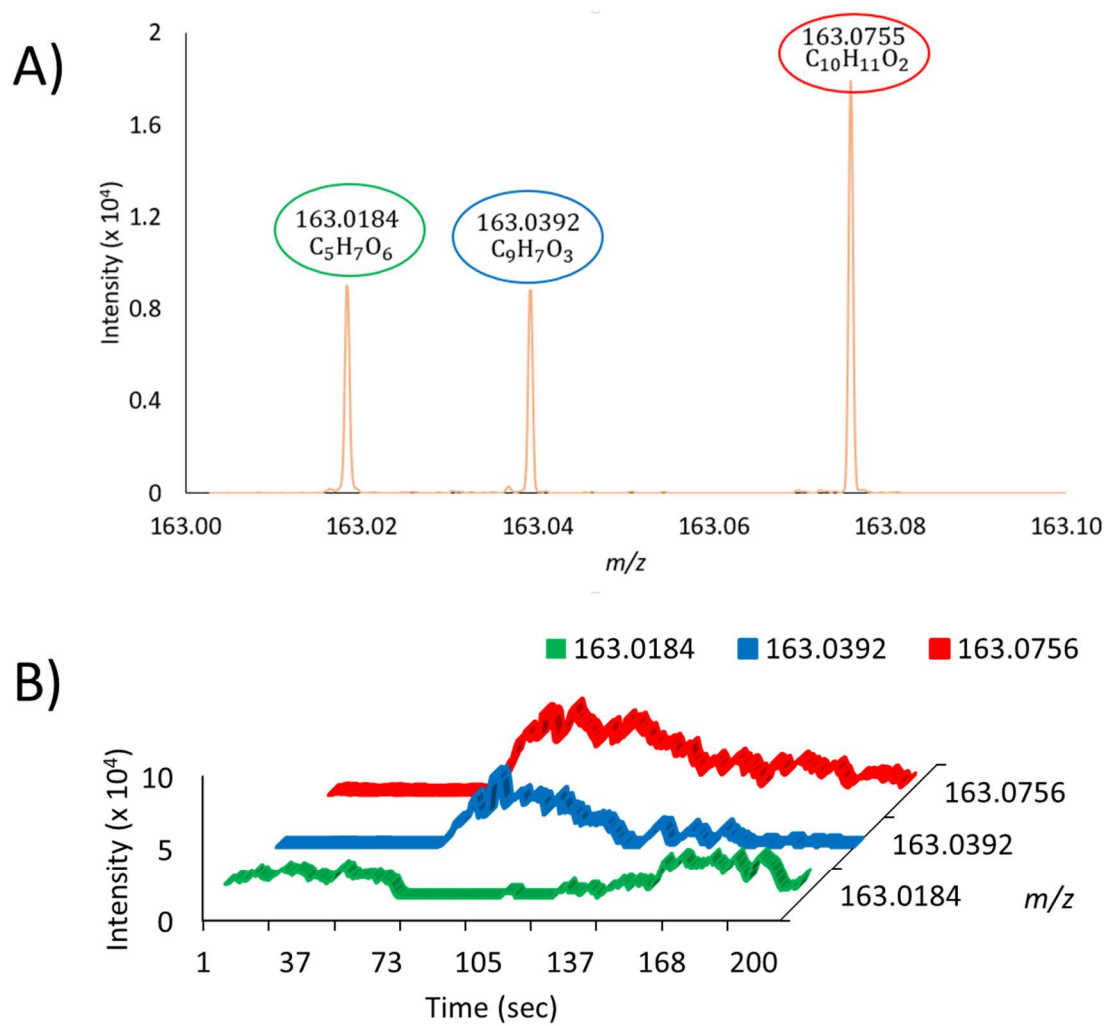
Figure 4.15. Accurate mass spectra of *m/z* 163 using the FT-ICR shown as A) single spectrum and B) time-resolved spectrum.

4.5.   Solvent Composition

One of the primary benefits of EESI over other ambient ionization techniques such as LTPI is the ability to change the solvent to affect extraction of compounds from an aerosol. In Chapter 3, solvent additives were shown to enhance ionization by using metal salts. Solubility of the analyte in the electrospray solvent is a primary factor to extraction in EESI, but no such study has been performed for the analysis of an aerosol by EESI[18]. Coaxial EESI was used for these studies for improved reproducibility and simplicity of setup on a Bruker Esquire ion trap mass spectrometer. Binary mixtures of water, methanol, acetonitrile, chloroform, toluene, and dichloromethane were tested as electrospray solvents for EESI with a formic acid additive at 1% by volume. Each solvent mixture was used for the analysis of the aerosol generated from pyrolysis of cellulose.

The mass spectra observed for each electrospray solvent are shown in Figure 4.16. The signal intensity of the base peak was greatest for the methanol, acetonitrile/methanol, and water/methanol mixtures. The signal intensity decrease in the base peak for water as the electrospray solvent compared to methanol and water/methanol is likely due to poor desolvation. The base peak when acetonitrile was used as the electrospray solvent was two orders of magnitude lower in signal intensity than the base peaks in methanol, acetonitrile/methanol and water/methanol. Toluene, chloroform, and dichloromethane were used as mixtures in methanol rather than water because of immiscibility of the solvents in water. The distribution and relative intensities of the peaks observed in the mass spectrum varied widely between solvents. To determine the number of peaks in the mass spectrum observed for each solvent composition, three replicate runs using each solvent mixture were compared. Only odd m/z peaks were counted because any protonated monoisotopic compound produced from cellulose pyrolysis has an odd m/z. To reduce noise in the data,
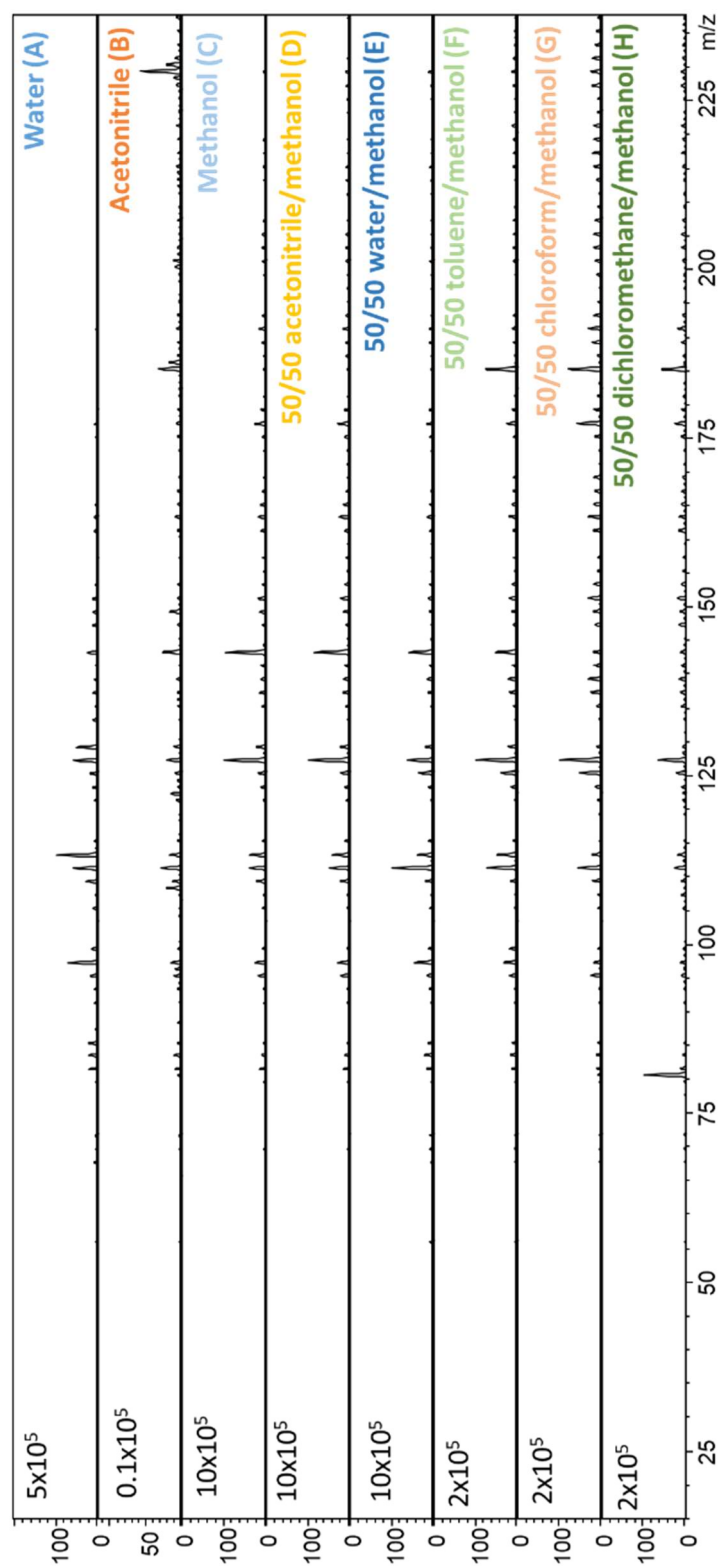
Figure 4.16. Mass spectra of the aerosol generated from the pyrolysis of cellulose ionized by coaxial EESI using different solvent compositions.

only peaks that were above 5% of the base peak intensity and were present in at least two of the three replicates were counted.

A summary of the peaks in the mass spectrum from the aerosol generated from pyrolysis of cellulose and analyzed by coaxial EESI is presented in Figure 4.17. The inset figure shows the total number of peaks counted in each solvent mixture given the data filtering criteria. The most total peaks were observed in acetonitrile/methanol (86 peaks), water/methanol (101 peaks) and toluene/methanol (94 peaks). Unique peaks were observed in toluene/methanol (7 peaks), dichloromethane/methanol (3 peaks), and acetonitrile (2 peaks). Interestingly, no unique peaks were observed in either water or methanol, but five unique peaks were observed in the water/methanol mixture. The histogram in Figure 4.17 describes how the peaks are shared among the solvent mixtures used in this study. The labels on the x-axis of the main figure correspond to the solvent labels on the x-axis of the inset figure. For example, twenty peaks are observed in all eight of the solvent mixtures as described by the left-most bar. Both graphs describe a total coverage of 113 peaks observed among all solvent compositions.

One of the key benefits to using EESI is the ability to easily change the solvent to extract different compounds in the aerosol. Practically, this is done by exchanging the solvent in the syringe for a different solvent mixture without altering the source arrangement in any way. For the analysis of the aerosol generated by the pyrolysis of cellulose by coaxial EESI, multiple solvent compositions could be used during a single analysis to obtain greater coverage of compounds present in the aerosol. According to Figure 4.17, a multiple solvent system of water/methanol and toluene/methanol gives the best coverage of the peaks (108 of 113) observed during pyrolysis.
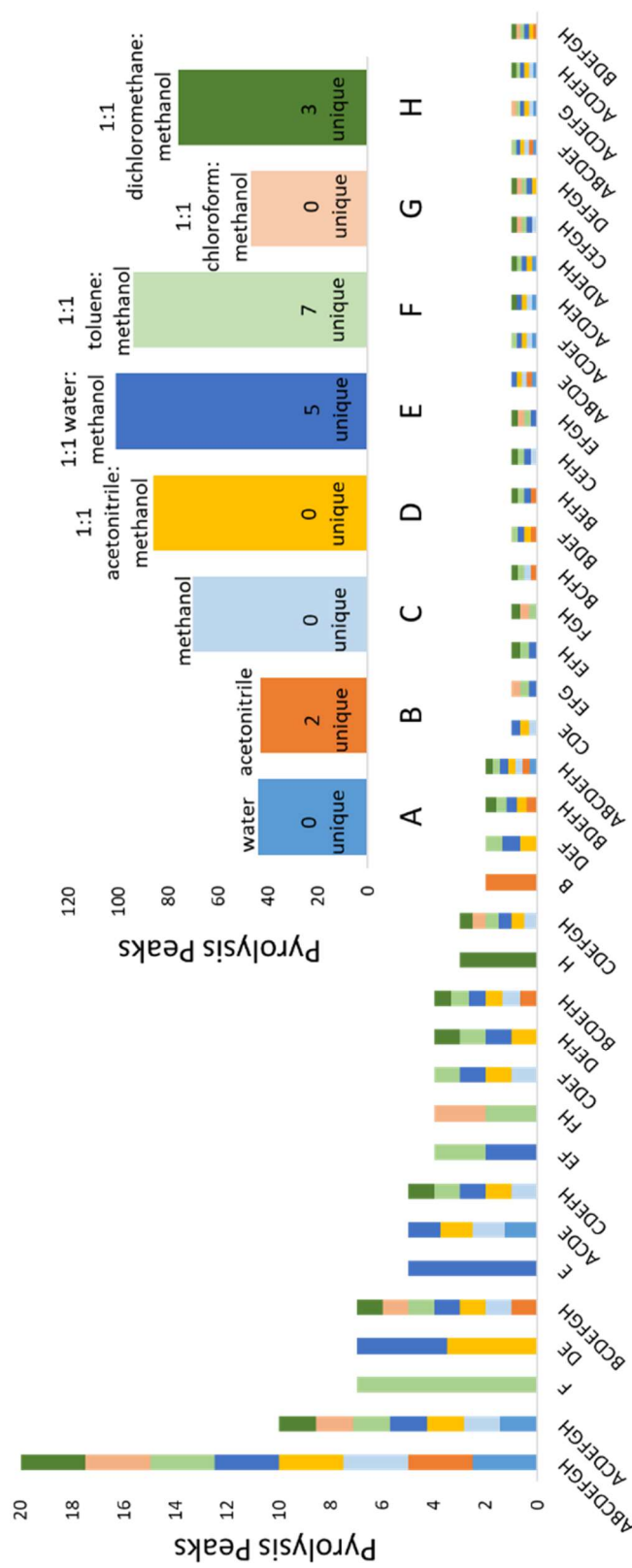
Figure 4.17. Histogram of peaks observed in the analysis of the aerosol generated from the pyrolysis of cellulose using coaxial EESI with different solvent compositions. The inset bar graph shows the total number of peaks observed for each solvent composition.

4.6.   Port Switching

As mentioned briefly in Section 4.3, the mode of coaxial EESI operation used involved input of the aerosol into the outermost capillary in the coaxial EESI emitter as shown in Figure 4.3. This configuration was chosen because of the mechanical stress that the aerosol generator places on the device. It was more appropriate to thread the output of the Pyroprobe into the bottom emitter of coaxial EESI (Figure 4.4K) because that emitter could be stabilized to the source housing with screws, placing the weight of the aerosol generator on the source housing rather than the emitter. Initial testing was done to determine if this mode of operation was sub-optimal, and preliminary results using aerosolized levoglucosan determined no difference in signal between the mode of operation described above and the mode which inputs the aerosol into the top emitter (Figure 4.4F) and the nebulization gas into the bottom emitter (Figure 4.4K). During testing of the second mode of operation, the coaxial EESI device was snapped in half at the 20 gauge needle (Figure 4.4G). When the device was repaired, plastic support was added to the device (Figure 4.4H) to provide mechanical stability, but the aerosol output was exclusively used in the outermost capillary for the majority of experiments presented in this chapter.

The plastic support in Figure 4.4H was made by cutting a 15 mL Falcon centrifuge tube to fit the gap between the two emitters (Figure 4.4F and K). Other supports were also added directly around the 20 gauge needle for protection as seen in Figure 4.18A. This support provided enough mechanical stability to support the nebulization gas input and solvent input. To more thoroughly explore the possibility of using this device in other modes, improvements to the structural stability of the device were necessary. Most notably, the plastic support (Figure 4.4H) was replaced with a 3D printed support that was sized adequately and allowed the top emitter (Figure 4.4F) to be secured into the 3D printed support with set screws. The improved device is shown in Figure 4.18B. The model
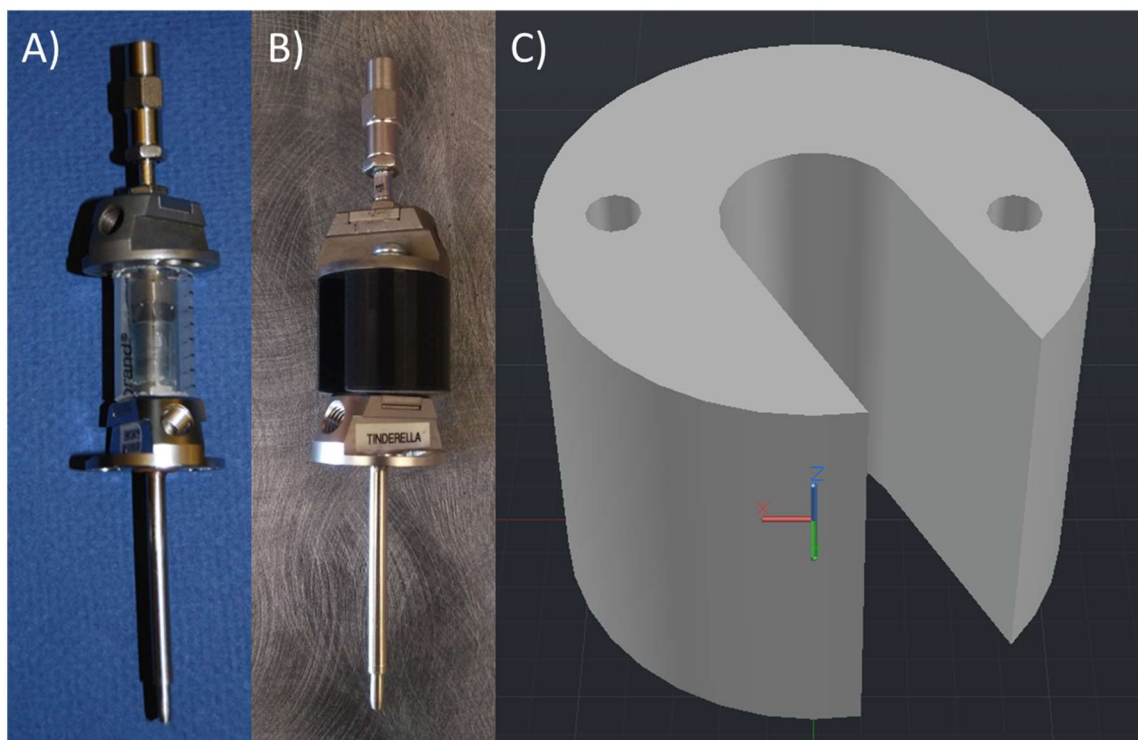
Figure 4.18. Pictures of the coaxial EESI device A) originally, B) after reinforcement, and C) an AutoCAD drawing of the plastic support.

of the improved support generated in AutoCAD is displayed in Figure 4.18C. The primary features of this design is the center cutout that allows the support to be placed onto the device without disassembly of the coaxial EESI emitter. The printed holes are positioned to allow the top emitter to secure into the 3D printed piece as it typically would secure to the source housing during standard operation. The open central cutout also allows unimpeded view of the 20 gauge needle and the silver-soldered joint for occasional inspection, a benefit that was not possible using the original plastic supports.

Using the reinforced coaxial EESI emitter, studies were carried out to determine if there was a difference in ionization from aerosol particles between the normal mode of operation where the aerosol is input into the bottom emitter and the inverted mode of operation, where the aerosol is piped into the top emitter. The effect of solvent flow rate was also assessed for each mode of operation for the analysis of the aerosol generated during pyrolysis of cellulose. The extracted ion chromatogram (EIC) for the most prominent peak in most cellulose pyrolysis spectra (*m/z* 127) is shown in Figure 4.19 for each set of conditions. Generally, the normal mode of operation gives about threefold better signal intensity than the inverted mode of operation. Further, increasing the solvent flow rate causes a twofold decrease in signal intensity. The normal mode of operation is confirmed to be at least as sensitive, if not more sensitive, as the inverted mode.

4.7. Effect on the Chemistry of Ion Formation

4.7.1. Analysis of Aerosolized Proteins by EESI

Although many of the differences between standard and coaxial EESI can be explained by improved fluid dynamics and reproducible geometry, some differences between the two sources have been observed that suggest the mechanism of ion formation is different
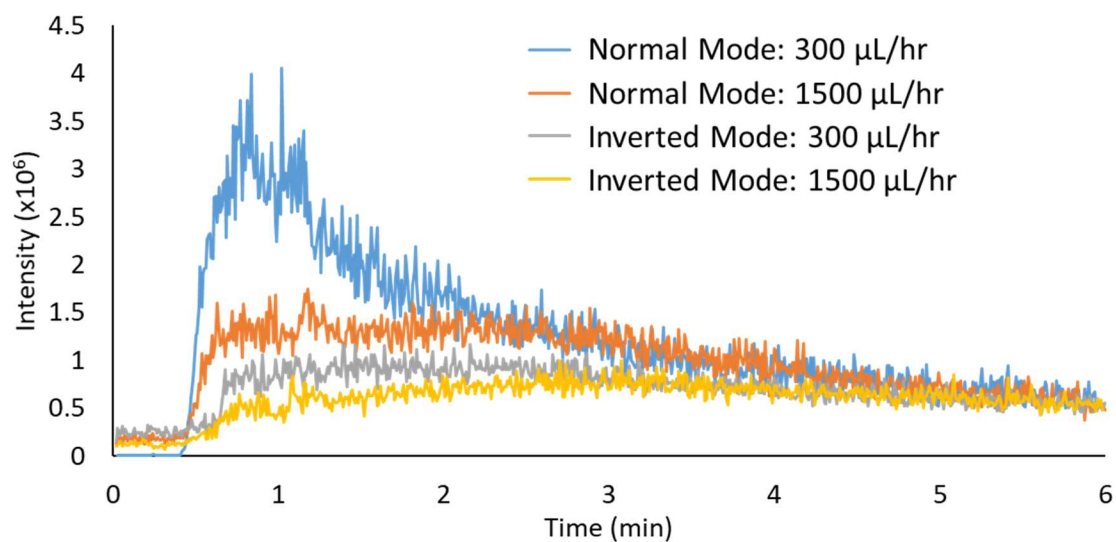
Figure 4.19. A chronogram of the analysis of the aerosol generated from the pyrolysis of cellulose using coaxial EESI in different modes of operation and at different flow rates.

between the two ionization sources. One such difference involves the ionization of protein from an aerosol generated using the COA. Typical COA operation requires a volatile solvent such as methanol for the aerosol solution; however, for protein solubility, 10% water was added to a solution of methanol and 100 μg/mL of protein. To demonstrate that an aerosol is formed, an aerosol size distribution is shown in Figure 4.20. The mean particle diameter for the lysozyme aerosol is 55 nm. For the analysis of lysozyme aerosol, a noticeable shift in average charge state is observed between the analysis using standard and coaxial EESI ion sources as shown in Figure 4.20. These mass spectra were taken on the same day using the same aerosol solution and instrument method. For reference, mass spectra of lysozyme analyzed by ESI under three different conditions are shown in Figure 4.21 as well. Lysozyme in the EESI spray solution places lysozyme in an acidic environment in a mixture of equal parts water and methanol. Lysozyme in the aerosol solution has no added acid, but is composed of 90% methanol and 10% water. Standard EESI suggests a lysozyme structure that is highly charged with many accessible sites of protonation. The charge state distribution observed using coaxial EESI suggests a lysozyme structure that looks more similar to nativespray ESI where lysozyme exists in a solvent comprised of mostly water with added ammonium acetate to avoid denaturation[22].

A similar analysis was performed using ubiquitin aerosol under the same conditions as shown in Figure 4.22. Interestingly, the difference between the average charge state using standard and coaxial EESI is small and shows the opposite trend as the lysozyme analysis. Standard and coaxial EESI produce charge state distributions that resemble a highly charged, denatured protein. These charge states are also observed in ESI of ubiquitin from the EESI solution and the aerosol solution. Nativespray ESI of ubiquitin produces low charge states, indicative of a protein in a native conformation. It was expected that
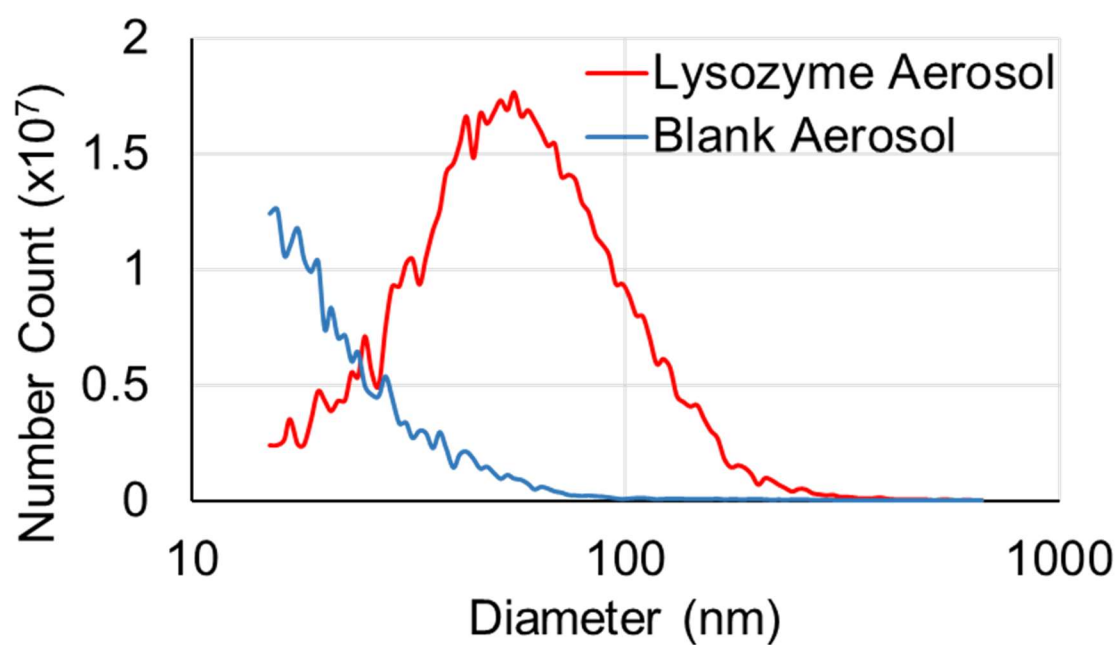
Figure 4.20. Aerosol size distribution of a blank aerosol and an aerosol containing lysozyme.
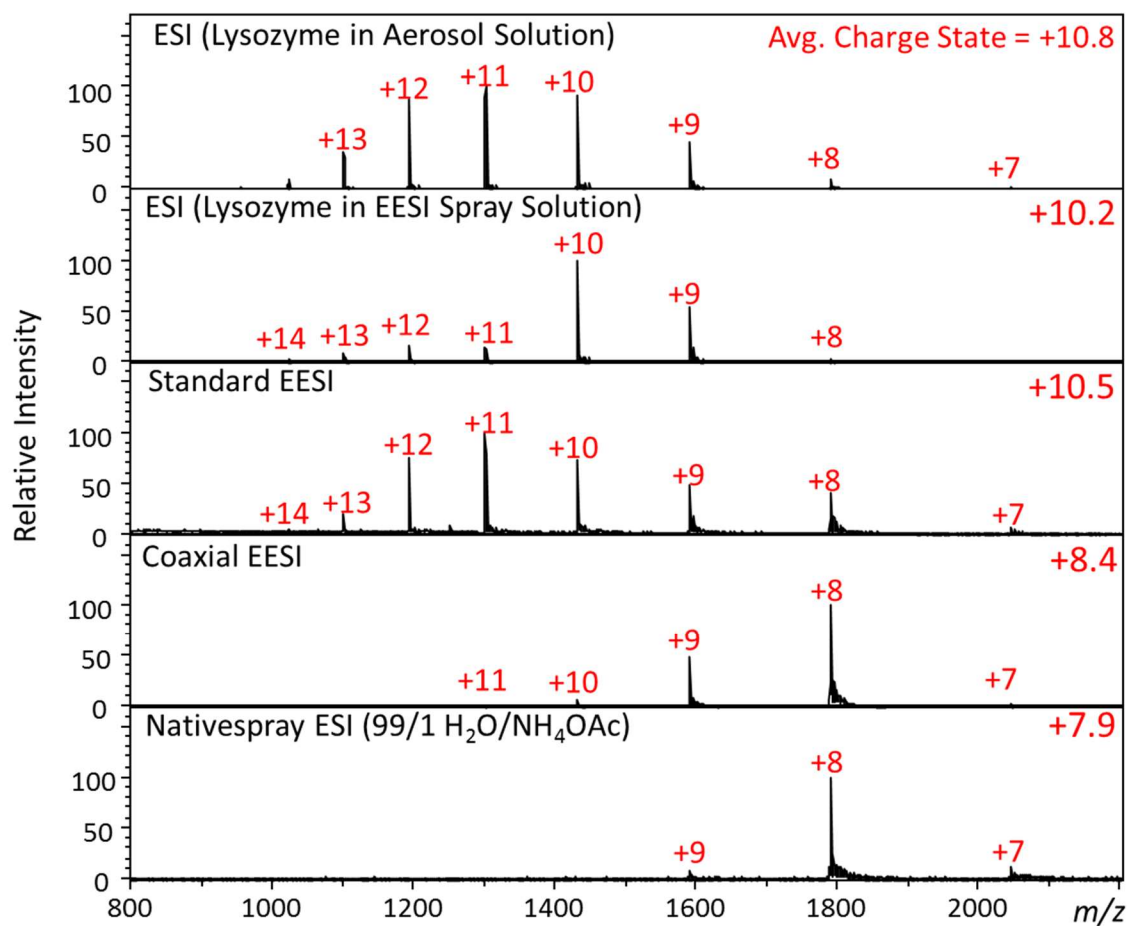
Figure 4.21. Analysis of lysozyme using different ionization techniques.
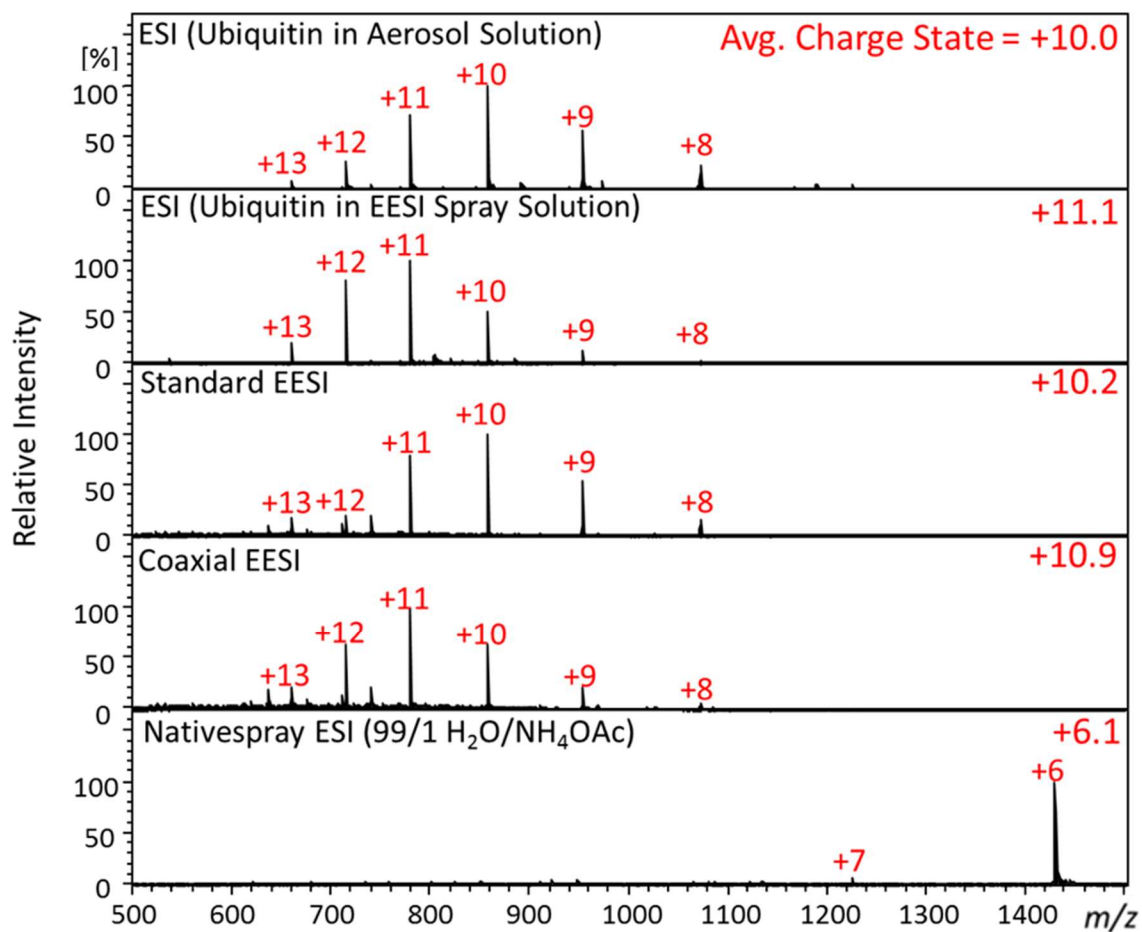
Figure 4.22. Analysis of ubiquitin using different ionization techniques.

ubiquitin analyzed by coaxial EESI would resemble the nativespray ESI charge state distribution based upon the lysozyme results, but the results were contradictory.

The electrospray solvent is a crucial part of EESI; however, it is not necessary for the ionization of proteins from an aerosol using a coaxial EESI emitter. For lysozyme aerosol analyzed by standard EESI, the results when the electrospray solvent is removed are shown in Figure 4.23. In this experiment, the syringe pump that forces solvent through the emitter was stopped, and the syringe plunger was pulled backwards to ensure no solvent was in the solvent line. No signal for lysozyme aerosol was observed in this case. For the same lysozyme aerosol analyzed using the coaxial EESI emitter, the results are very different as shown in Figure 4.24. The same procedure was followed from the standard EESI analysis to ensure no solvent was in the solvent line. No signal intensity is lost, and no change in the charge state distribution is observed. The presence of a charge state distribution with no solvent present suggests that ionization can occur without the assistance of an electrospray solvent as suggested by the similarity of the two spectra in Figure 4.24. Although not shown, direct ionization from the aerosol particle also occurs in the analysis of ubiquitin using the coaxial EESI emitter. No change in the spectra is observed when the electrospray solvent is removed.

4.7.2. Analysis of Aerosolized Small Molecules using EESI

Another difference between coaxial and standard EESI is observed in the metal cationization of levoglucosan. As discussed in Chapter 3.2, using standard EESI, the addition of lithium acetate to the electrospray solvent can enhance the analysis of levoglucosan by improving sensitivity. This is not the case when using coaxial EESI for metal cationization. As shown in Figure 4.25, signal intensity of lithiated levoglucosan (*m/z*
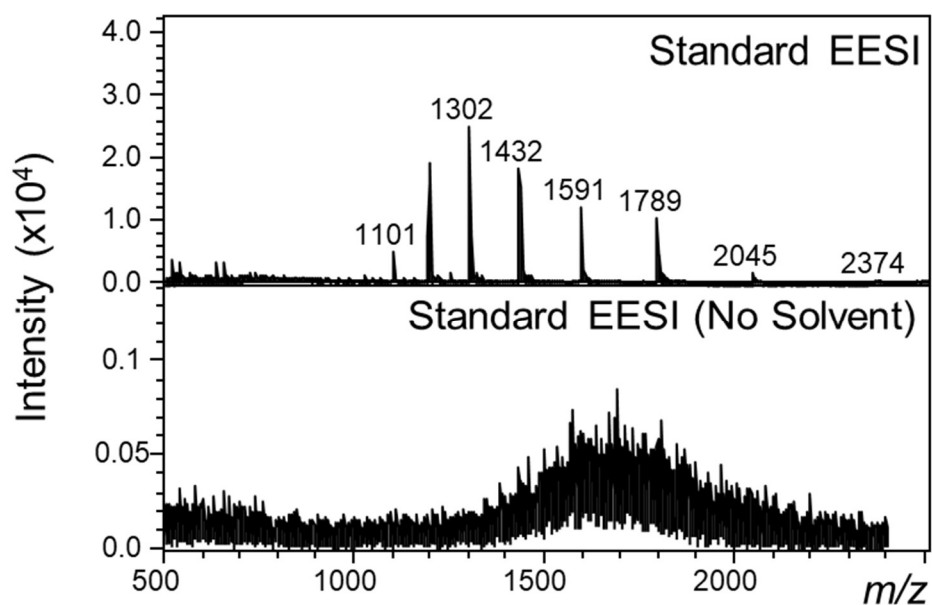
Figure 4.23. Mass spectra of lysozyme from an aerosol analyzed by standard EESI with and without the use of an electrospray solvent.
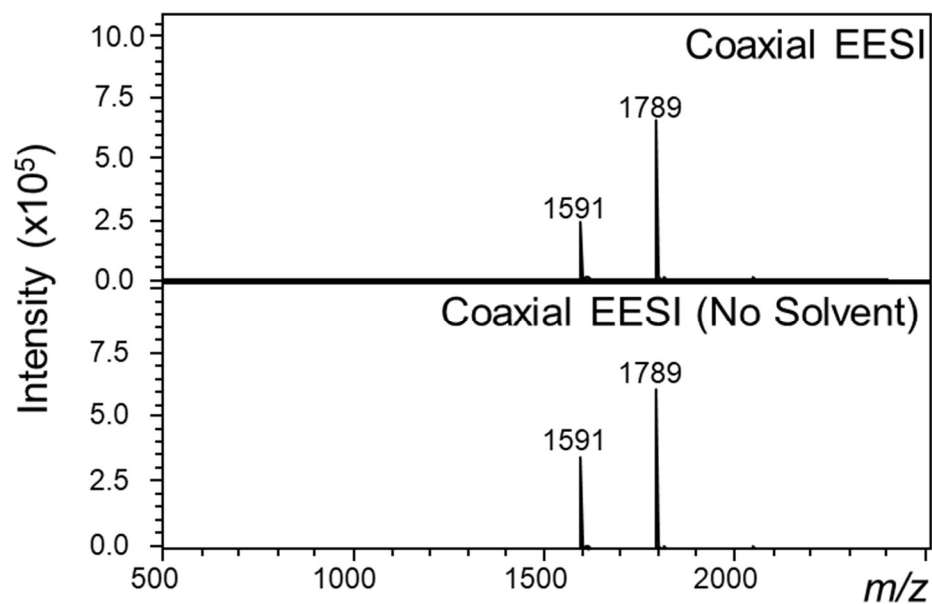
Figure 4.24. Mass spectra of lysozyme from an aerosol analyzed by coaxial EESI with and without the use of an electrospray solvent.
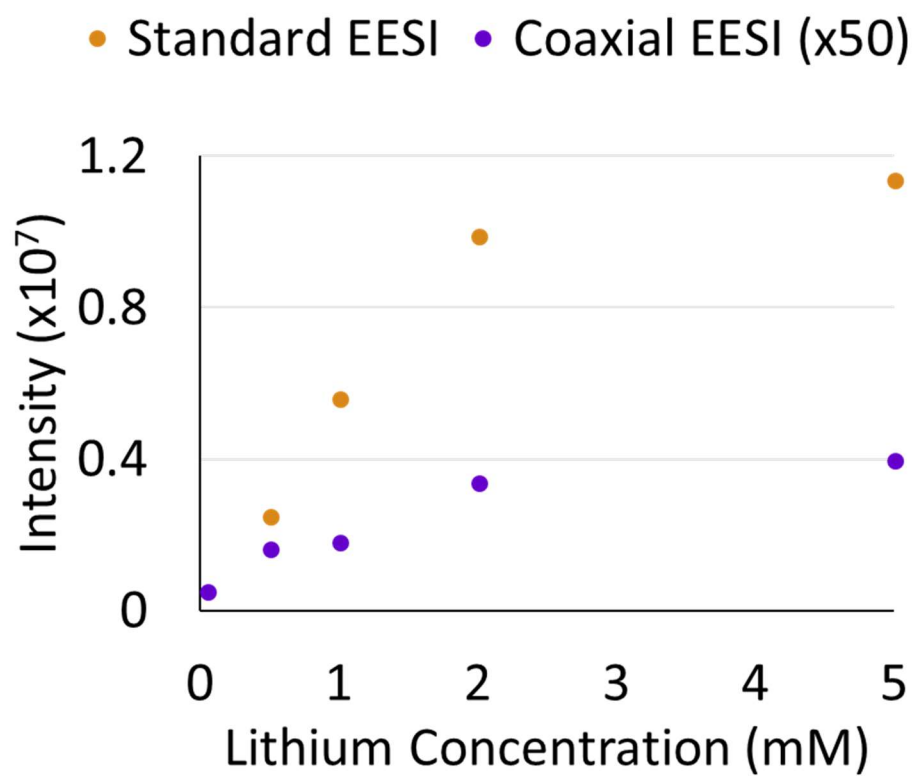
Figure 4.25. Comparison of the response of lithiated levoglucosan, *m/z* 169 to the addition of lithium to the electrospray solvent in both standard and coaxial EESI.

169) is observed as the concentration of lithium is increased using both ion sources. Notice the signal for coaxial EESI has been magnified 50 times. The trend as lithium concentration is increased is the same, but cationization efficiency for coaxial EESI is two orders of magnitude lower than standard EESI. A difference in ionization efficiency was observed in the left pane of Figure 4.6 as well for the analysis of deprotonated oleic acid (m/z 281), but to a lesser degree. The ionization efficiency during pyrolysis is not different between standard and coaxial EESI as shown in Figure 4.8. The dependence on aerosol composition and phase on ionization efficiency in coaxial EESI is an area of research that needs to be explored.

In an effort to compare to the results in Section 4.7.1, multiple small molecules were analyzed by coaxial EESI to determine the dependence of ionization on the electrospray solvent. For both the analysis of deprotonated oleic acid and protonated or metal cationized levoglucosan, no signal was observed when the electrospray solvent was removed, even when the aerosol solution contained 10% water. As shown in Figure 4.26, no signal was observed in the analysis of the aerosol generated from the pyrolysis of cellulose using the coaxial EESI emitter with no solvent. Small molecule analysis in aerosols by EESI is highly dependent on having an electrospray solvent for ionization to occur.

4.8.   Summary and Conclusions

In this chapter, the fabrication and testing of a novel design for extractive electrospray ionization of compounds from aerosol particles was described. The resulting coaxial EESI device improves upon the instability of signal inherent in EESI. The two primary factors this design addresses are reproducibility of the interaction between aerosol particles and charged solvent droplets from electrospray and reduction of turbulence caused by the intersecting nebulizing gas and aerosol transport gas flows. Both factors contribute to inter-
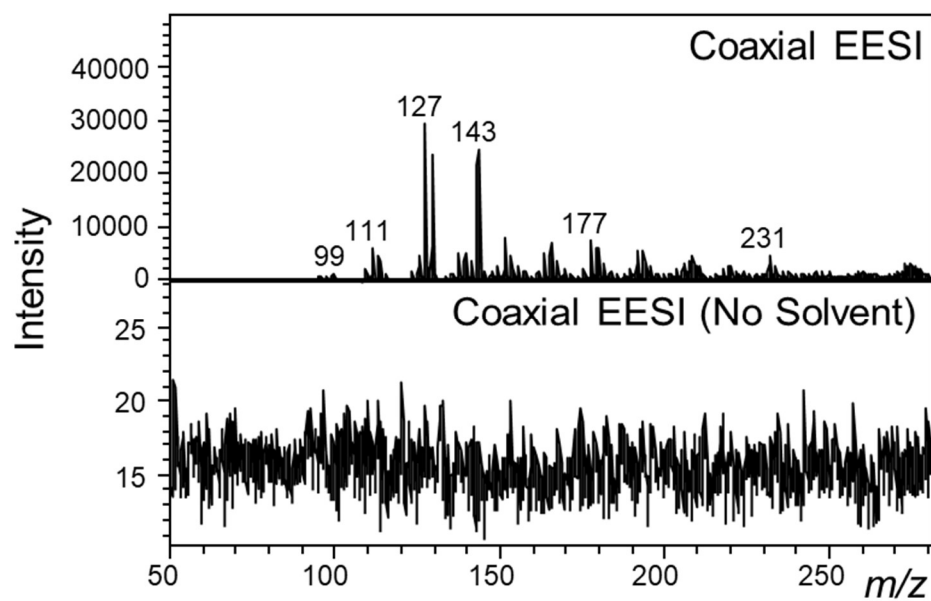
Figure 4.26. Mass spectra of the aerosol generated from the pyrolysis of cellulose analyzed by coaxial EESI with and without the use of an electrospray solvent.

experiment variation; however only the second factor, turbulence, contributes to the signal instability observed within a single experiment because no changes have been made to the relative positioning of the aerosol stream and the flow of charged solvent droplets. Coaxial EESI improves the inter-run variation by improving the signal stability and placing the capillaries that carry the aerosol, solvent, and nebulizing gas in a rigid configuration relative to one another and relative to the mass spectrometer inlet. The form factor of the device allows the coaxial EESI emitter to replace an emitter typically used for ESI without further instrument modifications. Unlike standard EESI, no further optimization of geometric parameters is required. This makes the setup for coaxial EESI much faster and simpler, such that the expertise required to perform a coaxial EESI-MS experiment is similar to the expertise needed to perform a direct infusion electrospray mass spectrometry experiment. Although the coaxial EESI emitter is designed to fit into the source of Bruker ion trap mass spectrometers, the coaxial EESI emitter, or similar designs, may be coupled with any type of mass spectrometer with an atmospheric pressure inlet for more reproducible, real-time aerosol analysis.

An existing ionization source designed for a Thermo Scientific LTQ-FT was repurposed for use as a coaxial EESI source and results show that it is a viable method for ambient ionization from aerosol particles with improvement in ease-of-setup, reproducibility, and signal stability. A solvent study was also undertaken to determine the best solvent composition, or combination of solvent compositions, for the analysis of the aerosol generated from the pyrolysis of cellulose. The results suggest that a binary solvent system that can switch between water/methanol and toluene/methanol gives the best coverage of the peaks observed during pyrolysis.

The effects that the EESI source design has on the chemistry of ion formation were also evaluated. One example of this is that ionization of protein can occur directly from an

aerosol generated by a COA using a coaxial EESI nebulizer without the use of an electrospray solvent. Ionization, in this case, occurs independent of the electrospray solvent. This does not occur for any of the small molecules studied, as interaction with the electrospray solvent is necessary for extraction and ionization of small molecules from an aerosol. It was also demonstrated that there are differences in charge state distribution in the analysis of aerosolized proteins by standard and coaxial EESI. For lysozyme, coaxial EESI produced a charge state distribution that mimics the protein in a native state. However, this shift in charge state distribution was not observed in the analysis of aerosolized ubiquitin by coaxial EESI.

REFERENCES

1.   Laskin, J. *et al.* High-Resolution Desorption Electrospray Ionization Mass Spectrometry for Chemical Characterization of Organic Aerosols. *Anal. Chem.* **82,** 2048–2058 (2010).

2.   Bateman, A. P., Nizkorodov, S. A., Laskin, J. & Laskin, A. High-Resolution Electrospray Ionization Mass Spectrometry Analysis of Water-Soluble Organic Aerosols Collected with a Particle into Liquid Sampler. *Anal. Chem.* **82,** 8010–8016 (2010).

3.   Turpin, B. J., Saxena, P. & Andrews, E. Measuring and simulating particulate organics in the atmosphere: Problems and prospects. *Atmos. Environ.* **34,** 2983–3013 (2000).

4.   Spencer, S. E., Tyler, C. A., Tolocka, M. P. & Glish, G. L. Low-temperature plasma ionization-mass spectrometry for the analysis of compounds in organic aerosol particles. *Anal. Chem.* **87,** (2015).

5.   Spencer, S. E., Santiago, B. G. & Glish, G. L. Miniature Flow-Through Low-Temperature Plasma Ionization Source for Ambient Ionization of Gases and Aerosols. *Anal. Chem.* **87,** (2015).

6.   Horan, A. J. *et al.* Online Characterization of Particles and Gases with an Ambient Electrospray Ionization Source. *Anal. Chem.* **84,** 9253–9258 (2012).

7.   Doezema, L. A. *et al.* Analysis of secondary organic aerosols in air using extractive electrospray ionization mass spectrometry (EESI-MS). *RSC Adv.* **2,** 2930 (2012).

8.   Gallimore, P. J. & Kalberer, M. Characterizing an extractive electrospray ionization (EESI) source for the online mass spectrometry analysis of organic aerosols. *Environ. Sci. Technol.* **47,** 7324–7331 (2013).

9.   Swanson, K. D., Spencer, S. E. & Glish, G. L. Metal Cationization Extractive Electrospray Ionization Mass Spectrometry of Compounds Containing Multiple Oxygens. *J. Am. Soc. Mass Spectrom.* **28,** 1030–1035 (2017).

10.   Chen, H., Venter, A. & Cooks, R. G. Extractive electrospray ionization for direct analysis of undiluted urine, milk and other complex mixtures without sample preparation. *Chem. Commun.* **19,** 2042–2044 (2006).

11.   Chen, H., Yang, S., Wortmann, A. & Zenobi, R. Neutral Desorption Sampling of Living Objects for Rapid Analysis by Extractive Electrospray Ionization Mass Spectrometry. *Angew. Chem.* **46,** 7591–7594 (2007).

12.   Chen, H. & Zenobi, R. Neutral desorption sampling of biological surfaces for rapid chemical characterization by extractive electrospray ionization mass spectrometry. *Nat. Protoc.* **3,** 1467–1475 (2008).

13. Chingin, K., Gamez, G., Chen, H., Zhu, L. & Zenobi, R. Rapid classification of perfumes by extractive electrospray ionization mass spectrometry (EESI-MS). *Rapid Commun. Mass Spectrom.* **22,** 2009–2014 (2008).

14. Venter, A., Nefliu, M. & Cooks, R. G. Ambient desorption ionization mass spectrometry. *TrAC Trends Anal. Chem.* **27,** 284–290 (2008).

15. Gu, H., Xu, N. & Chen, H. Direct analysis of biological samples using extractive electrospray ionization mass spectrometry (EESI-MS). *Anal. Bioanal. Chem.* **403,** 2145–2153 (2012).

16. Li, L.-P. *et al.* Applications of ambient mass spectrometry in high-throughput screening. *Analyst* **138,** 3097–3103 (2013).

17. Wang, Y., Liu, S., Hu, Y., Li, P. & Wan, J.-B. Current state of the art of mass spectrometry-based metabolomics studies – a review focusing on wide coverage, high throughput and easy identification. *RSC Adv.* **5,** 78728–78737 (2015).

18. Law, W. S. *et al.* On the Mechanism of Extractive Electrospray Ionization. *Anal. Chem.* **82,** 4494–4500 (2010).

19. Wang, R. *et al.* On the mechanism of extractive electrospray ionization (EESI) in the dual-spray configuration. *Anal. Bioanal. Chem.* **402,** 2633–2643 (2012).

20. Hail, M. E. & Mylchreest, I. C. Electrospray ion source and interface apparatus and method. (1992).

21. Lloyd, J. R. & Hess, S. A corona discharge initiated electrochemical electrospray ionization technique. *J. Am. Soc. Mass Spectrom.* **20,** 1988–1996 (2009).

22. Konermann, L. Addressing a Common Misconception: Ammonium Acetate as Neutral pH "Buffer" for Native Electrospray Mass Spectrometry. *J. Am. Soc. Mass Spectrom.* **28,** 1827–1835 (2017).

CHAPTER 5: OPEN PORT SAMPLING INTERFACE - ELECTROSPRAY IONIZATION

5.1.   Introduction

Since the early 2000's, self-aspirating continuous flow liquid microjunction sampling techniques have been implemented for numerous applications[1–10]. Such devices may be configured to use an upright open port with an exposed sampling interface for sample introduction[7]. This technology has been implemented with flow injection analysis[11], solid-phase microextraction[10], and liquid chromatography[4] prior to mass spectrometry. More recently, an open port sampling interface (OPSI) has been implemented with acoustic droplet generation for a touchless, ultra-high throughput bioanalytical platform[12].

In an OPSI, the solvent flow rate dictates the mode of operation. The most commonly used mode of operation is the vortex mode where the solvent flow rate into the open port is less than the aspiration rate out of the device. The vortex mode of operation is ideal for the introduction of liquid droplets. In contrast, if the solvent flow rate into the device is greater than the aspirated solvent flow rate out of the device, an overflow occurs where excess solvent flows away from the open port to waste. In this overflow mode, a dome-shaped solvent interface is formed where the sample may be introduced. When the sample (i.e. a liquid droplet, a solid tablet, or a gaseous stream) interacts with the dome-shaped solvent

interface, a portion of the sample is dissolved and the solvent extract is aspirated through an inner capillary for analysis by electrospray ionization - mass spectrometry (ESI-MS). An OPSI has been implemented for the study of both solid and liquid samples, but it has not been used to directly sample from aerosolized species. In this chapter, OPSI-ESI is presented as a method to sample from both liquid and solid organic aerosols by introducing the aerosolized sample to the solvent interface of the OPSI.

5.2.   Open Port Sampling Interface coupled to Electrospray Ionization

5.2.1. Design and Operation of OPSI-ESI

Open port sampling operates by flowing solvent into a vertical tube that is sealed at one end to form a small reservoir of solvent that is open at the top (open port). As shown in Figure 5.1, this reservoir is attached to an electrospray emitter by an inner capillary that extends into the reservoir of solvent. The electrospray emitter uses a nebulization gas (nitrogen) to produce small charged droplets and aid in desolvation. For an OPSI, the nebulization gas also acts as a Venturi pump to pull solvent from the reservoir through the inner capillary. If solvent is continuously provided to the reservoir, then solvent can be continuously aspirated from the reservoir.

For OPSI operation, there are two liquid flow rates to consider. One solvent flow rate is controlled by a syringe pump and pushes solvent into the device. The other solvent flow rate is the aspiration rate through the inner capillary which is determined by the linear velocity of the nebulization gas. Sampling using the vortex mode of operation was attempted, but the aerosol gas flow forced air through the inner capillary and no signal was observed. Instead, this device was operated in overflow mode where the flow of solvent into the device was greater than the aspiration rate. The surface tension of the solvent formed a dome-shaped solvent interface at the open port as shown in Figure 5.1A. Excess solvent flowed over the edge of the open port to waste. When aerosol is introduced to the dome-
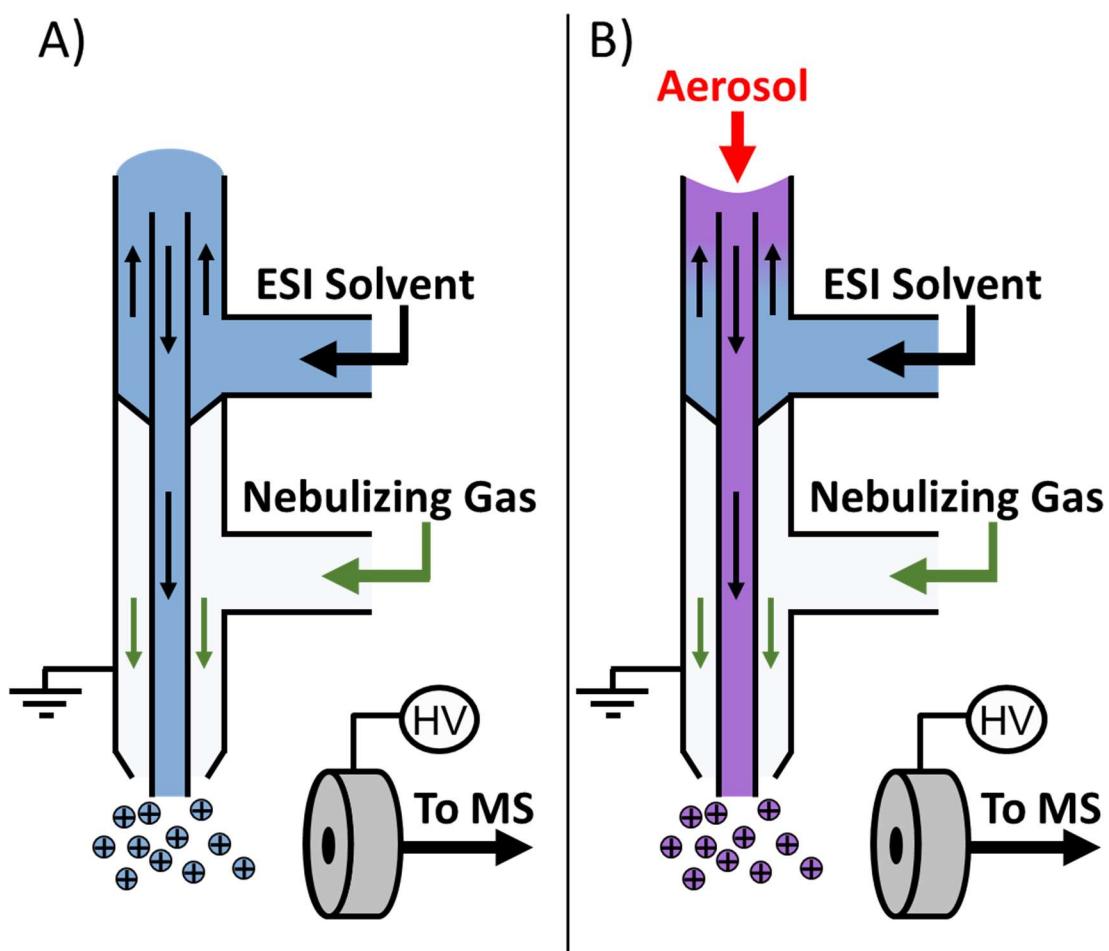
Figure 5.1. Schematic of open port sampling interface – electrospray ionization (OPSI-ESI) A) without aerosol introduction and B) with aerosol introduction

shaped solvent interface, there is a deformation of the solvent interface caused by the aerosol-gas flow as shown in Figure 5.1B.

For the OPSI-ESI design, shown in Figure 5.2, a Bruker ESI Emitter (P/N: A5940, Billerica, MA) was used without major modifications to the body of the emitter. The inner capillary was removed and replaced with a longer stainless steel inner capillary of matching inner and outer diameter, 0.1 mm and 0.22 mm, respectively (32RW gauge, Vitaneedle, Needham, MA). The inner capillary extended 130 mm from the tip of the electrospray emitter through both a zero dead volume (ZDV) union (accessory to P/N: A5940, Billerica, MA) and a Swagelok 1/16" union tee (SS-100-3, Solon, OH). The tip of the capillary recessed 0.5 mm from the surface of the open port. A second ZDV union was attached to the orthogonal connector of the tee for introduction of solvent to the system. The solvent used throughout this study was a 1:1 mixture of methanol and water with formic acid added at 1% by volume. In most cases, the solvent flow rate into the device was set to barely exceed the aspiration rate and ranged from 5 to 20 µL min^{-1}. If the solvent flow rate into the device is higher than the aspiration rate then solvent spills over the edge of the OPSI. The aspiration rate through the capillary was controlled by changing the nebulization gas (nitrogen) pressure in the Bruker control software, ranging from 0 to 50 psig. The gas velocity was calculated by measuring the volumetric flow rate of the gas using a flow meter (Bios Defender 510M, Butler, NJ) and dividing the volumetric flow rate by the area of the opening at the tip of the emitter (0.08 mm^2).

Aerosol was introduced to the solvent interface by positioning the output from the aerosol generator approximately 4 millimeters above the solvent interface. The aerosol gas flow caused a distortion in the solvent interface as the surface was depressed slightly,
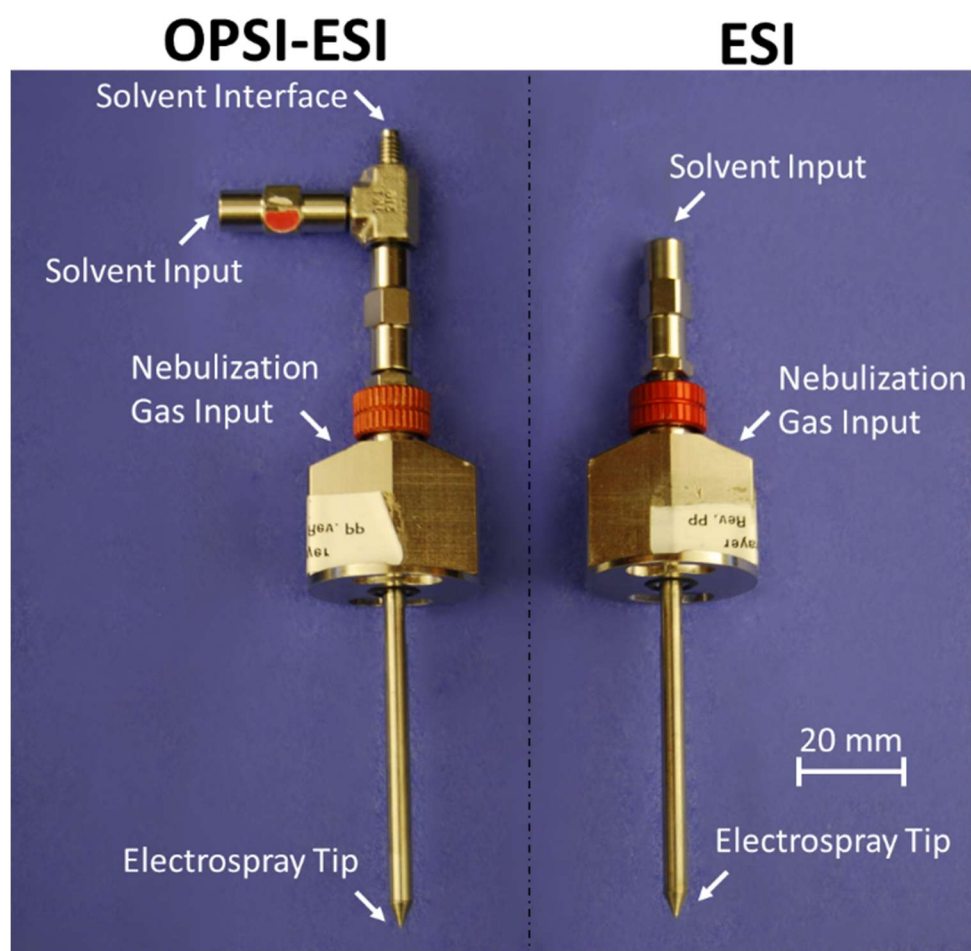
Figure 5.2. Comparison of OPSI-ESI emitter and a standard ESI emitter.

depicted in Figure 5.1. Too high of an aerosol gas flow rate should be avoided because the solvent interface can be depressed beyond the inner capillary so only air is pulled through the inner capillary. In this situation no signal is observed until the aerosol gas flow is removed and the particles that impacted exposed surfaces are dissolved and flowed through the system.

5.2.2. Measurement of Aspiration Rate

The aspiration rate determines the time from aerosol penetration into the solvent interface to electrospray ionization as well as the concentration of the analyte in the extraction solvent. If the solvent flow into the device is switched off, the device is allowed to dry by electrospraying solvent until signal is no longer observed. At this point, air is being pulled through the inner capillary resulting in no ion formation. To measure aspiration rate, 15 μL was injected into the solvent interface when dry and the signal was measured as a function of time. The injected volume was divided by the duration of signal to obtain an aspiration rate. An average aspiration rate was determined using five replicates for each gas velocity. In Figure 5.3, the data shows that the aspiration rate is slow to increase at gas velocity rates below 300 m s^{-1} then rapidly increases at higher velocities. The factors that affect the aspiration rate are nebulization gas pressure (and consequently nebulization gas flow) and the internal diameter (ID) of the inner capillary. The maximum gas velocity with the current instrumental setup is 500 m s^{-1}. The current design uses the existing needle holder from the Bruker ESI emitter with no modifications which is sized to match the outer diameter of an ESI needle. Modifications may be made to the needle holder to increase the appropriate needle gauge size for increased aspiration rate.
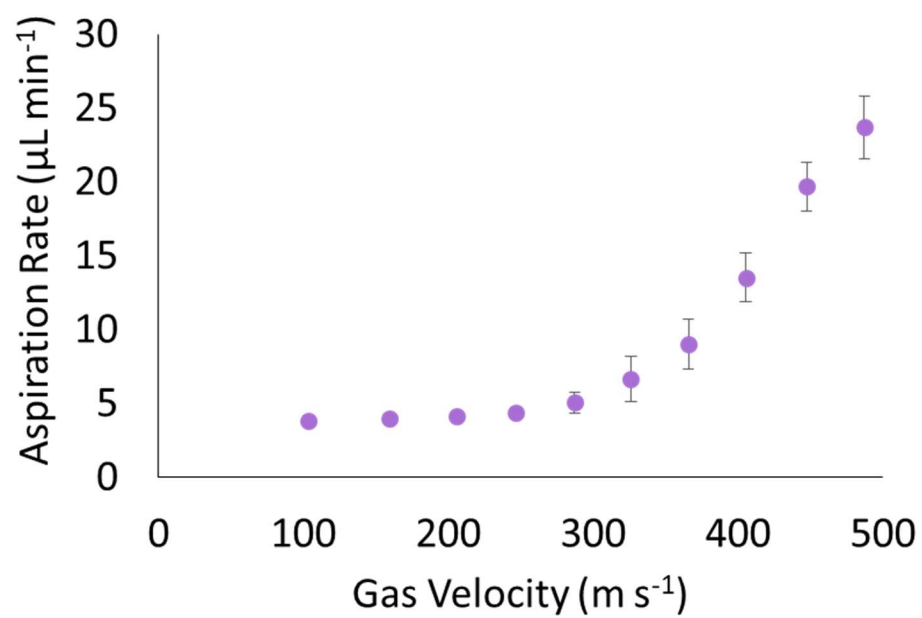
Figure 5.3. Plot of gas velocity versus aspiration rate through the inner capillary (N=5).

5.2.3. Nicotine Aerosol Response

When an aerosol of nicotine, generated using the COA, was introduced to the solvent interface of the OPSI-ESI device, a signal at *m/z* 163, [M+H]⁺, was observed. A three-port valve could be actuated to the "Aerosol OFF" position to send the entirety of the flow to a particle counter and none to the OPSI-ESI solvent interface. Alternatively, the three-port valve could be actuated to the "Aerosol ON" position to send the entirety of the flow to the OPSI-ESI solvent interface. This valve was actuated every 240 seconds beginning at 120 seconds for five periods at four different gas velocities as shown in Figure 5.4. For each gas velocity, the signal rises when the aerosol is in the ON position and the signal falls when the aerosol is in the OFF position. The residence times, solvent flow rates, and average signal intensities are given in Table 5.1. In each case, the solvent flow rate into the device was 16.6 µL min⁻¹. The solvent flow difference describes the rate of overflow for the OPSI. An increase in signal intensity is observed as aspiration rate is increased. The residence time decreases as the aspiration rate is increased, but not linearly. Although peak height was used for comparison in Table 5.1, average peak height correlates well to peak area as gas velocity is increased.

An abnormality is observed in the extracted ion chronogram when using OPSI-ESI for aerosol analysis in overflow mode. One example is in the top (blue) trace at 200 seconds, but this occurs consistently in the top two traces and occasionally for the bottom two. This effect occurs when the three-way valve has been switched to the Aerosol OFF position and the solvent interface is no longer depressed by the aerosol gas flow. Fresh solvent replaces nicotine-containing solvent at the tip of the inner capillary in the reservoir causing a rapid decrease in analyte signal. As local fresh solvent is used up, nicotine-containing solvent diffuses to the capillary and a slow decay of signal is observed. This abnormality is most
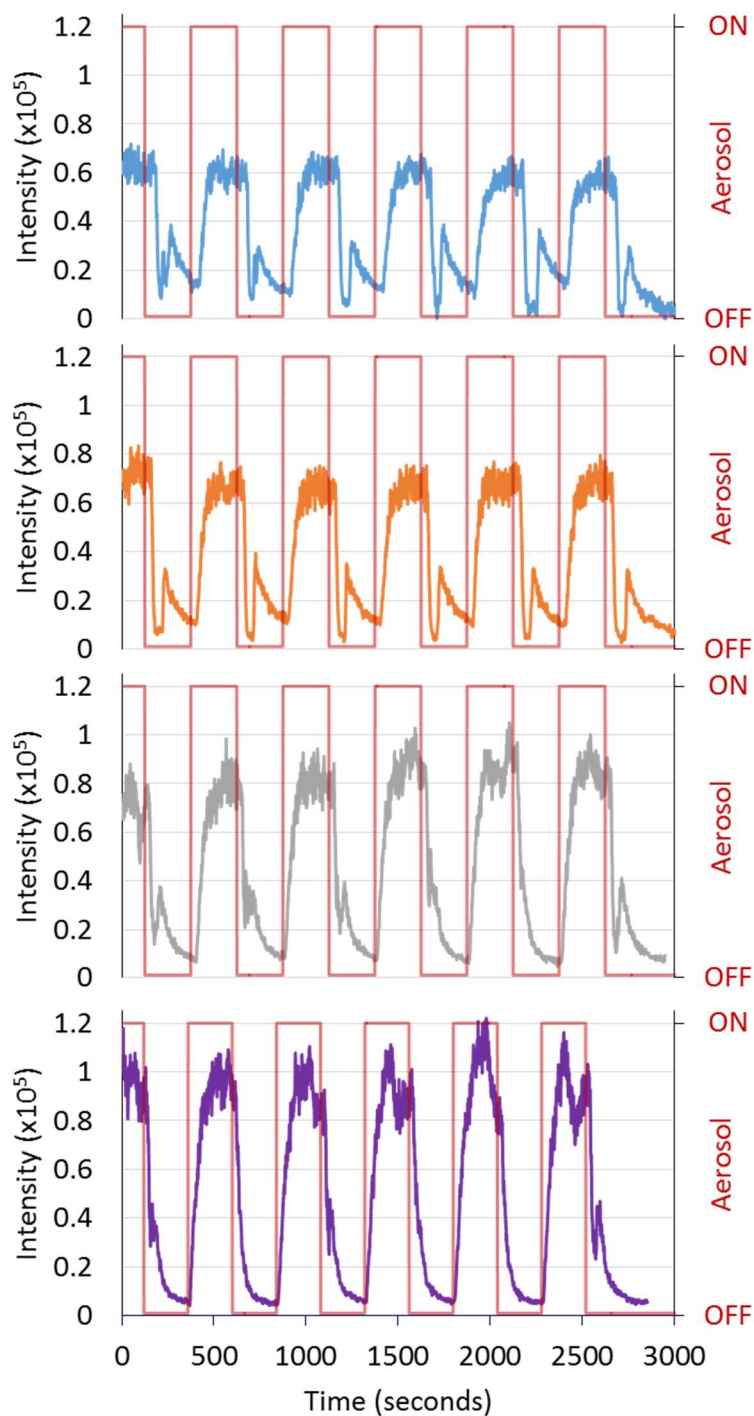
Figure 5.4. Figure showing the response of OPSI-ESI to an aerosol of nicotine at 159 m s^{-1}(blue), 247 m s^{-1}(orange), 326 m s^{-1} (grey), and 405 m s^{-1} (purple) gas velocities. The red trace indicates whether aerosol was directed toward the OPSI-ESI interface (ON) or away from the OPSI-ESI interface (OFF).

Table 5.1. OPSI-ESI of an aerosol of nicotine at varying gas velocities.

Gas Pressure (psig)	Gas Velocity (m s^{-1})	Aspiration Rate (uL min^{-1})	Solvent Flow Difference (uL min^{-1})	Residence Time (s)	Average Intensity (counts)
10	159	4.0	12.6	44.4	60768
20	247	4.3	12.3	29.2	63952
30	326	6.7	9.9	8.5	80939
40	405	13.5	3.1	7.3	93046

pronounced when the difference between solvent in and solvent out is the greatest as observed after every period of Aerosol ON in the top two traces. To reduce the occurrence of the artifact in the experiment, the system should be run with the aspiration rate and the solvent flow rate matched.

5.2.4. Comparison to Standard EESI

The aerosol generated from the pyrolysis of cellulose, lignin extracted from tobacco, and hemicellulose extracted from tobacco were analyzed by OPSI-ESI-MS and the data is displayed in Figure 5.5. Overall, the results obtained using OPSI-ESI are very similar to what is observed using EESI for each sample. One example of this is shown in the top two panels of Figure 5.5 in the mass spectral comparison of OPSI-ESI to EESI for the analysis of the aerosol generated from pyrolyzed cellulose. Although the primary peaks observed in the spectrum as well as their absolute intensities are very similar, there is an increase in the total ion current for OPSI by a factor of three. The lower relative intensity peaks in the EESI spectrum are increased in absolute intensity when using OPSI-ESI. The increase in the sum of all peaks is displayed in Figure 5.5 where the total ion count (TIC) is summed across the mass range 15 to 250 m/z for three replicates of each ionization method. OPSI-ESI improves upon EESI threefold in TIC intensity. The top two spectra in Figure 5.5 shows this is not due to an increase in sensitivity of the primary ions, due to the rise in the less-abundant ions from the aerosol.

When using OPSI-ESI the RSD in the measurement decreases by nearly a factor of three, an improvement similar to the results observed in Chapter 4.3 for coaxial EESI. One reason OPSI-ESI improves upon the inter-run reproducibility of EESI is that the sprayer positioning is consistent. For EESI, the source housing must be removed and the ESI emitter and aerosol outlet must be manually positioned with respect to the inlet to the mass spectrometer to optimize overlap between charged solvent droplets and aerosol particles as
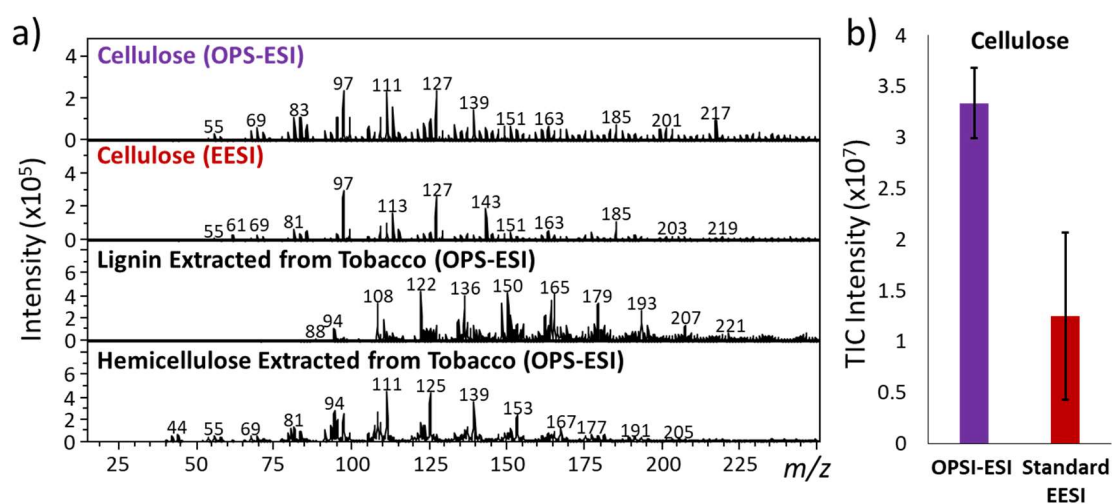
Figure 5.5. (a) Mass spectra obtained using OPSI-ESI for the analysis of pyrolyzed cellulose, EESI for the analysis of pyrolyzed cellulose, OPSI-ESI for the analysis of pyrolyzed lignin extracted from tobacco, and OPSI-ESI for the analysis of pyrolyzed hemicellulose extracted from tobacco. A comparison of the total ion count across the mass range 15 to 250 *m/z* for both OPSI-ESI and EESI of pyrolyzed cellulose (N=3) is shown in (b).

described in Chapter 3. In OPSI-ESI, the device has the same form factor as a standard ESI emitter so that it simply sits in the emitter slot in the source housing. The only optimization necessary from experiment to experiment is that the aerosol stream must be positioned to be above the device, directed toward the center of the solvent interface, which is very simple to optimize as compared to the EESI setup. OPSI-ESI also improves upon the intra-run reproducibility observed in EESI because there are no turbulent gas flows to suppress ionization at the inlet to the mass spectrometer. Previous studies have shown that the turbulent flow caused by interacting gas streams in EESI lead to an erratic signal[13]. The intra-run signal stability of OPSI-ESI is better than EESI by a factor of four and is the same as standard ESI. The setup process for OPSI-ESI is a little more complicated than the setup of coaxial EESI, but the intra-run signal stability is improved from 8% to 5% for coaxial EESI and OPSI-ESI respectively.

5.3.   Improvements on the OPSI-ESI design for Aerosol Analysis

One drawback to the OPSI-ESI design presented in Section 5.2 is the exclusivity of the design for use on Agilent/Bruker instruments. In ideal operation, the ESI source employed during OPSI-ESI will be optimized for the intended instrument. To use the OPSI-ESI device described in Section 5.2 on a non-Bruker mass spectrometer, the source housing must be removed and the OPSI-ESI device must be held near the inlet to the mass spectrometer using an insulating collar in a similar fashion to Figure 4.9. For operation in this mode, safety interlocks must be overridden and manual positioning of the device is required.

A simplified, modular OPSI device was designed and fabricated to thread directly onto any pneumatic ESI or APCI source that uses 1/16" solvent fittings, a common size used for LC introduction. The completed OPSI device is shown in Figure 5.6A. The design of this device is the same as the one described in Section 5.2, except the inner capillary (27RW

gauge, Vitaneedle, Needham, MA) has a larger ID (0.2 mm) and extends from the solvent interface, recessed 1 mm, to the exposed male 1/16" union, a length of 60.5 mm. The inner capillary extends from the solvent interface through a 1/16" Swagelok Tee (SS-100-3), a Valco ZDV union with a 0.75 mm internal bore (VWR, 10852-948), and a custom male-male ZDV union. The inner capillary was recessed farther than the standard OPSI device to allow higher aerosol-gas flow rates. The custom male-male ZDV union was made using PEEK tubing with 0.5 mm ID, Swagelok 1/16" union (SS-100-6), and 1/16" Swagelok ferrules on either side of the union (SS-100-SET). The inner capillary was affixed in place using a graphite ferrule with an ID of 0.5 mm between the Swagelok tee and the Valco ZDV union. A second ZDV union was attached to the orthogonal connector of the tee for introduction of solvent to the device. Solvent is pushed through this ZDV union into the Swagelok tee. The solvent is blocked on one side by the graphite ferrule and flows around the inner capillary to the solvent interface. If the device is attached to a pneumatic emitter, as in Figure 5.6B, with a flowing nebulizing gas, solvent is aspirated from the solvent interface, through the inner capillary, to the tip of the emitter.

This modular OPSI device operates similarly to the device described in Section 5.2. As shown in Figure 5.7, the solvent flow rate at each nebulization gas pressure is greater for the modular device than the standard OPSI device. The increase in solvent flow is due to the increased ID of the inner capillary. Otherwise, the modular device functions the same as the standard OPSI device using the Bruker Apollo I ESI ion source. This modular device was used on the Thermo Scientific LTQ-FT instrument, as shown in Figure 5.8, to demonstrate the functionality of the design for use on multiple vendor instruments. The OPSI device was threaded into the ESI probe of the Thermo Scientific Ion Max source. An aerosol of caffeine was generated using the COA and sampled using the modular OPSI
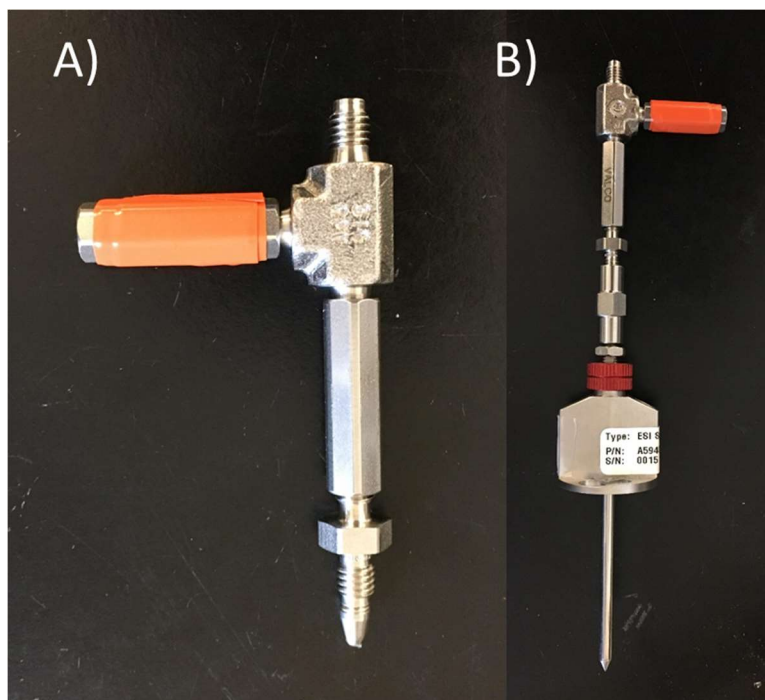
Figure 5.6. Picture of the modular OPSI-ESI device A) alone and B) attached to a Bruker ESI emitter.
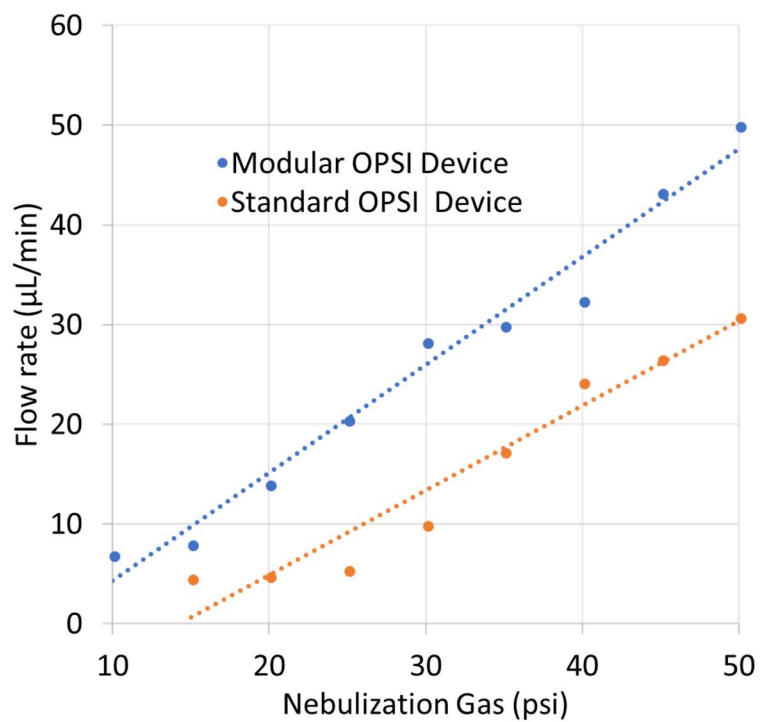
Figure 5.7. Plot showing the relationship of nebulization gas to aspiration rate for each the standard and modular OPSI-ESI devices.
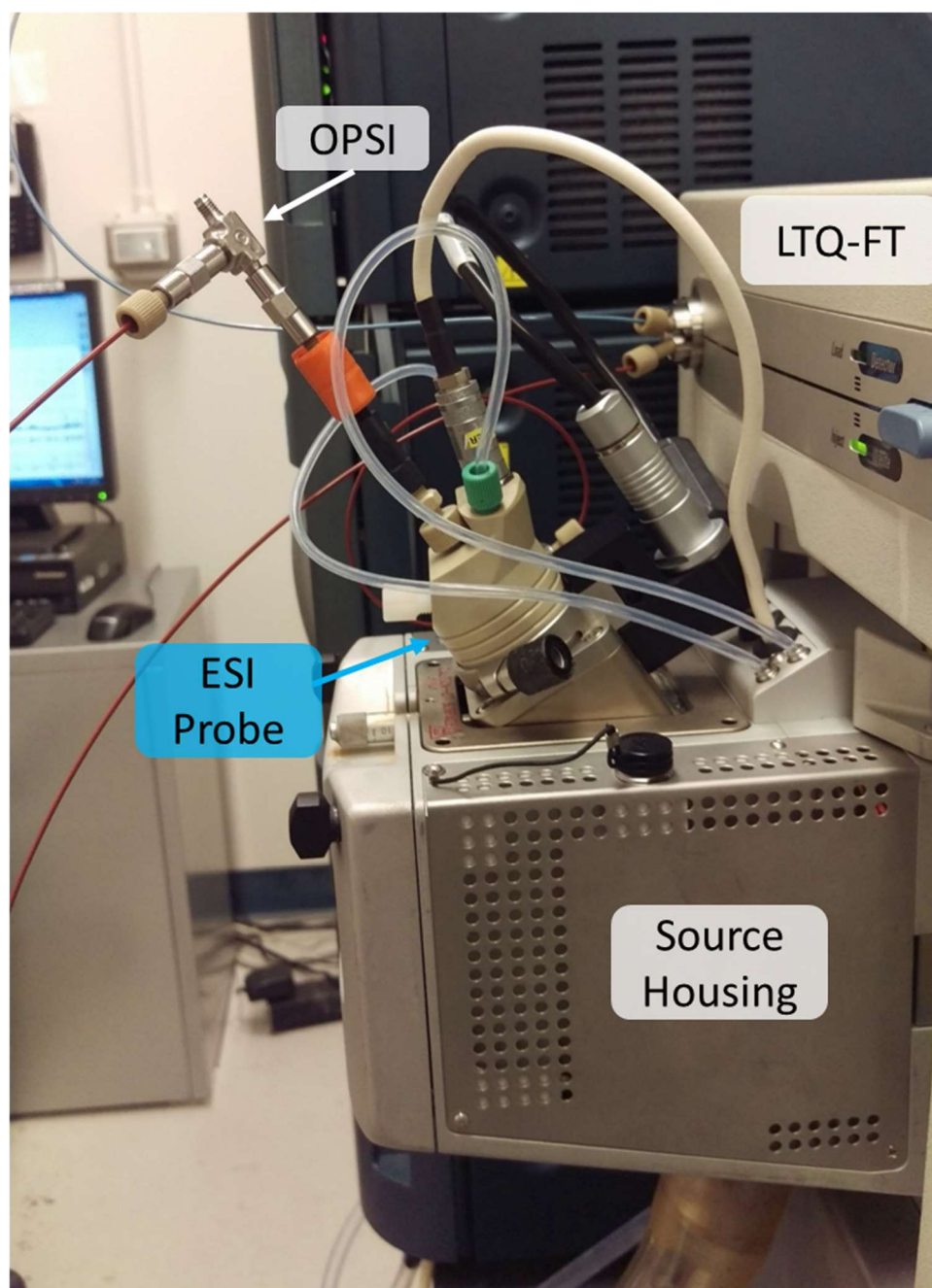
Figure 5.8. Picture of the modular OPSI-ESI device on a Thermo Scientific Ion Max source.

device attached to the ESI source on the Thermo Scientific LTQ-FT as shown in Figure 5.9. The signal for *m/z* 195 ([M+H]$^+$) has some instability at the beginning of the sampling period and the carry-over in between periods of aerosol introduction is more significant than typically seen on Bruker instruments. This is likely due to the sampling interface being held at the electrospray voltage due to electrical contact inside the ESI probe. The carry-over could be due to charged aerosol particles impacting on the sides of the device held at high voltage and dissolving over time. This could likely be solved by using an inner capillary of an insulating material like fused silica or using peak tubing to increase the distance between the ESI probe and the OPSI solvent interface while grounding the OPSI device. Another issue is that the ESI probe is held at an angle as shown in Figure 5.8, so gravity pulls the solvent dome away from the solvent interface. This results in a smaller volume capacity for the solvent dome. These issues are likely conserved among instruments that apply the electrospray voltage to the emitter rather than the inlet to the mass spectrometer.

5.4.   Solvent Composition

A study, similar to the study presented in Chapter 4.5, was carried out for the analysis of the aerosol generated from the pyrolysis of cellulose using OPSI-ESI. Solubility of the analyte in the electrospray solvent is expected to be a primary factor in sampling by OPSI. The modular OPSI-ESI source was used for this study on a Bruker Esquire ion trap mass spectrometer. Binary mixtures of water, methanol, acetonitrile, chloroform, toluene, and dichloromethane were tested as electrospray solvents for OPSI-ESI with a formic acid additive at 1% by volume. Each solvent mixture was used for the analysis of the aerosol generated from pyrolysis of cellulose.
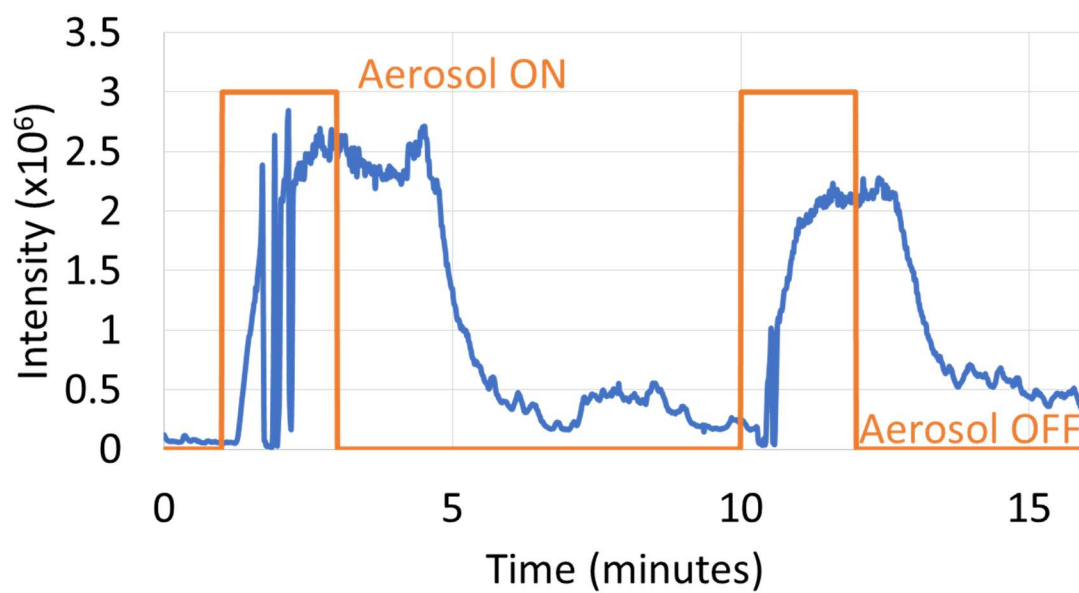
**Figure 5.9.** Extracted ion chronogram of caffeine, *m/z* 195, sampled from an aerosol with the modular OPSI-ESI device on the Thermo Scientific Ion Max source. The orange trace indicates the presence or absence of aerosol at the solvent interface.

The solvent flow rate in OPSI-ESI is inversely proportional to the viscosity of the solvent, and the solvent interface was most stable with water, a high viscosity solvent. The stability of the solvent interface decreased as the surface tension of the solvent mixture decreased. To perform analysis when low viscosity solvents such as methanol were used, very high flow rates were required to maintain the presence of the solvent interface. The mass spectra observed for each electrospray solvent are shown in Figure 5.10. The signal intensity of the base peak was relatively even for all mixtures tested. The signal intensity increase in the base peak for toluene/methanol as the electrospray solvent compared to the rest is due to the presence of a contaminant in the toluene as seen in the spectrum of a blank solvent. Toluene, chloroform, and dichloromethane were used as mixtures in methanol rather than water because of immiscibility of the solvents in water. The distribution and relative intensities of the peaks observed in the mass spectrum varied widely between solvents. To determine the number of peaks in the mass spectrum observed for each solvent composition, three replicate runs using each solvent mixture were compared. Only odd *m/z* peaks were counted because any protonated monoisotopic compound produced from cellulose pyrolysis has an odd *m/z*. To reduce noise in the data, only peaks that were above 5% of the base peak intensity and were present in at least two of the three replicates were counted.

A summary of the peaks in the mass spectrum from the aerosol generated from pyrolysis of cellulose and analyzed by OPSI-ESI is presented in Figure 5.11. The inset figure shows the total number of peaks counted in each solvent mixture given the data filtering criteria. The most total peaks were observed in acetonitrile/methanol (85 peaks), pure methanol (82 peaks), and water/methanol (71 peaks). Unique peaks were observed in pure methanol (10 peaks), acetonitrile/methanol (3 peaks), and water (1 peak). The histogram in Figure 5.11 describes how the peaks are shared among the solvent mixtures
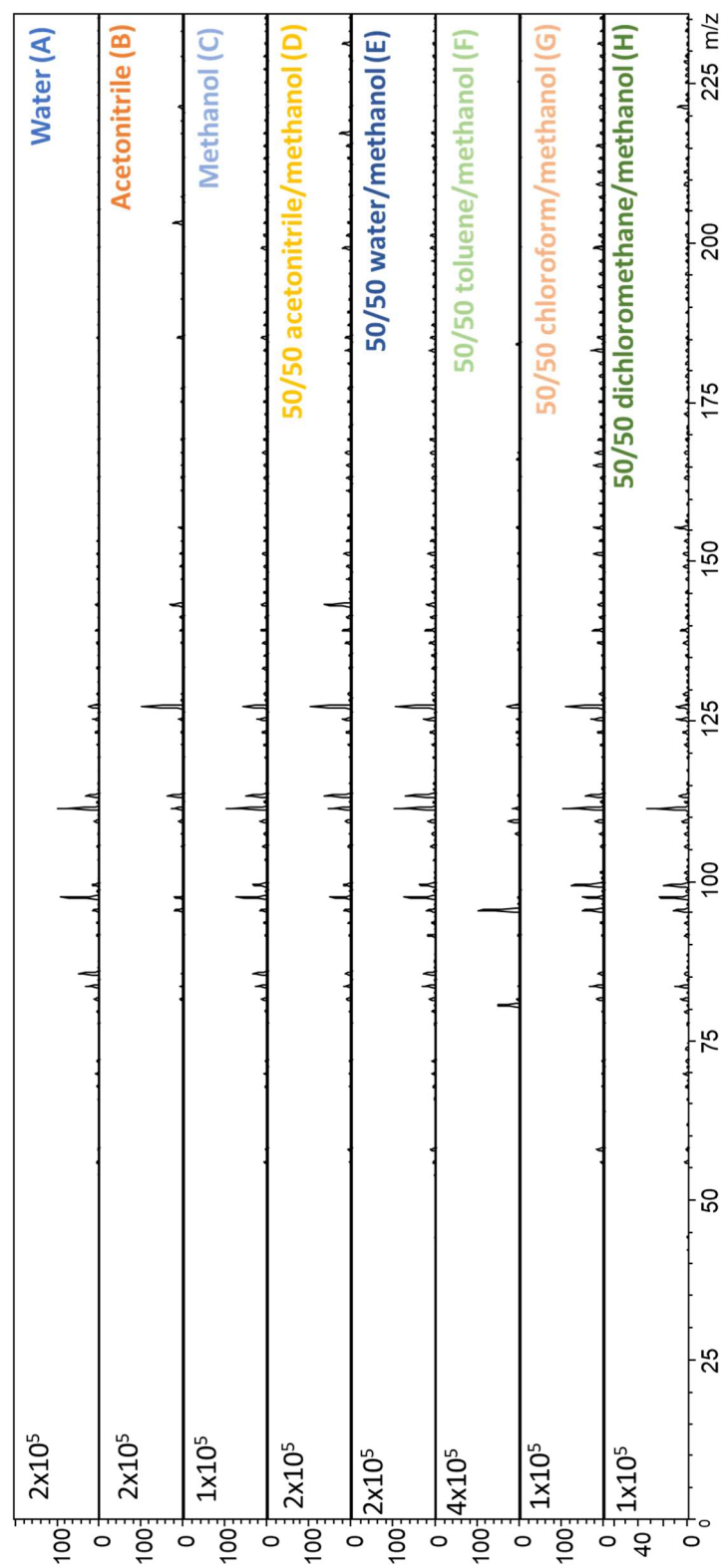
Figure 5.10. Mass spectra of the aerosol generated from the pyrolysis of cellulose ionized by OPSI-ESI using different solvent compositions.
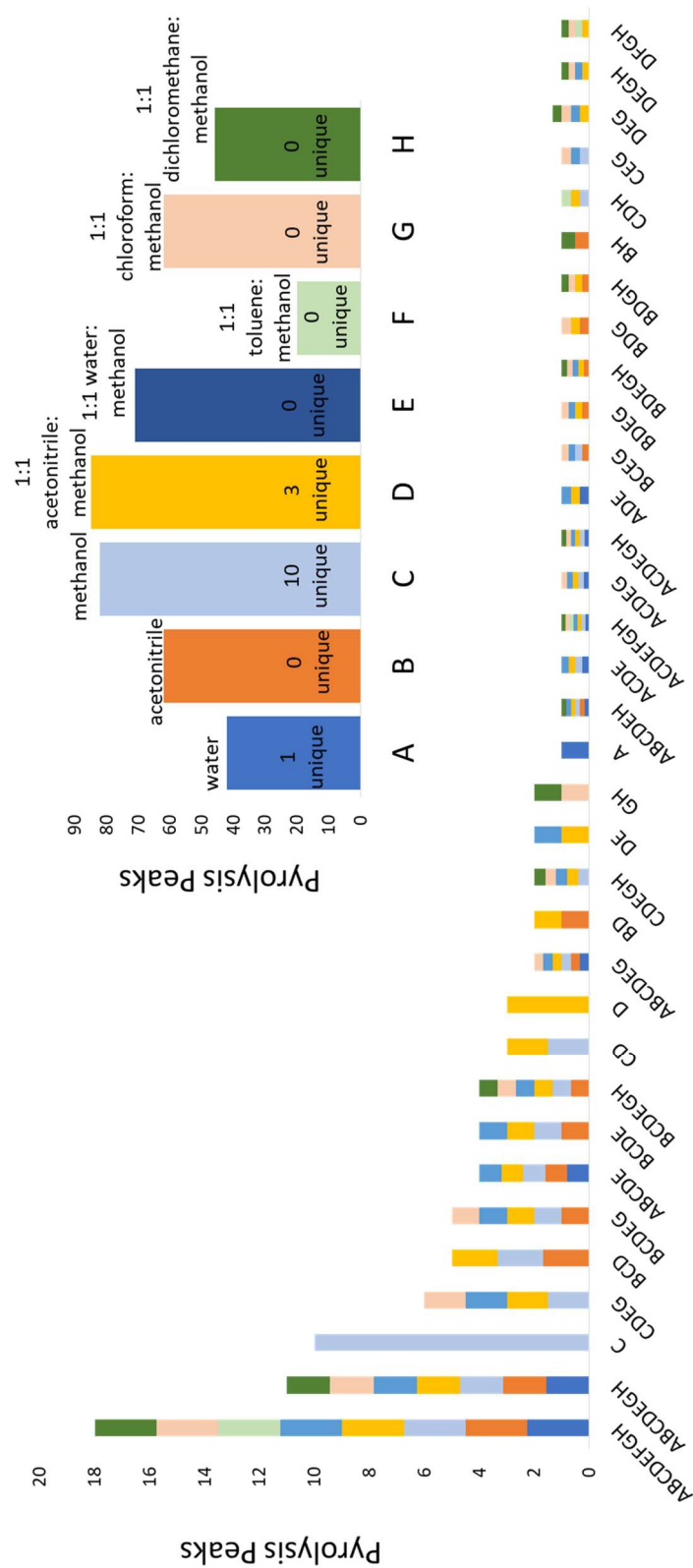
Figure 5.11. Histogram of peaks observed in the analysis of the aerosol generated from the pyrolysis of cellulose using OPSI-ESI with different solvent compositions. The inset bar graph shows the total number of peaks observed for each solvent composition.

used in this study. The labels on the x-axis of the main figure correspond to the solvent

labels on the x-axis of the inset figure. For example, eighteen peaks are observed in all

eight of the solvent mixtures as described by the left-most bar. Both graphs describe a total

coverage of 96 peaks observed among all solvent compositions.

One of the key benefits conserved between EESI and OPSI-ESI is the ability to easily

change the solvent to dissolve different compounds in the aerosol. Practically, this is done

by exchanging the solvent in the syringe for a different solvent mixture without altering the

source arrangement in any way. For the analysis of the aerosol generated by the pyrolysis

of cellulose by OPSI-ESI, multiple solvent compositions could be used during a single

analysis to obtain greater coverage of compounds present in the aerosol. According to

Figure 5.11, a multiple solvent system of methanol and an acetonitrile/methanol mixture

would extract all but one compound observed in this analysis. Differences between the

results shown here and those shown in Chapter 4.5 may be due to the difference in

extraction mechanism. In EESI, the electrospray solvent is electrosprayed into charged

solvent droplets. In a binary mixture, evaporation of the more volatile solvent can occur,

changing the droplet composition. Aerosol particles may have some surface charge which

may alter the mechanism of extraction. For OPSI-ESI, aerosol particles penetrate into a

solvent interface with constant solvent composition and no surface charge.

5.5.   Summary and Conclusions

OPSI is a robust sample introduction probe that is easily coupled to ionization

techniques such as APCI or ESI. In this chapter, a novel design for OPSI-ESI was described

for the sampling of aerosols. This device is an on-line sampling technique coupled directly

to electrospray ionization and requires no additional pumps compared to ESI or moving

parts and can be used with the existing source design on any Agilent/Bruker ESI source.

Because the ESI emitter, and thus the OPSI-ESI device, is grounded on Agilent/Bruker

instruments, no voltages are exposed and only the position of the aerosol outlet above the solvent interface requires optimization. This makes the setup for OPSI-ESI much faster and simpler as compared to conventional aerosol analysis techniques using ambient ionization. A modular design was presented where the OPSI device is easily threaded onto any ESI emitter without any instrument modifications. This new design was shown to work similarly to the standard OPSI-ESI design for Agilent/Bruker instruments. Some issues were observed when using the modular OPSI device on a Thermo Scientific ESI source and potential solutions were presented. A solvent study was also undertaken to determine the best solvent composition, or combination of solvent compositions, for the analysis of the aerosol generated from the pyrolysis of cellulose. The results suggest that a multiple solvent system of methanol and an acetonitrile/methanol mixture gives the best coverage of the peaks observed during pyrolysis.

REFERENCES

1. Van Berkel, G. J., And, A. D. S. & Quirke, J. M. E. Thin-Layer Chromatography and Electrospray Mass Spectrometry Coupled Using a Surface Sampling Probe. *Anal. Chem.* **74,** 6216–6223 (2002).

2. Asano, K. G., Ford, M. J., Tomkins, B. A. & Van Berkel, G. J. Self-aspirating atmospheric pressure chemical ionization source for direct sampling of analytes on surfaces and in liquid solutions. *Rapid Commun. Mass Spectrom.* **19,** 2305–2312 (2005).

3. ElNaggar, M. S., Barbier, C. & Van Berkel, G. J. Liquid Microjunction Surface Sampling Probe Fluid Dynamics: Computational and Experimental Analysis of Coaxial Intercapillary Positioning Effects on Sample Manipulation. *J. Am. Soc. Mass Spectrom.* **22,** 1157–1166 (2011).

4. Van Berkel, G. J. & Kertesz, V. Continuous-flow liquid microjunction surface sampling probe connected on-line with high-performance liquid chromatography/mass spectrometry for spatially resolved analysis of small molecules and proteins. *Rapid Commun. Mass Spectrom.* **27,** 1329–1334 (2013).

5. Hsu, C.-C. *et al.* Real-Time Metabolomics on Living Microorganisms Using Ambient Electrospray Ionization Flow-Probe. *Anal. Chem.* **85,** 7014–7018 (2013).

6. Lorenz, M., Ovchinnikova, O. S., Kertesz, V. & Van Berkel, G. J. Controlled-Resonant Surface Tapping-Mode Scanning Probe Electrospray Ionization Mass Spectrometry Imaging. *Anal. Chem.* **86,** 3146–3152 (2014).

7. Van Berkel, G. J. & Kertesz, V. An open port sampling interface for liquid introduction atmospheric pressure ionization mass spectrometry. *Rapid Commun. Mass Spectrom.* **29,** 1749–1756 (2015).

8. Van Berkel, G. J. & Kertesz, V. Rapid sample classification using an open port sampling interface coupled with liquid introduction atmospheric pressure ionization mass spectrometry. *Rapid Commun. Mass Spectrom.* **31,** 281–291 (2017).

9. Yu, Q., Zhang, J., Ni, K., Qian, X. & Wang, X. Characterization and application of a self-aspirating electrospray source with pneumatic-assisted ionization. *J. Mass Spectrom.* **52,** 109–115 (2017).

10. Gómez-Ríos, G. A. *et al.* Open Port Probe Sampling Interface for the Direct Coupling of Biocompatible Solid-Phase Microextraction to Atmospheric Pressure Ionization Mass Spectrometry. *Anal. Chem.* **89,** 3805–3809 (2017).

11. Van Berkel, G. J. *et al.* Combined Falling Drop/Open Port Sampling Interface System for Automated Flow Injection Mass Spectrometry. *Anal. Chem.* **89,** 12578–12586 (2017).

12. Zhang, H. *et al.* Acoustic-OPP-MS: The Next Generation BioAnalytical Platform For Drug Discovery With Ultra-High Throughput. in *The Proceedings of the 66th Annual ASMS Conference* (2018).

13. Swanson, K. D., Worth, A. L. & Glish, G. L. A coaxial extractive electrospray ionization source. *Anal. Methods* **9,** 4997–5002 (2017).

CHAPTER 6: SUMMARY AND FUTURE DIRECTIONS

6.1.   General Summary

The work presented in this dissertation has focused on the direct sampling and ionization of compounds from aerosol particles in real-time. After an introduction to traditional aerosol analysis and ambient ionization, an explanation of the experimental details behind each system used was included. Two viable methods of sampling and ionization are discussed in this dissertation. EESI is presented in Chapter 3 as a way to simultaneously sample and ionize compounds in the aerosol. Many of the challenges associated with EESI were addressed in Chapter 4 by a new coaxial design that improved the reproducibility of aerosol analysis. In Chapter 5, OPSI was presented as a novel approach to aerosol sampling that can be coupled to ESI for analysis on the timescale of seconds. This final chapter provides a brief summary of the results described in Chapters 3-5 and the potential future directions that can follow from this work.

6.2.   Chapter Summaries

6.2.1. Chapter 3: Extractive Electrospray Ionization

EESI occurs when a stream of droplets or aerosol particles intersects a plume of electrosprayed droplets.[1] The extraction in EESI is based on the solubility of an analyte in the electrospray solvent.[2] The solvent composition can be changed to alter the chemistry of ionization. The solvent composition was changed by adding a metal salt to the electrospray solvent and observing a metal cationized analyte using the mass spectrometer. For glucose and levoglucosan, the addition of lithium improved signal intensity.[3] Metal cationization was also used in the analysis of the aerosol generated from the pyrolysis of cellulose with

an increase of signal intensity observed by using lithium in the experiment. The chapter

concludes with a discussion of acid additives and identification of a source of contamination,

an isobar at *m/z* 163, that interferes with the analysis of protonated levoglucosan from an

aerosol.

6.2.2. Chapter 4: Coaxial Extractive Electrospray Ionization

EESI in the standard configuration, as described in Chapter 3, suffers from poor

reproducibility and poor signal stability. In this chapter, a new source design was presented

to overcome those two challenges and simplify the experimental setup. This design was

used to construct a coaxial EESI emitter that fits into the existing source housing and

replaces the ESI emitter with no further modifications to the instrument. This device uses

coaxial capillaries to deliver solvent, nebulizing gas, and aerosol to the tip of the emitter in

a reproducible manner.[4] Coaxial EESI was shown to improve both the signal stability and

run-to-run reproducibility. A similar design was used to implement coaxial EESI on a

Thermo Scientific Ion Max source by repurposing the heated ESI probe. This chapter also

discusses some differences observed between standard EESI and coaxial EESI, including

unexpected differences in the chemistry of ion formation.

6.2.3. Chapter 5: Open Port Sampling Interface – Electrospray Ionization

OPSI is a robust sample introduction method[5] that was used to analyze aerosol particles

for the first time.[6] The sampling device consists of a solvent interface into which aerosol

particles are impacted and dissolved. A pneumatic ESI emitter is used to aspirate dissolved

analyte from the solvent interface to the tip of the emitter for nebulization and ionization.

The first design presented in this chapter implemented OPSI into a Bruker ESI emitter.

This OPSI-ESI device was used to sample aerosol as efficiently as standard EESI with

improved reproducibility and signal stability. A modular design was also presented that

could be used with any pneumatic ESI emitter without any instrument modifications. This

device was used with a Thermo Scientific Ion Max ESI probe successfully, but with some issues regarding source geometry and high voltage placement.

6.3.   Future Directions

6.3.1. Quantification of Compounds in an Aerosol using OPSI-ESI

E-cigarettes are hand-held battery powered devices which deliver a liquid solution of nicotine, flavorings, or other additives in aerosol form when a user inhales, or vapes.[7] EESI and OPSI-ESI are well-suited for qualitative analysis of these e-cigarette aerosols, and should be evaluated for the quantitative analysis of nicotine and other flavorings as well. When a user vapes, gas is pulled through a gas inlet, across a heated coil and carries aerosol to the user for inhalation. Since the user is acting as the pump, placing either coaxial EESI or OPSI-ESI in-line with this system is difficult. An alternative method to flowing air through the system is to apply a positive pressure to the gas inlet to push air across the heated coil and out the mouthpiece of the e-cigarette. This method allows the aerosol output from the mouthpiece to be analyzed by OPSI-ESI. A 3D printed piece to adapt Swagelok fittings to the e-cigarette gas inlet to reproducibly apply a positive pressure of air was provided by a collaborator. To evaluate the difference between the methods of providing air flow, aerosol filter collection with Cambridge filter pads (Borgwaldt, 44mm) was used for each method followed by solvent extraction and gas chromatography – mass spectrometry (GC-MS) analysis. Three replicates were taken for each method, and one representative chromatogram from each method is displayed in Figure 6.1. No differences were observed in the chromatograms between the two methods; thus positive pressure on the gas inlet can be used as a viable method to generate aerosol. Standards and internal standards can be spiked into the liquid and mixed prior to aerosol generation for quantitative studies.
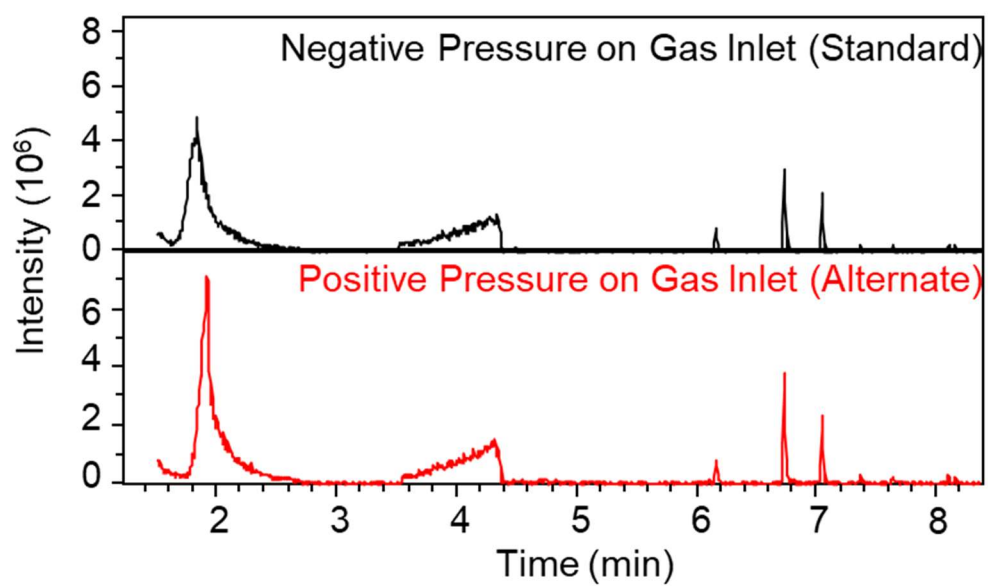
Figure 6.1. GC-MS chromatograms of aerosol collected onto a filter and extracted in methanol for two different methods of aerosol generation.

6.3.2. Structural Investigation of Compounds in Aerosol by Water Adduction

As discussed in Chapter 3.4, isomers and/or isobars can be distinguished in an ion trap using the ion-molecule reaction of water adduction to lithiated molecules.[8–10] The basis of this distinguishing ability is the preference of a lithium cationized molecule to bind to adventitious water. If the lithium can have a tridentate or tetradentate interaction with a structure, the reaction of the complex with water is less likely to be observed using an ion trap. This water adduction method can be used to measure deviations in structure due to ionization mechanism. In Chapter 3.2.1, results were presented to suggest that there is some difference in the ionization of levoglucosan by ESI compared to EESI of an aerosol of levoglucosan. When an acid is used as an additive, the protonated species is observed in EESI, but the sodiated species is observed in ESI. To investigate if there are differences that can be attributed to ionization mechanism, both ionization techniques can be used to cationize molecules with lithium, and the water adduction reaction in the ion trap can be used to compare the structures. Standard EESI must be used for this study due to the poor metal cationization efficiency using coaxial EESI, described in Chapter 4.7.2.

It is very important to ensure the instrumental parameters and trap conditions are the same between ESI and EESI. An example of the importance of this is displayed in Figure 6.2. A glucose derivative, α-methylglucoside, was chosen because of high water reactivity and an inability to isomerize to the less reactive β-methylglucoside. When using 5 L/min gas flow for the drying gas, a great difference in the water reactive species (orange) is observed between ESI and EESI. This difference is due to methanol from the aerosol particles reaching the ion trap and reacting with the lithiated analyte. In this case, a methanol adduct of α-methylglucoside, $[M+H+CH_3OH]^+$, is observed. For these experiments,
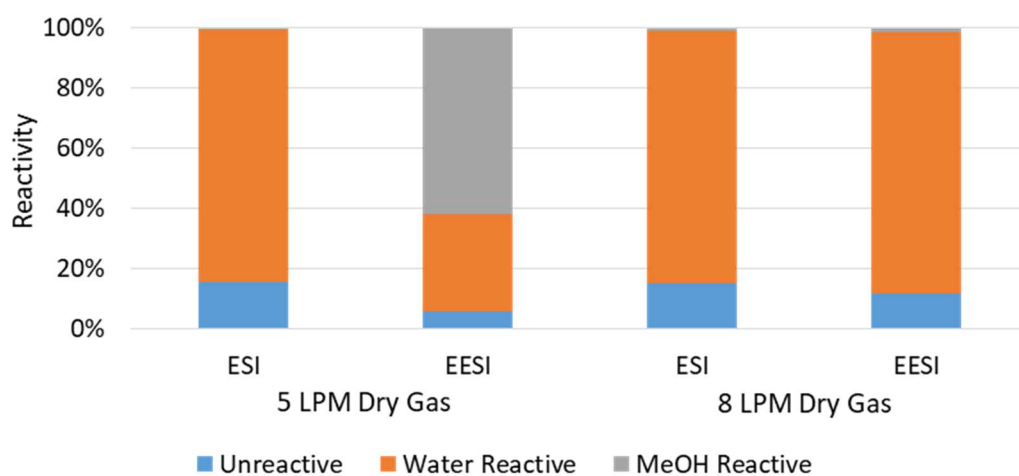
Figure 6.2. Bar graph showing the reactivity of α-methylglucoside ionized by ESI and EESI under two different dry gas flow rates.

the drying gas flow must be 8 L/min or higher to prevent methanol from reaching the trap in EESI.

For levoglucosan, it was observed that the unreactive fraction of lithiated molecules is a function of the electrospray solvent composition by ESI as shown in Figure 6.3. This is also the case for EESI of aerosolized levoglucosan where the electrospray solvent and the aerosol solution both have solvent composition below 50% water. No data points are plotted for solvent compositions above 50% water for EESI analysis because no signal was observed due to the inability to generate aerosol particles using a high viscosity solvent. Typical analysis of an aerosol generated with a COA requires the analyte be in a volatile solvent, such as methanol. Thus, in typical EESI analysis the solvent composition of the aerosol solution differs from the electrospray solvent. The unreactive fraction of levoglucosan in a typical EESI experiment could be used to determine the solvent composition of the droplet from which the lithiated analyte is ejected in EESI, yielding information on the mechanism of extraction and ionization.

A good design for this experiment would include an isotopically labeled internal standard spiked into the electrospray solvent. In this experiment, switching between EESI and only ESI would involve switching off the aerosol generator. During EESI, ions generated by both ESI and EESI would be present in the same mass spectra. Preliminary experiments of this type, using glucose-^{12}C and glucose-^{13}C, show that ESI and EESI produce similar structures, but there seems to be some interaction that is not conserved between glucose-^{12}C and glucose-^{13}C as shown in Figure 6.4. Glucose-^{13}C was present in each experiment. For the experiments represented by the blue dots, no aerosol was present. For the experiments represented by the gray dots, only methanol aerosol was present. When both glucose-^{12}C (aerosol) and glucose-^{13}C are present (green and orange dots, respectively), a larger unreactive fraction is observed for both species compared to the
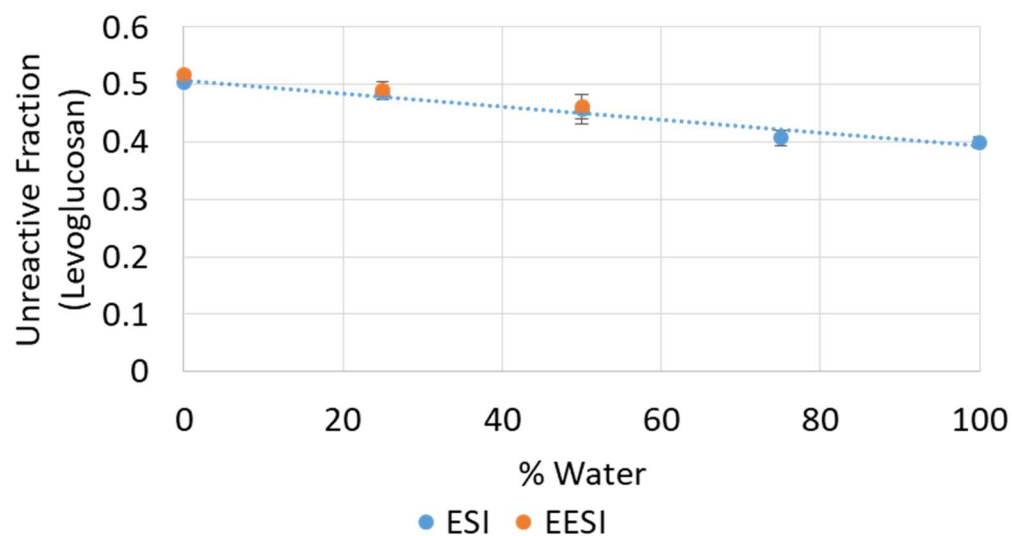
Figure 6.3. Graph showing the relationship of unreactive fraction of levoglucosan to the water content of the solvents in ESI and EESI.
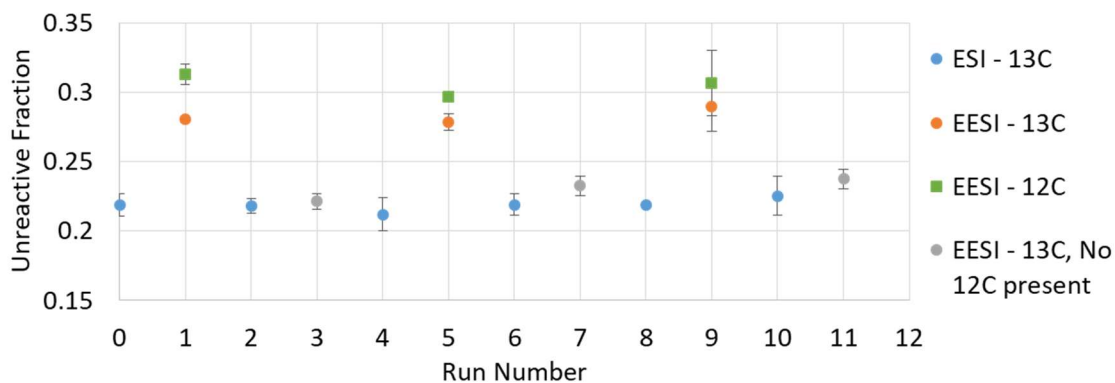
Figure 6.4. Graph showing the unreactive fraction of glucose-^{12}C and glucose-^{13}C under ESI and EESI conditions.

experiments with no glucose-^{12}C present. Further experiments need to be carried out to understand this isotope effect and its role in ion formation in EESI.

6.3.3. Separations coupled to OPSI-ESI for Complex Aerosol Analysis

One of the challenges of ambient ionization is the difficulty in overcoming sample complexity.[11] Separations are often coupled to mass spectrometry to reduce sample complexity, particularly for the identification of isomeric/isobaric species in a sample.[12,13] Differential ion mobility spectrometry (DIMS) is a post-ionization separation technique that has been applied to analysis of the aerosol particles from the pyrolysis of cellulose after ionization by EESI and LTPI.[14] Any ion mobility technique that is typically used with ESI could be coupled to OPSI-ESI, but most require extensive instrument modification as the separation most often occurs in vacuum.

Although time-resolved information is lost, there are multiple benefits to using a pre-ionization separation technique such as liquid chromatography, including the robustness of commercial instruments and the ability to tune a separation by altering the solvent composition of the mobile phases. Another benefit to chromatographic separations is the ability to separate an analyte from potential ionization supressors.[15] OPSI has previously been coupled to LC-MS for the study of both small molecules and proteins.[16] The experimental design uses a simple 6-port valve with a sample loop for injection to an LC system. One important study for which an aerosol-OPSI-LC-MS/MS system would be ideal is comparing the effects of filter collection and solvent extraction to an ambient sampling technique.

REFERENCES

1. Chen, H., Venter, A. & Cooks, R. G. Extractive electrospray ionization for direct analysis of undiluted urine, milk and other complex mixtures without sample preparation. *Chem. Commun.* **19,** 2042–2044 (2006).

2. Law, W. S. *et al.* On the Mechanism of Extractive Electrospray Ionization. *Anal. Chem.* **82,** 4494–4500 (2010).

3. Swanson, K. D., Spencer, S. E. & Glish, G. L. Metal Cationization Extractive Electrospray Ionization Mass Spectrometry of Compounds Containing Multiple Oxygens. *J. Am. Soc. Mass Spectrom.* **28,** 1030–1035 (2017).

4. Swanson, K. D., Worth, A. L. & Glish, G. L. A coaxial extractive electrospray ionization source. *Anal. Methods* **9,** 4997–5002 (2017).

5. Van Berkel, G. J. & Kertesz, V. An open port sampling interface for liquid introduction atmospheric pressure ionization mass spectrometry. *Rapid Commun. Mass Spectrom.* **29,** 1749–1756 (2015).

6. Swanson, K. D., Worth, A. L. & Glish, G. L. Use of an Open Port Sampling Interface Coupled to Electrospray Ionization for the On-Line Analysis of Organic Aerosol Particles. *J. Am. Soc. Mass Spectrom.* **29,** (2018).

7. Aszyk, J., Kubica, P., Kot-Wasik, A., Namieśnik, J. & Wasik, A. Comprehensive determination of flavouring additives and nicotine in e-cigarette refill solutions. Part I: Liquid chromatography-tandem mass spectrometry analysis. *J. Chromatogr. A* **1519,** 45–54 (2017).

8. Campbell, M. T., Chen, D. & Glish, G. L. Identifying the D-Pentoses Using Water Adduction to Lithium Cationized Molecule. *J. Am. Soc. Mass Spectrom.* **28,** 1420–1424 (2017).

9. Campbell, M. T., Chen, D., Wallbillich, N. J. & Glish, G. L. Distinguishing Biologically Relevant Hexoses by Water Adduction to the Lithium-Cationized Molecule. *Anal. Chem.* **89,** 10504–10510 (2017).

10. Campbell, M. T., Chen, D. & Glish, G. L. Distinguishing Linkage Position and Anomeric Configuration of Glucose–Glucose Disaccharides by Water Adduction to Lithiated Molecules. *Anal. Chem.* **90,** 2048–2054 (2018).

11. Li, X. *et al.* Sampling and analyte enrichment strategies for ambient mass spectrometry. *Anal. Bioanal. Chem.* **410,** 715–724 (2018).

12. Kocadağlı, T., Yılmaz, C. & Gökmen, V. Determination of melatonin and its isomer in foods by liquid chromatography tandem mass spectrometry. *Food Chem.* **153,** 151–156 (2014).

13. Isaacman, G. *et al.* Improved Resolution of Hydrocarbon Structures and Constitutional Isomers in Complex Mixtures Using Gas Chromatography-Vacuum

Ultraviolet-Mass Spectrometry. *Anal. Chem.* **84,** 2335–2342 (2012).

14.   Spencer, S. E. Development of an Aerosol Mass Spectrometry System for the Analysis of the Composition of Aerosol Particles in Real Time. *Ph. D. Dissertation* (University of North Carolina, 2015).

15.   Mei, H. *et al.* Investigation of matrix effects in bioanalytical high-performance liquid chromatography/tandem mass spectrometric assays: application to drug discovery. *Rapid Commun. Mass Spectrom.* **17,** 97–103 (2003).

16.   Van Berkel, G. J. & Kertesz, V. Continuous-flow liquid microjunction surface sampling probe connected on-line with high-performance liquid chromatography/mass spectrometry for spatially resolved analysis of small molecules and proteins. *Rapid Commun. Mass Spectrom.* **27,** 1329–1334 (2013).